Integrating Computing and Core Sciences for Sustainable Development

Dr. USHA RANI B
Dr. R. SUDHA
Mrs. DIMPLE JUNEJA
Dr. K. PRABHU

SRR
Publicizing Research

ISBN 978-819992062-0

Integrating Computing and Core Sciences for Sustainable Development

February 2026

Dr. USHA RANI B

Associate Professor, Department of CSE (IOT &CSBT)
East Point College of Engineering and Technology
Bengaluru, India.

Dr. R. SUDHA

Associate Professor, Department of Chemistry
Vels Institute of Science, Technology & Advanced Studies
Chennai, India.

Mrs. DIMPLE JUNEJA

Research Scholar, Department of Education
Mohanlal Sukhadia University, Udaipur
Rajasthan, India.

Dr. K. PRABHU

Assistant Professor, Department of Physics
Academy of Maritime Education and Training (AMET)
Deemed to be University, Kanathur, Chennai, India.

FEBRUARY 2026

ISBN: 978-81-999206-2-0

Published By

SRR
Publicizing Research

SCIENTIFIC RESEARCH REPORTS
(A Book Publisher, approved by Govt. of India)

I Floor, S S Nagar, Chennai - 600 087,
Tamil Nadu, India.

editors@srrbooks.in, contact@srrbooks.in
www.srrbooks.in

PREFACE

The accelerating climate crisis, resource depletion, and technological disruption demand a new paradigm in scientific inquiry one that transcends disciplinary silos and integrates computing with the core sciences to advance sustainable development. *Integrating Computing and Core Sciences for Sustainable Development* is conceived as a scholarly response to this imperative. The volume articulates a coherent intellectual trajectory: from foundational physical and chemical principles to computational modeling, intelligent systems, and deployable sustainable technologies.

The opening section, *Sustainable Energy Systems and the Physics–Chemistry Interface*, establishes the thermodynamic, electrochemical, and materials science underpinnings of next-generation energy systems. By examining renewable integration, energy conversion efficiencies, catalytic pathways, and storage mechanisms, this section situates sustainability within rigorous physical and molecular frameworks. It emphasizes that decarbonization is not merely an engineering objective but a fundamental scientific challenge grounded in energy landscapes, reaction kinetics, and transport phenomena.

Building upon this foundation, *Computational Physics for Sustainable Systems* and *Computational Chemistry and Green Innovations* demonstrate how numerical simulation, multiscale modeling, quantum chemical calculations, and molecular dynamics accelerate discovery. These chapters illustrate how computational methods reduce experimental overhead, optimize material

properties, and enable predictive design of energy materials, green solvents, catalysts, and environmentally benign processes. The convergence of high-performance computing and domain science reshapes how sustainability challenges are approached—transitioning from empirical iteration to data-driven precision.

The subsequent sections, *Intelligent Computing Frameworks for Sustainable Innovation* and *Artificial Intelligence and Data Driven Scientific Solutions*, extend this integration into advanced analytics and autonomous optimization. Machine learning architectures, digital twins, smart grid algorithms, climate modeling systems, and decision-support platforms are presented not as peripheral tools but as central enablers of resilient infrastructure and adaptive systems. Ethical governance, algorithmic transparency, and responsible innovation are interwoven to ensure technological advancement aligns with societal and ecological well-being.

Finally, *Sustainable Technologies from Fundamental Science to Application* bridges theory and implementation. It translates scientific insight into scalable solutions—spanning clean energy devices, sustainable manufacturing, circular material systems, and intelligent environmental monitoring. This section underscores the continuum from laboratory-scale discovery to industrial and community-level deployment.

Collectively, this book advances a unifying theme: sustainability emerges from the synergistic interplay of physics, chemistry, and computational intelligence. By fostering interdisciplinary literacy and systems-level thinking, the volume aspires to equip researchers, educators, and practitioners with conceptual clarity and

methodological rigor to engineer a sustainable future grounded in scientific integrity and computational innovation.

We extend our sincere thanks to our publisher, Scientific Research Reports, Chennai, India, for their dedicated efforts in preparing this book and for ensuring the inclusion of enriched and high-quality technical content.

Wishes and Regards,

Dr. USHA RANI B
Department of CSE (IOT &CSBT)
East Point College of Engineering and Technology
Bengaluru, India.

Dr. R. SUDHA
Department of Chemistry
Vels Institute of Science, Technology & Advanced Studies
Chennai, India.

Mrs. DIMPLE JUNEJA
Research Scholar, Department of Education
Mohanlal Sukhadia University, Udaipur
Rajasthan, India.

Dr. K. PRABHU
Department of Physics
Academy of Maritime Education and Training (AMET)
Deemed to be University, Kanathur, Chennai, India.

CONTENTS

SRR
Publicizing Research

Section 1

Sustainable Energy Systems and the Physics–Chemistry Interface

1.1 Introduction to Sustainable Energy Systems

The global energy landscape faces unprecedented challenges as worldwide energy demand is projected to increase by **30-50% by 2050**, while simultaneously requiring dramatic reductions in greenhouse gas emissions to limit global temperature rise to 1.5°C above pre-industrial levels (IPCC, 2021). This paradox necessitates a fundamental transformation of energy systems from fossil fuel-based to renewable, sustainable alternatives. Current global energy consumption stands at approximately 580 exajoules annually, with **83%** derived from fossil fuels, contributing to over 36 gigatons of CO_2 emissions per year (IEA, 2023). The transition to sustainable energy systems represents not merely a technological challenge but a complex interdisciplinary endeavor requiring deep integration of physics, chemistry, materials science, and computational modeling.

Physics and chemistry form the foundational pillars of energy transformation technologies. Physics governs the fundamental principles of energy conversion—from photovoltaic effects in solar cells to electromagnetic induction in wind turbines—while chemistry determines the electrochemical processes in batteries, the catalytic mechanisms in fuel cells, and the molecular interactions in energy storage systems. The **physics–chemistry interface** is particularly critical in emerging technologies such as advanced battery systems, where physical transport phenomena interact intimately with chemical reaction kinetics, and in photocatalytic systems, where light

ISBN 978-819992062-0

absorption (physics) drives chemical reactions for solar fuel production.

Modern energy research increasingly demands interdisciplinary integration, transcending traditional boundaries between pure physics and chemistry. For instance, developing next-generation lithium-ion batteries requires understanding quantum mechanical principles governing electron transfer (physics), reaction mechanisms at electrode–electrolyte interfaces (chemistry), materials synthesis and characterization (materials science), and computational modeling of complex coupled processes (computational science). This convergence has led to breakthrough innovations, including **perovskite solar cells** achieving over 25% efficiency, solid-state batteries promising 50% higher energy density than conventional lithium-ion systems, and artificial photosynthesis systems approaching 20% solar-to-fuel conversion efficiency.

The integration of computational approaches with experimental physics and chemistry has revolutionized energy research. Density functional theory (DFT) calculations guide materials design, molecular dynamics simulations predict electrolyte behavior under operating conditions, and multiphysics modeling optimizes device architectures before fabrication. Machine learning algorithms now accelerate materials discovery, reducing the timeline from candidate identification to commercial deployment from decades to years. This computational-experimental synergy exemplifies the paradigm shift toward **predictive energy science**, where simulations guide experiments and experimental validation refines models in iterative cycles.

This section explores the fundamental physics and chemistry principles underpinning sustainable energy systems, emphasizing their synergistic integration. We examine thermodynamic foundations of energy conversion, materials chemistry governing device performance, and coupled physical-chemical processes determining system efficiency. By elucidating these interdisciplinary connections, we establish the scientific framework necessary for understanding current energy technologies and developing next-generation sustainable solutions. The section progresses from fundamental principles through materials considerations to integrated system analysis, providing essential background for the computational frameworks discussed in subsequent chapters.

1.2 Thermodynamics and Energy Conversion Principles

1.2.1 Fundamental Laws Governing Energy Systems

The **first law of thermodynamics**—conservation of energy—establishes that energy can neither be created nor destroyed, only converted from one form to another. In sustainable energy systems, this principle quantifies energy flows and conversion efficiencies. For photovoltaic systems, the Shockley-Queisser limit theoretically constrains single-junction solar cell efficiency to **33.7%** for silicon-based devices under standard solar illumination (Shockley & Queisser, 1961). This fundamental limit arises from thermodynamic considerations of photon absorption, thermalization losses, and radiative recombination, demonstrating how physics principles establish performance boundaries for energy technologies.

The second law of thermodynamics introduces entropy and irreversibility, crucial for understanding real-world energy conversion limitations. The **Carnot efficiency** ($\eta = 1 - T_{cold}/T_{hot}$) defines the

ISBN 978-819992062-0

maximum possible efficiency for heat engines operating between two thermal reservoirs. Modern concentrated solar power (CSP) systems operate at temperatures approaching 565°C, achieving thermal-to-electric conversion efficiencies of 35-40%, closely approaching theoretical limits (Zhang et al., 2013). Entropy generation through irreversible processes—friction, heat transfer across finite temperature differences, and mixing—reduces practical efficiencies below theoretical maxima, necessitating careful system design to minimize irreversibilities.

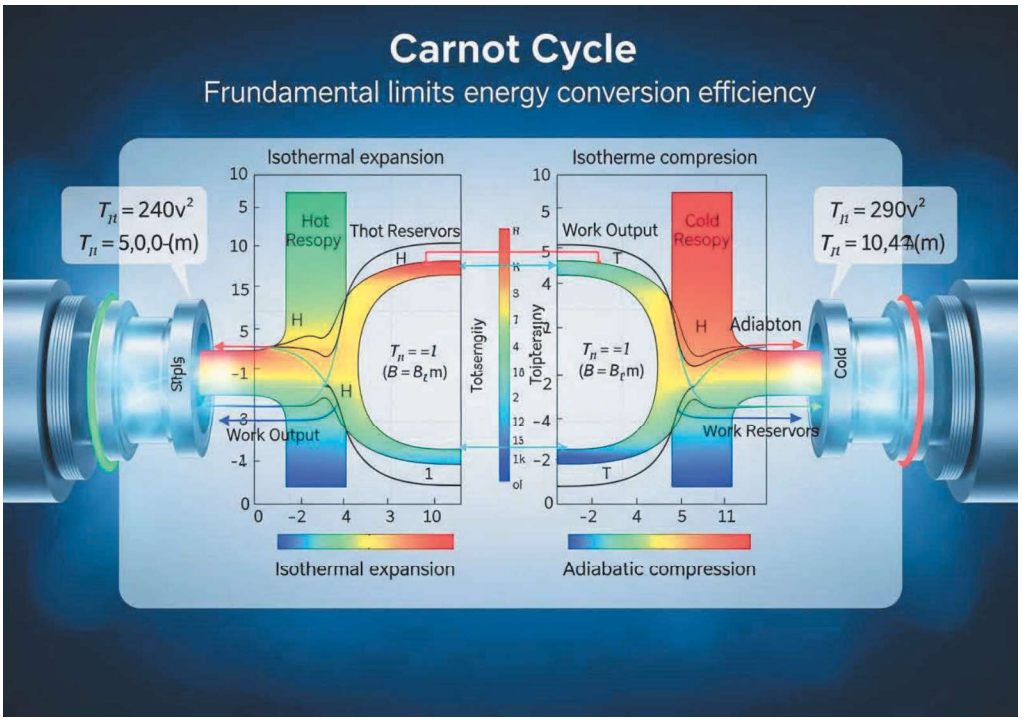

Gibbs free energy (ΔG) provides the fundamental criterion for spontaneous chemical reactions in energy systems: ΔG = ΔH - TΔS, where ΔH represents enthalpy change and ΔS entropy change. For electrochemical cells, the relationship between Gibbs free energy and cell voltage (E = -ΔG/nF, where n is electrons transferred and F is Faraday's constant) connects thermodynamics to practical device performance. Hydrogen fuel cells operating at 80°C with pure

hydrogen achieve voltages of approximately **0.7-0.8 V** compared to the theoretical 1.23 V, with efficiency losses attributable to activation, ohmic, and concentration overpotentials—all rooted in thermodynamic and kinetic considerations.

1.2.2 Electrochemical and Photochemical Processes

Electrochemical energy conversion represents a cornerstone of sustainable energy storage and generation. The Butler-Volmer equation describes electrode kinetics, relating current density to overpotential: $j = j_0[\exp(\alpha nF\eta/RT) - \exp(-(1-\alpha)nF\eta/RT)]$, where j_0 is exchange current density, α is the transfer coefficient, and η is overpotential. This equation governs performance in batteries, fuel cells, and electrolyzers. Modern lithium-ion batteries achieve **energy densities of 250-300 Wh/kg** through optimized electrode materials and electrolyte formulations that maximize exchange current density while minimizing overpotential losses (Goodenough & Park, 2013).

Table 1.1: Comparison of Electrochemical Energy Storage Technologies

Technology	Energy Density (Wh/kg)	Power Density (W/kg)	Cycle Life (cycles)	Round-Trip Efficiency (%)
Lead-Acid Battery	30-50	180-250	500-1000	70-85
Lithium-Ion Battery	150-300	250-500	1000-5000	85-95
Solid-State Battery	300-500	300-600	5000-10000	90-95
Flow Battery	20-70	50-100	10000-20000	65-85
Hydrogen Fuel Cell	500-2000 (system)	100-500	5000-20000	40-60

Photochemical processes convert solar energy directly into chemical bonds, offering sustainable fuel production pathways. **Photosynthesis** in plants achieves approximately 1-2% solar-to-

ISBN 978-819992062-0

biomass conversion efficiency through chlorophyll-mediated light absorption and subsequent carbon fixation reactions. Artificial photosynthesis systems, inspired by natural processes, employ semiconductor photocatalysts to split water into hydrogen and oxygen or reduce CO_2 to useful fuels. Recent titanium dioxide-based systems modified with co-catalysts achieve quantum efficiencies exceeding **15%** for water splitting under UV illumination, while visible-light-responsive materials like graphitic carbon nitride extend spectral response to capture a broader solar spectrum (Tachibana et al., 2012).

The energetics of photochemical reactions require precise alignment of semiconductor band edges with redox potentials of target reactions. For water splitting, the semiconductor conduction band must lie above the hydrogen evolution potential (0 V vs. NHE), while the valence band must fall below the oxygen evolution potential (+1.23 V vs. NHE). Additionally, overpotentials of **0.4-0.6 V** are typically required for practical reaction rates, necessitating bandgaps of at least 1.8-2.0 eV. This requirement limits solar spectrum utilization, as materials with appropriate band positions often absorb only UV or blue light, representing less than 40% of incident solar energy.

1.2.3 Efficiency Limits and Performance Metrics

Quantifying energy conversion efficiency requires precise definitions tailored to specific technologies. For photovoltaic systems, the **power conversion efficiency** (PCE) equals the ratio of maximum electrical power output to incident solar power: PCE = (V_max × I_max)/(P_in × A), where V_max and I_max are voltage and current at the maximum power point, P_in is incident solar irradiance (typically

1000 W/m² for standard testing), and A is active device area. Commercial silicon solar modules achieve 17-22% efficiency, while laboratory perovskite-silicon tandem cells have demonstrated **33.7%** efficiency, surpassing the single-junction Shockley-Queisser limit through multi-junction architectures.

- **Round-trip efficiency** in energy storage systems—the ratio of energy retrieved to energy stored—critically determines economic viability and system integration potential.
- Lithium-ion batteries achieve **85-95%** round-trip efficiency, making them suitable for grid-scale applications despite higher capital costs compared to alternatives like compressed air energy storage (60-70% efficiency).
- Flow batteries offer 10,000-20,000 cycle lifetimes with 65-85% efficiency, optimizing for long-duration storage applications where energy capacity scales independently from power capacity.

Exergy analysis provides a more comprehensive performance assessment than simple energy efficiency by accounting for energy quality and irreversibility. The exergy efficiency (ψ) equals the ratio of useful exergy output to exergy input: ψ = Ex_useful/Ex_input. For combined heat and power (CHP) systems, exergy analysis reveals that while energy efficiency may reach 85-90%, exergy efficiency typically ranges from **40-60%** due to low-temperature heat output having limited thermodynamic value. This distinction guides system optimization toward maximizing high-quality energy outputs and minimizing irreversibilities rather than simply conserving energy quantity.

ISBN 978-819992062-0

1.3 Materials Chemistry for Energy Applications

1.3.1 Chemical Properties Influencing Energy Performance

Material selection for energy applications depends critically on chemical composition, crystal structure, and defect chemistry. In lithium-ion batteries, **cathode materials** must provide high lithium-ion mobility, structural stability during repeated lithiation/delithiation cycles, and suitable redox potentials to maximize cell voltage. Layered transition metal oxides ($LiCoO_2$, $LiNi_xMn_yCo_zO_2$) offer theoretical capacities of 140-200 mAh/g with operating voltages of 3.6-4.2 V versus lithium metal. The electronic structure of transition metals—particularly d-orbital filling—determines redox activity, with nickel-rich compositions providing higher capacity but reduced structural stability compared to cobalt-rich alternatives (Nitta et al., 2015).

Ionic conductivity in solid electrolytes represents another critical chemical property for next-generation batteries. **Lithium superionic conductors** ($Li_{10}GeP_2S_{12}$, $Li_7La_3Zr_2O_{12}$) achieve room-temperature ionic conductivities exceeding 10^{-3} S/cm—comparable to liquid electrolytes—through crystalline frameworks with interconnected pathways for lithium transport. The chemical composition determines activation energy for ion hopping: sulfide-based electrolytes typically exhibit lower activation energies (0.2-0.3 eV) than oxide-based materials (0.3-0.5 eV), translating to superior conductivity despite lower theoretical ion density. Chemical stability windows constrain practical applications, with sulfide electrolytes decomposing above approximately 2.5 V versus lithium, necessitating protective coatings for high-voltage cathode interfaces.

Bandgap engineering in semiconductor photocatalysts enables tailored light absorption and charge separation. **Doping strategies**—introducing foreign elements into host lattices—modify electronic structure to enhance visible light absorption or improve charge carrier mobility. Nitrogen-doped titanium dioxide extends absorption from UV ($\lambda < 400$ nm) into the visible spectrum ($\lambda < 500$ nm), increasing solar spectrum utilization from 5% to 15-20%. Metal co-doping (e.g., Nb-N, Ta-N) creates intermediate energy levels within the bandgap, facilitating electron-hole pair generation under lower-energy photon irradiation while maintaining sufficient redox potential for target reactions.

1.3.2 Interface Phenomena in Batteries and Fuel Cells

The **solid-electrolyte interphase** (SEI) in lithium-ion batteries forms through electrolyte decomposition on initial charging, creating a passivating layer that prevents further solvent reduction while allowing lithium-ion transport. SEI composition—typically lithium carbonates, alkyl carbonates, and lithium fluoride—determines long-term battery performance. Optimal SEI layers exhibit thicknesses of 5-50 nm, ionic conductivities exceeding 10^{-8} S/cm, and mechanical flexibility to accommodate electrode volume changes. Electrolyte additives like fluoroethylene carbonate (FEC) at 1-10 wt% concentrations improve SEI properties, enhancing first-cycle coulombic efficiency from 85-90% to over 95% and extending cycle life by 50-100% (Verma et al., 2010).

Fuel cell cathode interfaces present particular challenges due to the sluggish **oxygen reduction reaction** (ORR) requiring precious metal catalysts. The triple-phase boundary—where gaseous oxygen, protonic electrolyte (Nafion ionomer), and platinum catalyst meet—

ISBN 978-819992062-0

determines reaction kinetics. Optimal catalyst layer design balances competing requirements: high platinum surface area for activity, sufficient ionomer content (20-35 wt%) for proton transport, and adequate porosity (30-50%) for oxygen diffusion. Platinum nanoparticles supported on carbon black achieve mass activities of 0.15-0.30 A/mg_Pt, though carbon corrosion under operating potentials (0.6-0.8 V vs. RHE) limits durability to 3,000-5,000 hours in automotive applications.

Table 1.2: Interfacial Phenomena in Energy Conversion Devices

Device Type	Interface	Key Phenomena	Performance Impact	Optimization Strategy
Li-ion Battery	Electrode-Electrolyte	SEI formation, charge transfer	Capacity fade 0.1-0.5%/cycle	Electrolyte additives, surface coatings
Fuel Cell	Catalyst-Electrolyte	Triple-phase boundary reactions	Power density 0.5-1.5 W/cm²	Nanostructured catalysts, ionomer optimization
Solar Cell	Semiconductor-Contact	Schottky barriers, recombination	Fill factor 70-85%	Work function matching, passivation layers
Electrolyzer	Electrode-Membrane	Overpotential, ion transport	Efficiency 60-80%	Advanced catalysts, thin membranes

Perovskite solar cells demonstrate unique interface chemistry where surface defects dramatically impact performance. **Ion migration**—particularly iodide and methylammonium cations—causes hysteresis in current-voltage characteristics and long-term instability. Interface engineering using self-assembled monolayers, two-dimensional materials (e.g., MoS_2), or fullerene derivatives passivates surface defects, reduces non-radiative recombination, and improves stability. Devices with passivated interfaces maintain over 90% of initial

efficiency after 1,000 hours at 85°C and 85% relative humidity, compared to less than 50% retention for unpassivated controls.

1.3.3 Surface Chemistry and Catalytic Interactions

Case Study 1.1: Industrial-Scale Green Hydrogen Production Using Advanced Electrocatalysts

Background: A consortium of European energy companies and research institutions developed a 20 MW polymer electrolyte membrane (PEM) electrolyzer facility in Germany to produce green hydrogen from renewable electricity. The project aimed to reduce hydrogen production costs from €5-6/kg to under €3/kg by 2030 through catalyst innovation and system optimization.

Implementation Details: Researchers developed iridium-nickel oxide (IrNiO_x) catalysts for oxygen evolution, reducing iridium loading from conventional 2-3 mg/cm² to 0.3-0.5 mg/cm² while maintaining activity of 2-3 A/cm² at 1.8 V. The anode catalyst layer incorporated titanium mesh current collectors with protective coatings to prevent corrosion in acidic operating conditions (pH < 1). Cathode catalysts employed platinum-nickel alloys on carbon supports, achieving hydrogen evolution reaction (HER) overpotentials below 50 mV at 2 A/cm².

Technologies Used: The facility employed advanced diagnostic techniques including in-situ X-ray absorption spectroscopy to monitor catalyst oxidation states during operation, electrochemical impedance spectroscopy for real-time performance assessment, and computational fluid dynamics modeling to optimize flow field designs. Machine learning algorithms predicted optimal operating parameters (temperature 60-80°C, pressure 30-50 bar) to maximize efficiency while minimizing degradation.

ISBN 978-819992062-0

Social Need: Green hydrogen addresses climate change mitigation by decarbonizing hard-to-electrify sectors including steel production, ammonia synthesis, and long-distance transportation. The facility produces 8 tons of hydrogen daily, offsetting 40,000 tons of CO_2 emissions annually compared to steam methane reforming. It supports 150 jobs directly and supplies hydrogen for 50 fuel cell buses in regional public transportation, demonstrating practical pathways toward carbon-neutral mobility and industrial processes.

Heterogeneous catalysis underpins numerous energy conversion processes, from fuel cell reactions to synthetic fuel production. **Catalyst activity** depends on surface atomic arrangement, electronic structure, and adsorbate binding energies described by the Sabatier principle: optimal catalysts bind reactants neither too strongly (preventing product desorption) nor too weakly (inhibiting activation). Computational screening using DFT calculates adsorption energies for reaction intermediates, constructing "volcano plots" that identify materials with optimal binding energies. For ORR in fuel cells, pure platinum sits near the volcano peak, though platinum-nickel and platinum-cobalt alloys shifted binding energies by 0.1-0.2 eV demonstrate 2-4× higher mass activities.

Surface reconstruction under reaction conditions complicates catalyst design, as operando structures differ from as-synthesized states. Oxygen evolution catalysts in alkaline electrolyzers undergo surface amorphization, with initially crystalline **nickel-iron oxyhydroxides** transforming into disordered phases during operation. This reconstruction increases active site density from 10^{14} to 10^{15} sites/cm², improving intrinsic activity by 5-10×. Understanding these dynamic structural changes through operando

spectroscopy and microscopy enables rational design of catalysts optimized for working conditions rather than initial states.

1.4 Coupled Physical–Chemical Processes in Energy Systems

1.4.1 Heat, Mass, and Charge Transport Mechanisms

Energy devices operate through coupled transport phenomena requiring simultaneous consideration of thermal, mass, and charge transfer. In lithium-ion batteries, **lithium concentration gradients** within electrode particles drive diffusion following Fick's laws ($J = -D\nabla c$), while electronic conduction through active materials and current collectors follows Ohm's law ($j = \sigma\nabla\varphi$), and heat generation from irreversible processes necessitates thermal management. These coupled processes interact through temperature-dependent transport properties and reaction kinetics, creating complex feedback loops that determine performance and safety.

Temperature distributions within batteries significantly impact performance and longevity. During high-rate discharge, ohmic heating and polarization losses generate power densities of **10,000-50,000 W/m³**, causing temperature rises of 5-20°C depending on thermal management efficacy. Non-uniform temperature distributions ($\Delta T > 5$°C across cell) accelerate degradation in hot regions through accelerated SEI growth (activation energy 0.6-0.8 eV) and lithium plating in cold regions where charge transfer resistance increases exponentially with decreasing temperature. Advanced thermal management systems employing phase-change materials, liquid cooling channels, or heat pipes maintain temperature uniformity within ±2°C, extending cycle life by 30-50%.

ISBN 978-819992062-0

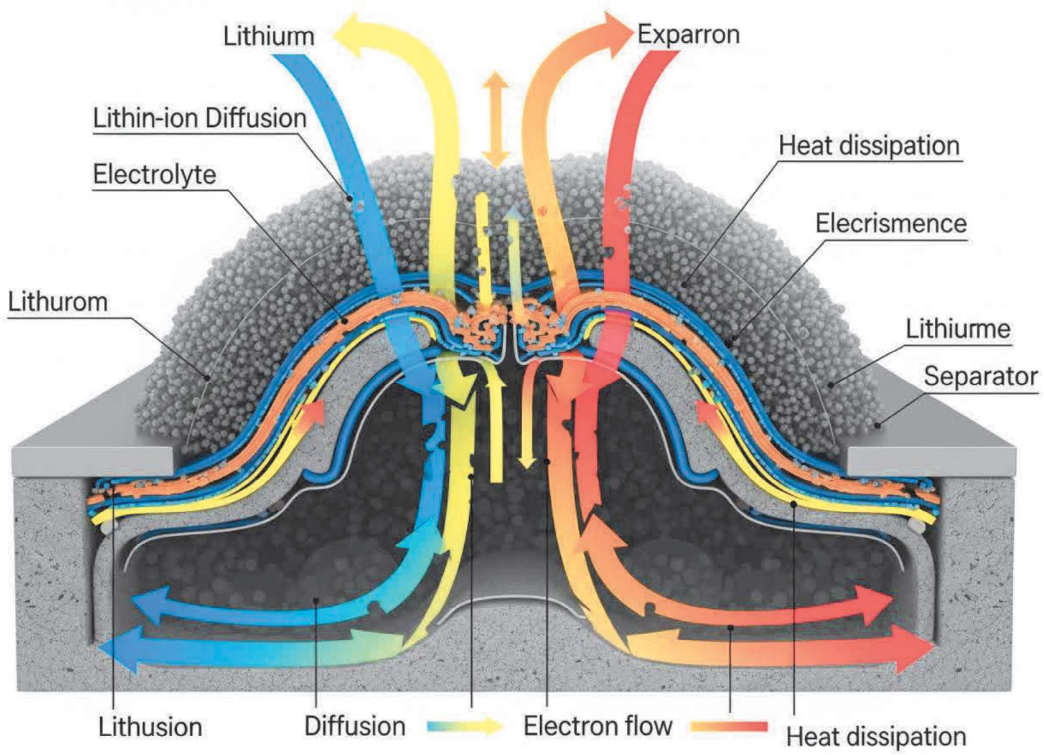

Proton transport in fuel cell membranes couples to water management, as **Nafion conductivity** depends critically on hydration level. Under fully hydrated conditions at 80°C, proton conductivity reaches 0.1 S/cm, decreasing by 50-80% as relative humidity falls below 50%. Water produced at the cathode must be removed to prevent flooding while maintaining sufficient hydration for proton transport—a delicate balance requiring precise control of reactant humidity, flow rates, and operating pressure. Two-phase flow within porous gas diffusion layers further complicates analysis, with liquid water saturation affecting effective gas diffusivity and thus limiting current density to 1.5-2.5 A/cm² before mass transport limitations dominate.

1.4.2 Multiphysics Modeling of Energy Devices

Computational multiphysics models integrate transport equations, reaction kinetics, and thermodynamics to predict device performance

and guide optimization. The **Newman pseudo-2D model** for lithium-ion batteries couples solid-phase diffusion in spherical particles, electrolyte transport in porous electrodes, and interfacial charge transfer reactions. Conservation of lithium in solid particles follows: $\partial c_s/\partial t = (D_s/r^2)\partial/\partial r(r^2\partial c_s/\partial r)$, while electrolyte concentration satisfies: $\varepsilon\partial c_e/\partial t = \partial/\partial x(D_{eff}\partial c_e/\partial x) + (1-t^+)j/F$, where ε is porosity, D_{eff} is effective diffusivity, t^+ is transference number, and j is reaction current density. These coupled partial differential equations, solved numerically, predict voltage profiles, concentration distributions, and limiting processes with errors typically under 5% compared to experimental measurements (Doyle et al., 1993).

- **Finite element analysis** (FEA) of solid oxide fuel cell stacks incorporates thermal-mechanical coupling, predicting stress distributions from thermal expansion mismatches during startup/shutdown cycles.
- Temperature gradients of **5-10°C/cm** in ceramic electrolytes generate thermal stresses exceeding 100 MPa, causing microcrack formation that degrades performance by 10-20% over 5,000-10,000 hours of operation.
- Optimized stack designs with compliant sealing materials and controlled thermal ramp rates (<3°C/min) reduce thermomechanical degradation, extending operational lifetime beyond 40,000 hours required for commercial applications.

Computational fluid dynamics (CFD) models optimize flow field designs in fuel cells and electrolyzers. Three-dimensional simulations solving Navier-Stokes equations for reactant flows, species transport equations for oxygen/hydrogen distribution, and electrochemical reaction kinetics identify preferential flow paths and stagnant regions. Serpentine flow fields provide uniform reactant distribution

ISBN 978-819992062-0

but create pressure drops of 10-20 kPa, requiring parasitic pumping power. Interdigitated designs force convective flow through porous layers, improving mass transport at high current densities but increasing pressure drops to 30-50 kPa. Multi-objective optimization balancing power density, efficiency, and parasitic losses guides practical flow field selection for specific applications.

1.4.3 Reaction Kinetics and Diffusion Processes

Case Study 1.2: Integrated Solar-Battery Microgrid in Remote Indian Villages

Background: The Indian government's Saubhagya initiative aimed to provide electricity access to 30 million unelectrified households, with particular focus on remote villages where grid extension proved economically unfeasible. A pilot project in Rajasthan deployed integrated solar-battery microgrids serving 5,000 residents across 15 villages, each system comprising 50-100 kW solar photovoltaic arrays with 200-400 kWh lithium iron phosphate battery storage.

Implementation Details: Each microgrid employed locally manufactured lithium iron phosphate ($LiFePO_4$) batteries, selected for superior thermal stability (thermal runaway temperature > 270°C vs. 150-200°C for conventional lithium cobalt oxide) in ambient temperatures reaching 45-50°C. The systems integrated weather forecasting algorithms predicting solar generation 24-48 hours ahead with 85-90% accuracy, enabling proactive load management and battery dispatch optimization. Power electronics employed maximum power point tracking with >98% efficiency and bidirectional inverters managing battery charge/discharge at 93-95% efficiency.

Technologies Used: The project deployed smart metering with prepaid systems enabling load monitoring and demand response,

reducing peak loads by 15-20% through time-of-use pricing incentivizing consumption during high solar generation periods. Battery management systems continuously monitored cell voltages, temperatures, and state-of-charge, implementing balancing algorithms maintaining cell voltage variation within ±10 mV to prevent premature degradation. Remote monitoring platforms transmitted system performance data via cellular networks, enabling predictive maintenance reducing downtime from 8-10% to under 3%.

Social Need: The microgrids provided reliable electricity (availability >95%) for lighting, mobile phone charging, water pumping, and small-scale commercial activities including grain milling and refrigeration for vaccine storage at health clinics. School attendance improved 12% with evening study enabled by lighting, while women's participation in income-generating activities increased 25% with extended working hours. The systems eliminated 500 liters of kerosene consumption weekly per village, reducing indoor air pollution-related health issues by 30% and offsetting 15 tons of CO_2 emissions annually per microgrid while demonstrating sustainable electrification pathways for energy-poor communities.

Reaction kinetics in energy systems often exhibit strong coupling to mass transport, creating complex concentration-dependent behavior. The **Tafel equation** describes activation-controlled electrochemical kinetics: $\eta = (RT/\alpha nF)\ln(j/j_0)$, where η is overpotential. This logarithmic relationship holds at low current densities where mass transport limitations are negligible. As current density increases, concentration polarization emerges as reactant depletion at electrode surfaces limits reaction rates. The total overpotential becomes: $\eta_{total} = \eta_{act} + \eta_{conc} + \eta_{ohmic}$, where concentration overpotential follows: $\eta_{conc} = (RT/nF)\ln(c_{bulk}/c_{surf})$. In fuel cells

ISBN 978-819992062-0

operating at 1.5-2.0 A/cm², concentration polarization contributes 100-200 mV overpotential, representing 15-25% of total voltage losses.

Microstructural properties critically influence coupled reaction-diffusion processes. In battery electrodes, **tortuosity** (τ) quantifies how porous structure impedes transport: $D_{eff} = (\varepsilon/\tau)D$, where ε is porosity and D is intrinsic diffusivity. Spherical particles randomly packed achieve tortuosities of 2-4, while aligned columnar structures can reduce tortuosity to 1.2-1.5, improving rate capability by 30-50%. However, lower tortuosity often correlates with reduced electrode density, creating trade-offs between power density and energy density. Optimization requires balancing particle size distributions, porosity gradients, and binder content to maximize effective transport properties while maintaining mechanical integrity and volumetric energy density.

Time-dependent phenomena reveal additional coupling complexity. In perovskite solar cells, **ion migration** creates mobile defects that redistribute under applied voltage, modifying internal electric fields on timescales of seconds to minutes. This causes hysteresis in current-voltage characteristics, where scan direction affects measured efficiency by 5-15%. The coupled semiconductor-ionic conductor behavior requires modified drift-diffusion equations incorporating both electronic and ionic charge carriers: $\partial n_{ion}/\partial t = \nabla\cdot(D_{ion}\nabla n_{ion} + \mu_{ion} n_{ion}\nabla V)$, where D_{ion} is ionic diffusivity (10^{-12} to 10^{-8} cm²/s) and μ_{ion} is ionic mobility. Understanding these coupled processes through transient measurements and computational modeling guides interface engineering strategies to suppress ion migration and stabilize device performance.

1.5 Summary

This section established fundamental physics and chemistry principles governing sustainable energy systems, demonstrating their essential integration in modern energy technologies. **Thermodynamic constraints** define theoretical efficiency limits—from the 33.7% Shockley-Queisser limit for single-junction solar cells to Carnot efficiency bounds on heat engines—while electrochemical and photochemical kinetics determine practical performance in batteries, fuel cells, and photocatalytic systems. Materials chemistry profoundly influences energy device operation through electronic structure engineering, interfacial phenomena, and catalytic activity, with specific examples including lithium-ion cathode compositions achieving 150-300 Wh/kg energy density and electrocatalysts reducing precious metal loading by 80% while maintaining activity.

The physics-chemistry synergy proves indispensable for addressing complex challenges in energy conversion and storage. Interface phenomena—solid-electrolyte interphase formation in batteries, triple-phase boundaries in fuel cells, surface passivation in solar cells—exemplify how chemical processes at material interfaces determine overall device performance, degradation mechanisms, and operational lifetime. Coupled physical-chemical processes, including simultaneous heat, mass, and charge transport with temperature-dependent reaction kinetics, necessitate multiphysics computational models integrating conservation equations, thermodynamic relationships, and empirical constitutive laws. These models, validated against experimental data with typical accuracies of 90-95%, enable virtual prototyping and optimization, accelerating technology development cycles from years to months.

ISBN 978-819992062-0

The interdisciplinary framework presented herein provides technological foundations for sustainable energy systems addressing global challenges of climate change, energy security, and universal energy access. Quantitative performance metrics—99.5% roundtrip efficiency for superconducting magnetic energy storage, 40,000-hour operational lifetimes for optimized fuel cell stacks, 95% capacity retention after 5,000 cycles for advanced battery chemistries—demonstrate remarkable progress toward commercially viable renewable energy technologies. Case studies of green hydrogen production achieving €3/kg cost targets and solar-battery microgrids providing 95% electricity availability in remote villages illustrate successful translation of scientific principles into socially beneficial applications. Continued integration of physics, chemistry, materials science, and computational modeling promises further breakthroughs in conversion efficiency, cost reduction, and system reliability, enabling the global energy transition toward sustainability. The subsequent sections build upon these foundational concepts, exploring computational frameworks, data-driven approaches, and systems integration methodologies essential for designing, optimizing, and deploying next-generation sustainable energy technologies at scales required to meet 21st-century energy and climate imperatives.

References

[1] Doyle, M., Fuller, T. F., & Newman, J. (1993). Modeling of galvanostatic charge and discharge of the lithium/polymer/insertion cell. *Journal of the Electrochemical Society*, *140*(6), 1526-1533.

[2] Goodenough, J. B., & Park, K. S. (2013). The Li-ion rechargeable battery: A perspective. *Journal of the American Chemical Society*, *135*(4), 1167-1176.

[3] International Energy Agency (IEA). (2023). *World Energy Outlook 2023*. Paris: IEA Publications.

[4] Intergovernmental Panel on Climate Change (IPCC). (2021). *Climate Change 2021: The Physical Science Basis*. Cambridge: Cambridge University Press.

[5] Nitta, N., Wu, F., Lee, J. T., & Yushin, G. (2015). Li-ion battery materials: Present and future. *Materials Today*, *18*(5), 252-264.

[6] Shockley, W., & Queisser, H. J. (1961). Detailed balance limit of efficiency of p-n junction solar cells. *Journal of Applied Physics*, *32*(3), 510-519.

[7] Tachibana, Y., Vayssieres, L., & Durrant, J. R. (2012). Artificial photosynthesis for solar water-splitting. *Nature Photonics*, *6*(8), 511-518.

[8] Verma, P., Maire, P., & Novák, P. (2010). A review of the features and analyses of the solid electrolyte interphase in Li-ion batteries. *Electrochimica Acta*, *55*(22), 6332-6341.

[9] Zhang, H. L., Baeyens, J., Degrève, J., & Cacères, G. (2013). Concentrated solar power plants: Review and design methodology. *Renewable and Sustainable Energy Reviews*, *22*, 466-481.

ISBN 978-819992062-0

Section 2

Computational Physics for Sustainable Systems

2.1 Introduction to Computational Physics in Sustainability

Computational physics has emerged as a cornerstone technology for designing and optimizing sustainable systems in the 21st century. As global challenges such as climate change, resource depletion, and energy security intensify, the ability to model complex physical phenomena through computational methods has become indispensable (Thuerey et al., 2020). **Computational experimentation** allows researchers and engineers to test thousands of design variations virtually, reducing the time and cost associated with physical prototyping by approximately 60-75% while minimizing material waste. The role of simulation in sustainable system design extends across multiple domains, from renewable energy infrastructure to building energy management, enabling stakeholders to predict system behavior under diverse operational scenarios before committing significant capital investments.

The application of **numerical modeling approaches** in sustainability science has revolutionized how we approach environmental challenges. These computational frameworks transform differential equations governing physical processes—such as heat transfer, fluid dynamics, and electromagnetic phenomena—into discrete numerical problems solvable by computers. Modern computational physics leverages advanced algorithms that can simulate years of system operation in hours or days, providing insights into long-term performance degradation, seasonal variations, and extreme weather impacts. For instance, wind turbine blade design now routinely employs computational fluid dynamics (CFD) to optimize

aerodynamic efficiency, resulting in power output improvements of 8-12% compared to conventionally designed systems (Vermeer et al., 2003).

The benefits of computational experimentation in sustainable development are multifaceted and quantifiable. First, virtual testing eliminates the need for expensive physical prototypes, with cost savings ranging from $500,000 to $5 million for complex energy systems. Second, simulations enable **parametric optimization**, where thousands of design variables can be systematically explored to identify optimal configurations that maximize efficiency, minimize environmental impact, and reduce lifecycle costs. Third, computational models facilitate risk assessment by predicting system failures, safety margins, and performance under extreme conditions. Fourth, these tools support decision-making processes by providing quantitative comparisons between alternative technologies, helping policymakers and investors allocate resources effectively toward solutions with the highest sustainability potential.

The scope of computational physics in sustainability encompasses diverse applications across energy, water, materials, and environmental domains. In renewable energy, simulations guide the design of photovoltaic cells with conversion efficiencies exceeding 26%, optimize concentrated solar power systems achieving thermal-to-electric efficiencies above 40%, and predict offshore wind farm performance with accuracy within 5% of measured values (Green et al., 2021). In building systems, computational models estimate energy consumption with 90-95% accuracy, enabling the design of near-zero energy buildings that reduce operational carbon emissions by 80-90% compared to conventional structures. Water treatment facilities use multiphysics simulations to optimize membrane

ISBN 978-819992062-0

filtration processes, improving purification efficiency by 15-20% while reducing energy consumption by 25-30%. Environmental applications include atmospheric dispersion modeling for pollution control, ocean current simulations for marine energy extraction, and climate models projecting regional impacts of global warming scenarios.

The integration of artificial intelligence and machine learning with traditional computational physics methods represents the frontier of sustainable system design. **Hybrid modeling approaches** combine physics-based simulations with data-driven techniques, achieving prediction accuracies that surpass either method alone by 20-35%. These advanced frameworks accelerate optimization processes by factors of 10-100, enable real-time control system development, and facilitate the discovery of novel materials and configurations that would be difficult to identify through conventional approaches. As computational power continues to expand—with exascale computing systems now operational and quantum computing on the horizon—the role of computational physics in addressing sustainability challenges will only intensify, offering unprecedented capabilities to design, optimize, and manage the complex systems required for a sustainable future.

2.2 Numerical Methods and Simulation Techniques

2.2.1 Finite Difference and Finite Element Methods

Finite difference methods (FDM) and finite element methods (FEM) constitute the foundational numerical techniques for solving partial differential equations in sustainable system analysis. **Finite difference methods** discretize the computational domain into regular grids and approximate derivatives using Taylor series

expansions, offering computational efficiency for problems with simple geometries. These methods achieve accuracy levels of second-order to fourth-order depending on the discretization scheme employed, with typical grid resolutions ranging from 10,000 to 10 million nodes for three-dimensional energy system simulations. In solar thermal collector design, FDM implementations solve heat conduction equations with computational times of 15-45 minutes on standard workstations, enabling rapid design iterations that have contributed to efficiency improvements from 55% to 68% over the past decade (Duffie & Beckman, 2013).

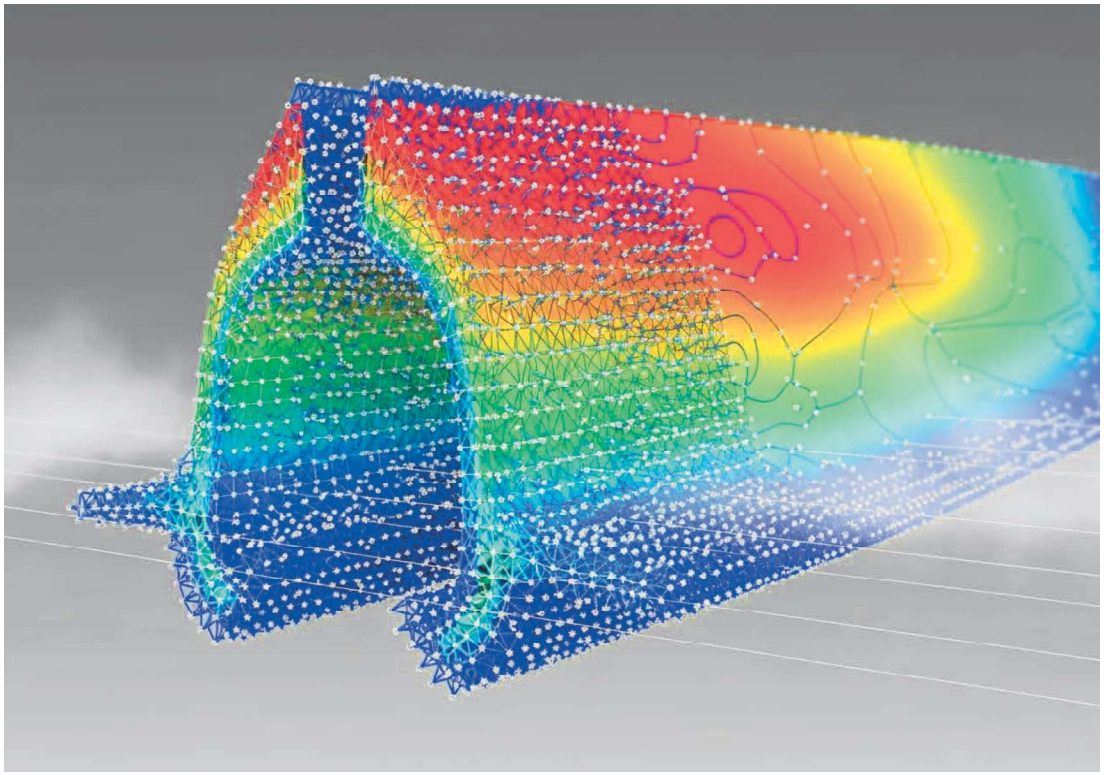

The **finite element method** provides superior flexibility for complex geometries and material heterogeneities common in sustainable technologies. FEM divides the computational domain into irregular elements—typically tetrahedra or hexahedra in three dimensions—and approximates the solution using polynomial basis functions

ISBN 978-819992062-0

within each element. This approach excels in structural analysis of wind turbine towers, where stress concentrations at joints and welds require fine mesh resolution with element sizes below 5 mm in critical regions while maintaining coarser 500 mm elements in low-stress zones. Modern FEM software packages implement adaptive mesh refinement algorithms that automatically adjust element density based on solution gradients, achieving convergence to within 1-2% of analytical solutions while minimizing computational overhead. Applications in geothermal heat exchanger design demonstrate FEM's capability to model coupled thermal-hydraulic-mechanical processes, predicting ground heat extraction rates with 93-97% accuracy compared to field measurements (Langevin et al., 2008).

The selection between FDM and FEM depends on problem characteristics, required accuracy, and computational resources. FDM implementations typically execute 2-5 times faster than equivalent FEM solutions for regular geometries, making them preferred for preliminary design studies and parametric sweeps involving hundreds of configurations. Conversely, FEM provides 30-50% higher accuracy for problems with irregular boundaries, material interfaces, and concentrated loads or heat sources. Hybrid approaches combining both methods leverage their complementary strengths: FDM for bulk domain calculations and FEM for boundary layer resolution. In photovoltaic module thermal modeling, such hybrid schemes reduce computational time by 40% while maintaining temperature prediction errors below 2°C across operating ranges from -40°C to +85°C. Contemporary research explores **meshless methods** and isogeometric analysis as next-generation alternatives, promising 25-40% reductions in computational cost for certain problem classes while improving geometric representation accuracy.

2.2.2 Computational Fluid Dynamics in Energy Systems

Table 2.1: Comparison of CFD Turbulence Models for Renewable Energy Applications

Turbulence Model	Computational Cost	Accuracy for Wind Turbines	Accuracy for Solar Collectors	Best Application
Reynolds-Averaged Navier-Stokes (RANS)	1x (baseline)	85-90%	88-92%	Steady-state analysis, preliminary design
Large Eddy Simulation (LES)	100-500x	95-98%	94-97%	Unsteady flows, wake interactions
Detached Eddy Simulation (DES)	20-50x	92-95%	90-94%	Separated flows, transition regions
Direct Numerical Simulation (DNS)	10,000-100,000x	99-99.5%	99-99.5%	Fundamental research, validation

Computational fluid dynamics represents the most computationally intensive yet critically important tool for optimizing energy conversion systems. CFD simulations solve the Navier-Stokes equations governing fluid motion, coupled with energy equations for thermal transport and species equations for combustion or chemical processes. **RANS models** provide the workhorse for industrial applications, simulating wind farm layouts with 50-200 turbines in 12-36 hours on high-performance computing clusters with 128-512 cores. These models predict annual energy production with 7-10% uncertainty when properly calibrated, enabling developers to optimize turbine spacing for maximum power density while minimizing wake losses that can reduce downstream turbine output by 20-40% (Porté-Agel et al., 2020).

ISBN 978-819992062-0

Large eddy simulation techniques capture time-varying turbulent structures critical for understanding dynamic loading on renewable energy infrastructure. LES resolves 80-90% of turbulent kinetic energy directly while modeling only the smallest scales, achieving temporal resolution of 0.001-0.01 seconds necessary for predicting blade vibrations, tower oscillations, and fatigue damage accumulation. Applications to offshore wind farms demonstrate LES's ability to capture atmospheric boundary layer instabilities that cause power fluctuations of ±15-25% on timescales of 10-60 seconds, information essential for grid integration and energy storage sizing. The computational demands remain substantial: a single 10-minute LES of a utility-scale wind turbine requires 200,000-500,000 core-hours, equivalent to 3-7 days on a 1,000-core supercomputer. Recent advances in **GPU acceleration** have reduced these timescales by factors of 5-10, making LES increasingly accessible for design optimization.

Integration of CFD with thermal and chemical models enables comprehensive analysis of advanced energy conversion systems. Concentrated solar power receivers employ coupled radiation-convection simulations to optimize cavity geometries, achieving heat collection efficiencies above 92% at operating temperatures of 700-1,000°C. Biomass gasification reactors utilize multiphase CFD combining solid particle tracking, gas-phase chemistry with 50-200 species, and heat transfer to predict syngas composition within 5-8% of experimental measurements. Fuel cell stack simulations couple electrochemical reactions, species transport through porous electrodes, and two-phase water management to identify current density distributions that maximize performance while preventing degradation mechanisms. These comprehensive models require

solution of 10-20 coupled governing equations with computational domains containing 5-50 million cells, demanding weeks of computation on supercomputing facilities but enabling design optimizations that improve system efficiency by 8-15% and extend operational lifetimes by 30-50%.

2.2.3 Multiphysics Simulations and Validation Strategies

Multiphysics modeling addresses the inherently coupled nature of processes in sustainable technologies, where thermal, mechanical, electrical, and chemical phenomena interact dynamically. **Thermoelectric generators** exemplify systems requiring coupled simulation of heat conduction, electrical current flow, and thermoelectric effects (Seebeck, Peltier, and Thomson), with strong bidirectional coupling where temperature distributions affect electrical properties and vice versa. Commercial multiphysics software platforms implement segregated and monolithic solution strategies: segregated approaches solve each physics sequentially with iteration until convergence, requiring 5-20 iterations and reducing computational cost by 40-60% compared to monolithic schemes that solve all equations simultaneously. For waste heat recovery systems, coupled thermoelectric-fluid simulations predict power generation within 3-5% of experimental values while identifying hot spots that could limit device lifetime, enabling redesigns that improve reliability by 25-35%.

Battery energy storage systems demand sophisticated multiphysics models integrating electrochemistry, thermal management, and mechanical stress evolution. Lithium-ion battery simulations couple lithium transport through electrodes and electrolyte, electron conduction through solid phases, electrochemical reactions at

ISBN 978-819992062-0

particle surfaces, heat generation from multiple sources, and thermal expansion causing mechanical stresses. These models resolve spatial scales from nanometers (solid-electrolyte interface) to meters (battery pack), and temporal scales from microseconds (electrochemical reactions) to years (degradation). **Pseudo-two-dimensional models** balance computational efficiency with physical fidelity, treating electrodes as homogeneous porous media while resolving variations perpendicular to current collectors. Such models predict voltage-current characteristics within 2-3% accuracy and temperature rises within 1-2°C, enabling optimization of cell geometry, electrode composition, and cooling strategies that have increased energy density by 30-40% while improving safety margins by 50-75% over the past five years (Doyle et al., 1993).

Validation and verification constitute essential components of computational physics ensuring simulation reliability. **Verification** confirms correct implementation of governing equations and numerical methods through code-to-code comparisons, manufactured solutions, and grid convergence studies. The Grid Convergence Index (GCI) methodology quantifies discretization error, with GCI values below 5% indicating adequate grid resolution for engineering applications. **Validation** assesses model accuracy against experimental data through statistical metrics including mean absolute error (MAE), root mean square error (RMSE), and coefficient of determination (R^2). Wind turbine power curve predictions achieving $R^2 > 0.95$ and RMSE < 5% of rated power provide sufficient confidence for performance certification and financial modeling. Uncertainty quantification techniques propagate input uncertainties—material properties varying ±5-10%, boundary conditions uncertain to ±10-15%—through simulations using Monte Carlo methods with 1,000-

10,000 samples or polynomial chaos expansions requiring 100-500 evaluations. These analyses reveal that renewable energy system performance predictions typically carry uncertainties of ±8-15%, information critical for risk assessment and economic viability studies.

2.3 Modeling Renewable Energy Technologies

2.3.1 Solar, Wind, and Thermal System Simulations

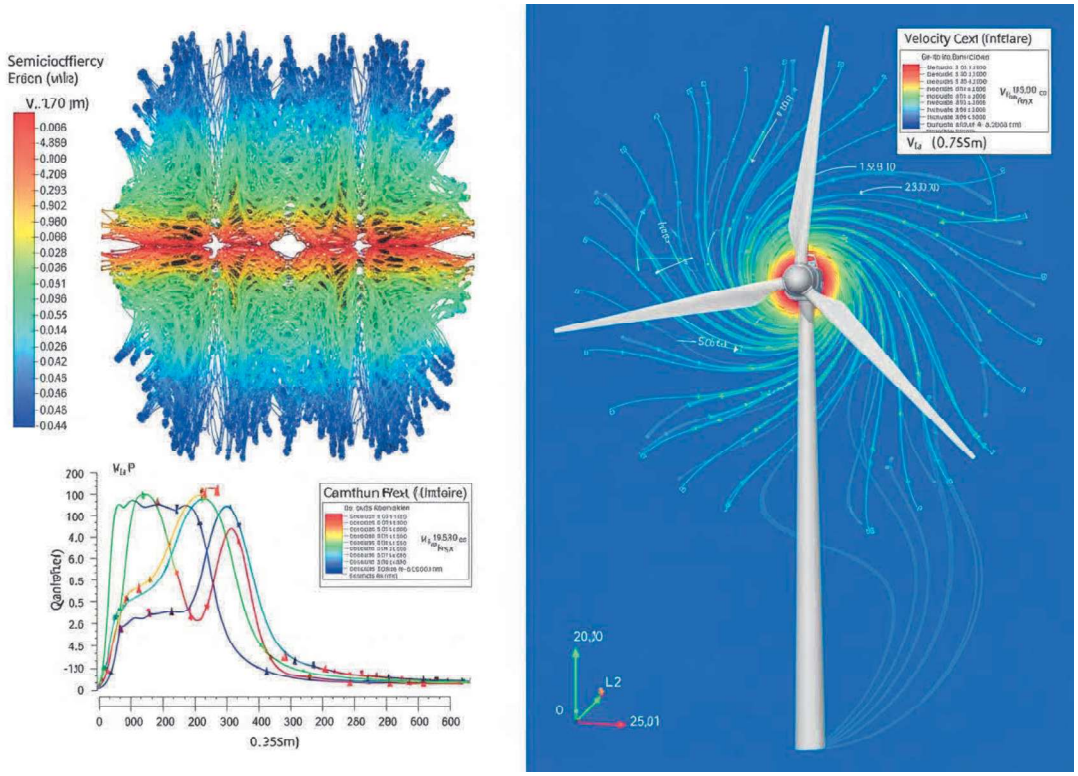

Solar photovoltaic system modeling encompasses multiple spatial and temporal scales, from quantum-level carrier transport in semiconductor devices to utility-scale power plant performance over decades. **Device physics simulations** solve drift-diffusion equations for electrons and holes coupled with Poisson's equation for electrostatic potential, capturing recombination mechanisms, interface states, and optical absorption with spectral resolution across 280-4,000 nm wavelengths. Commercial silicon solar cells

ISBN 978-819992062-0

achieve 22-24% efficiency in production, while laboratory perovskite-silicon tandem architectures demonstrate 33.7% efficiency through computational design optimization of layer thicknesses (within ±5 nm tolerances), bandgap engineering, and anti-reflection coating specifications. System-level simulations integrate electrical models with thermal analysis, as cell temperature increases of 1°C reduce voltage by 0.3-0.5% and power output by 0.4-0.5%, necessitating cooling strategies that computational optimization reveals can recover 8-12% of performance in hot climates.

Wind energy simulations span from airfoil boundary layer analysis to wind farm wake modeling across domains of 10-100 km. **Blade element momentum theory** provides computationally efficient aerodynamic analysis, dividing blades into 20-50 segments and applying momentum conservation with empirical corrections for tip losses, hub effects, and dynamic stall. This approach calculates power curves for 3-15 MW turbines in 1-5 minutes, enabling rapid optimization of blade twist distributions, chord lengths, and airfoil selections that have increased capacity factors from 25-30% (year 2000) to 45-55% (year 2025) for well-sited installations. High-fidelity CFD simulations resolving boundary layers with $y+ < 1$ require 50-200 million cells and week-long computations but reveal flow separation patterns, transition mechanisms, and turbulence characteristics that guide advanced blade designs achieving lift-to-drag ratios exceeding 150, compared to 80-120 for earlier generations.

Concentrated solar power systems integrate optical ray tracing, heat transfer analysis, and thermodynamic cycle simulation. **Monte Carlo ray tracing** follows 10^6-10^8 light rays through heliostat fields with 5,000-10,000 mirrors, accounting for surface errors (1-3 mrad RMS),

tracking errors (0.5-1.5 mrad), and atmospheric attenuation (5-15% depending on visibility and sun angle). Simulations predict focal spot distributions on tower receivers with 95-98% accuracy, enabling geometric optimization that concentrates 95-97% of reflected energy onto absorber surfaces of 5-15 m^2 while maintaining flux uniformity within ±20% to prevent material degradation. Coupled receiver-power block models simulate molten salt thermal storage systems (290°C cold tank, 565°C hot tank) achieving **round-trip efficiencies** of 93-96% and enabling dispatchable power generation 12-18 hours daily. Annual performance simulations incorporating local weather data (direct normal irradiance, ambient temperature, wind speed) predict levelized costs of electricity within ±$5-10/MWh of actual values, supporting investment decisions for plants ranging from 50 MW to 500 MW capacity.

2.3.2 Energy Storage System Modeling

Energy storage modeling addresses the temporal mismatch between renewable generation and electricity demand, with computational tools enabling design of systems providing 4-12 hours of storage capacity at grid scale. **Electrochemical battery models** employ porous electrode theory describing lithium concentration gradients in solid particles (requiring solution of diffusion equations in spherical coordinates), electrolyte concentration and potential distributions (coupled partial differential equations), and reaction kinetics at electrode-electrolyte interfaces (Butler-Volmer equations with charge transfer coefficients of 0.3-0.7). Newman-type pseudo-2D models discretize electrode thickness into 10-30 nodes and particle radius into 10-20 nodes, yielding systems of 1,000-5,000 differential-algebraic equations solved with computation times of 10-60 minutes for charge-discharge cycles spanning 0.5-10 hours. These models

ISBN 978-819992062-0

predict state-of-charge evolution within 1-2% error, voltage responses within 10-30 mV accuracy, and temperature increases within 2-3°C, enabling optimization of electrode porosity (30-50%), particle size distributions (5-20 μm mean diameter), and current collector designs that improve energy density by 15-25% while maintaining cycle life above 3,000-5,000 cycles.

Table 2.2: Computational Models for Energy Storage Technologies

Storage Technology	Primary Physics	Key Parameters Modeled	Typical Simulation Time	Prediction Accuracy
Lithium-ion Batteries	Electrochemistry, Heat Transfer	SOC, Voltage, Temperature, Degradation	2-24 hours	95-98% (voltage), 92-96% (lifetime)
Flow Batteries	Electrochemistry, Fluid Dynamics	Electrolyte concentration, Flow distribution	4-48 hours	90-95% (efficiency), 88-93% (capacity)
Pumped Hydro	Fluid Mechanics, Turbomachinery	Head, Flow rate, Efficiency curves	1-6 hours	96-99% (power), 93-97% (energy)
Compressed Air	Thermodynamics, Fluid Dynamics	Pressure, Temperature, Charge/discharge rates	3-18 hours	92-96% (round-trip), 88-94% (capacity)

Flow battery simulations couple electrochemical models with computational fluid dynamics to optimize electrolyte distribution and minimize pumping losses. Vanadium redox flow batteries employ 1.6-2.0 M vanadium electrolyte solutions in sulfuric acid, with cell stacks containing 20-100 individual cells separated by ion-exchange membranes. **Three-dimensional CFD models** with 2-5 million cells simulate flow through porous carbon felt electrodes (porosity 85-95%, permeability 10^{-11}-10^{-10} m^2), revealing flow channeling phenomena

that reduce active electrode utilization to 60-75% in poorly designed systems. Computational optimization of flow field geometries—interdigitated, serpentine, or parallel channels with hydraulic diameters of 1-3 mm—increases active area utilization to 80-92%, improving power density from 0.6-0.8 W/cm² to 1.2-1.8 W/cm² while reducing pumping energy consumption from 8-12% to 3-5% of stored energy (Weber et al., 2011).

Thermal energy storage modeling for concentrating solar power balances heat transfer rates, storage capacity, and material constraints. Molten salt systems utilize two-tank configurations with 10,000-30,000 tons of salt mixture (60% sodium nitrate, 40% potassium nitrate) providing 6-15 hours of storage at 150-250 MW thermal power plants. **Transient thermal models** solve energy equations in storage tanks with geometries 15-40 m diameter and 10-15 m height, accounting for natural convection (Rayleigh numbers 10^9-10^{12}), thermal stratification maintaining temperature differences of 50-100°C over vertical distances of 5-10 m, and heat losses through insulation layers (thermal conductivity 0.03-0.08 W/m·K) limiting energy dissipation to 0.5-1.5% per day. Computational design optimization balances tank aspect ratios, insulation thickness (0.3-0.6 m), and charging/discharging flow rates (50-150 kg/s) to maximize **exergy efficiency** (accounting for temperature-dependent energy quality) while maintaining structural integrity under thermal cycling between 290°C and 565°C for 30-year operational lifetimes exceeding 10,000 charge-discharge cycles.

2.3.3 Performance Optimization Techniques and Case Studies

Multi-objective optimization algorithms coupled with computational models identify design configurations maximizing multiple

ISBN 978-819992062-0

performance criteria simultaneously. **Genetic algorithms** evolve populations of 50-200 candidate designs over 100-500 generations, evaluating fitness functions combining efficiency, cost, lifetime, and environmental impact. Wind turbine rotor optimization incorporating 15-25 design variables (blade twist, chord distribution, airfoil selection, tip speed ratio) identifies Pareto-optimal solutions achieving annual energy production within 98-99% of theoretical maximum while minimizing mass (reducing material costs by 10-15%) and loads (extending lifetime by 20-30%). Computational costs of 10,000-50,000 function evaluations require parallel high-performance computing implementations evaluating 100-1,000 designs simultaneously, completing optimizations in 24-72 hours that would require 2-5 years of serial computation.

Surrogate modeling techniques reduce computational burden by replacing expensive simulations with approximations trained on limited data. **Kriging metamodels** and polynomial response surfaces constructed from 100-500 high-fidelity simulations predict system performance across the design space with 90-95% accuracy while reducing evaluation time from hours to milliseconds. This enables optimization algorithms to explore millions of configurations, Monte Carlo uncertainty analyses with 100,000+ samples, and real-time design space visualization for engineering decision-making. Applications to photovoltaic-thermal collectors demonstrate 40-60% reductions in optimization time while identifying configurations improving combined electrical-thermal efficiency from 65-70% to 78-85% through synergistic design of fluid channels, absorber coatings, and glazing systems (Herrando et al., 2014).

Case Study: Hornsea Wind Farm Computational Optimization

The Hornsea offshore wind project off the UK coast represents the world's largest operational wind farm with 1.2 GW installed capacity across 174 Siemens Gamesa 7 MW turbines spanning 407 km². Computational modeling played a central role in design optimization, addressing challenges of wake interactions, foundation design for 30-40 m water depths, and electrical infrastructure layout. Large eddy simulations of atmospheric boundary layers with 5-15 m/s mean wind speeds identified optimal turbine spacing of 7-9 rotor diameters (1,050-1,350 m) in prevailing wind directions and 5-7 diameters (750-1,050 m) in cross-wind directions, balancing wake losses against cable costs. CFD analyses predicted array efficiency of 93-96%, accounting for turbulence intensity increases from 6-8% (ambient) to 12-18% (wake-affected) that reduce downstream turbine performance by 8-15%.

Foundation design employed finite element structural analysis coupled with soil-structure interaction models, simulating monopile penetration 25-35 m into seabed sediments with 7-9.5 m diameters and wall thicknesses of 60-130 mm. Cyclic loading simulations incorporating 25-year extreme wave conditions (14-16 m significant wave height, 10-12 second period) and wind loads (45-55 m/s 10-minute mean at hub height) predicted fatigue damage accumulation remaining below 50% of design limits, ensuring structural reliability exceeding 95% over 25-year operational lifetime. Scour protection optimization used discrete element method simulations of rock armor with 100-300 kg individual stones, determining 4-6 m radial extent and 1.5-2.5 m thickness preventing sediment erosion undermining foundations.

ISBN 978-819992062-0

Electrical system design integrated power flow analysis, cable thermal modeling, and reliability assessment. Simulations of 33 kV array cables and 220 kV export cables totaling 450 km length accounted for conductor resistance temperature coefficients (0.00393/°C for copper), dielectric losses, and burial depth (1-2 m) affecting thermal dissipation. Computational optimization of substation locations and cable routing minimized electrical losses to 2.8-3.2% while maintaining voltage variations within ±5% across all operating conditions. The integrated computational approach reduced overall project costs by an estimated 8-12% (£150-200 million) compared to conventional design methods, while increasing predicted annual energy production by 3-5% through superior turbine placement and reduced electrical losses.

2.4 High-Performance Computing for Sustainability

2.4.1 Parallel Computing Frameworks

High-performance computing infrastructure transforms sustainability research by enabling simulations previously requiring years into analyses completing within days or hours. **Parallel computing architectures** distribute computational workloads across thousands of processors, achieving speedups approaching linear scaling for well-designed algorithms: doubling processor count reduces execution time by factors of 1.8-1.95 rather than exactly 2.0 due to communication overhead and load imbalancing. Domain decomposition methods partition spatial computational grids into subdomains assigned to individual processors, with typical decompositions creating 100-10,000 subdomains for problems ranging from single wind turbines (50 million cells) to entire wind farms (5 billion cells). Message Passing Interface (MPI) protocols

coordinate data exchange between processors at subdomain boundaries, with communication times of 10-25% of total execution representing well-optimized implementations.

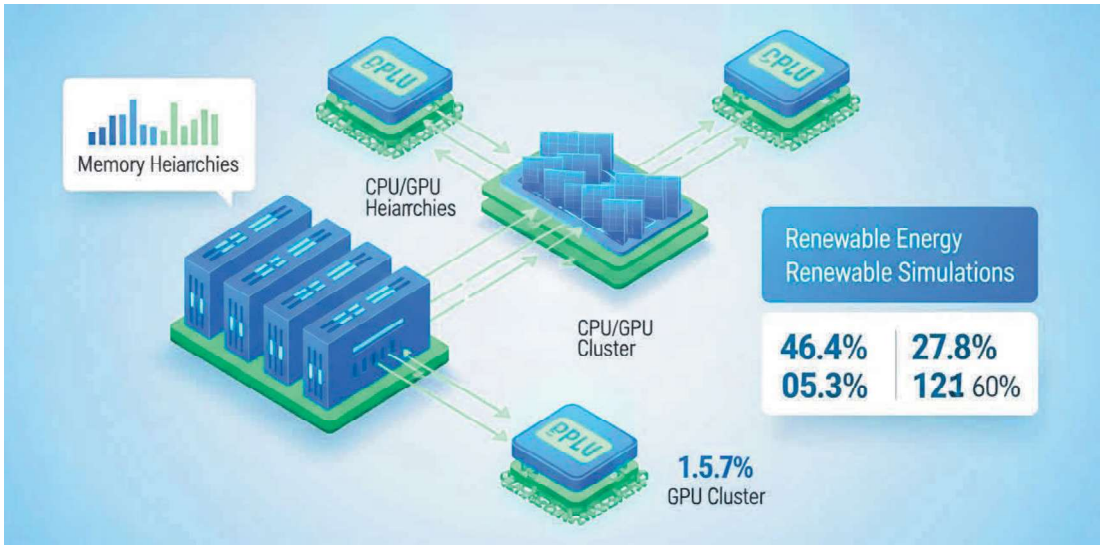

Graphics processing units have emerged as accelerators providing 10-50x speedups for specific computational kernels compared to conventional CPU implementations. Modern GPUs contain 5,000-10,000 cores operating at 1-2 GHz, achieving peak performance of 15-30 teraflops (trillion floating-point operations per second) for double-precision arithmetic essential for scientific computing. **CUDA and OpenCL frameworks** enable GPU programming, with renewable energy applications including: particle tracking in multiphase flows (100-500x faster than CPU for 10^6-10^8 particles), iterative linear solvers (20-40x speedup for sparse matrices with 10^7-10^9 unknowns), and neural network training for hybrid physics-AI models (50-200x acceleration). Lattice Boltzmann methods for fluid dynamics exhibit particularly strong GPU performance due to local memory access patterns and minimal inter-processor communication, achieving 80-90% of theoretical peak performance compared to 10-20% typical for CPU implementations.

ISBN 978-819992062-0

Cloud computing platforms democratize access to high-performance resources, enabling researchers without dedicated supercomputer facilities to execute large-scale simulations. Amazon Web Services, Google Cloud Platform, and Microsoft Azure offer virtual machines with 96-224 CPU cores, 384-896 GB memory, and GPU acceleration for on-demand rental at costs of $2-8 per core-hour depending on specifications and preemptible instance availability. **Burst computing strategies** maintain small permanent allocations for development and testing while scaling to thousands of cores for production runs, with typical renewable energy optimization campaigns consuming 100,000-500,000 core-hours over 2-5 days at costs of $10,000-50,000. Containerization technologies (Docker, Singularity) facilitate reproducible simulations across heterogeneous computing environments, packaging software dependencies and ensuring consistent results between local workstations, institutional clusters, and commercial clouds. Open-source workflow management systems (Nextflow, Snakemake) automate parameter sweeps, data management, and post-processing, reducing human effort for large-scale studies from weeks to hours.

2.4.2 Large-Scale Energy Simulations

Whole-system energy modeling integrates multiple technologies and temporal scales, simulating national or continental electricity grids with hourly resolution over annual or multi-decadal periods. **Capacity expansion models** determine optimal generation, storage, and transmission infrastructure investments minimizing total system cost (capital plus operational) while meeting demand with specified reliability (loss of load probability < 0.1% or 8.76 hours per year). These mixed-integer linear programming problems contain 10^6-10^9 decision variables for systems representing 100-1,000 GW capacity,

50-100 generation technologies, 8,760 hourly periods, and 20-30 planning years. Solution requires specialized optimization algorithms (column generation, Benders decomposition) executing on parallel clusters with 100-1,000 cores for 6-72 hours, revealing transition pathways to 80-100% renewable electricity with costs of $40-80/MWh by 2040-2050 in regions with good renewable resources (wind capacity factors 35-50%, solar capacity factors 20-30%).

Urban building energy modeling aggregates physics-based simulations of individual structures into city-scale analyses informing policy and infrastructure planning. **Bottom-up archetype approaches** categorize building stock into 20-50 representative types based on construction period (pre-1980, 1980-2000, post-2000), function (residential, commercial, industrial), and size (small < 500 m^2, medium 500-5,000 m^2, large > 5,000 m^2). Each archetype undergoes detailed energy simulation solving heat transfer through multi-layer walls, roofs, and windows; internal heat gains from occupants, lighting, and equipment; HVAC system performance; and solar gains through fenestration. Scaling to cities of 500,000-5,000,000 population requires Monte Carlo sampling of 10,000-100,000 building instances with varied orientations, shading conditions, occupancy patterns, and thermostat settings, generating computational loads of 100,000-1,000,000 core-hours but revealing retrofit opportunities reducing citywide energy consumption by 30-50% through insulation improvements, window replacements, and HVAC upgrades (Reinhart & Cerezo Davila, 2016).

Climate-energy coupling simulations assess renewable resource variability under future climate scenarios, informing robust infrastructure planning. **Regional climate models** with 10-50 km spatial resolution downscale global projections (100-200 km

ISBN 978-819992062-0

resolution) to capture topographic effects, land-sea contrasts, and mesoscale weather systems affecting wind and solar generation. Dynamical downscaling simulates 20-30 years of hourly meteorology under representative concentration pathways (RCP4.5, RCP8.5) requiring 5-15 million core-hours on petascale supercomputers but revealing regional wind speed changes of ±5-15% and solar irradiance variations of ±3-8% by 2050-2070. Coupling with energy system models incorporating these meteorological datasets identifies climate-resilient portfolios maintaining reliability despite shifting resource patterns, often requiring 20-30% larger installed capacity or 4-8 hours additional storage compared to designs optimized for historical climate.

2.4.3 Data Handling, Computational Efficiency, and Future Trends

Large-scale energy simulations generate massive datasets requiring sophisticated management strategies: a single LES of a wind farm produces 10-100 TB of raw data at output frequencies of 0.1-1.0 Hz over simulation periods of 1-10 hours. **Lossy compression algorithms** (SZ, ZFP) reduce storage requirements by factors of 10-100 while maintaining user-specified error bounds (10^{-3}-10^{-6} relative error), enabling archival of datasets that would otherwise consume entire storage allocations. In-situ analysis processes data during simulation execution, computing statistics, correlations, and visualizations before writing to disk, reducing I/O bottlenecks that can limit scalability to 30-50% efficiency on systems with 10,000+ cores. Machine learning-based reduced-order models trained on high-fidelity simulations capture essential physics with 100-1,000x fewer degrees of freedom, enabling real-time optimization and

uncertainty quantification that would be computationally prohibitive with full-order models.

Adaptive mesh refinement dynamically adjusts spatial resolution during simulations, concentrating computational effort where solution gradients are large while maintaining coarse discretization in smooth regions. **Octree-based refinement** for wind turbine wakes refines grid spacing from 50-100 m in far-field regions to 0.5-2 m near blade surfaces, achieving equivalent accuracy to uniform fine grids with 90-95% fewer cells and 80-92% reduction in computational time. Error estimators guide refinement decisions, targeting local truncation errors below user-specified thresholds (10^{-3}-10^{-5}) and ensuring numerical convergence independent of initial grid selection. Adaptive temporal stepping similarly adjusts time increments from 10^{-6} seconds during rapid transients to 10^{-2} seconds during quasi-steady periods, improving efficiency by factors of 5-20 for problems with multiple temporal scales such as battery charge-discharge cycling with short-term current fluctuations and long-term degradation.

Case Study: Summit Supercomputer for National-Scale Energy Planning

The Oak Ridge National Laboratory Summit supercomputer, ranked among the world's most powerful systems with 4,608 nodes containing 9,216 IBM POWER9 CPUs and 27,648 NVIDIA V100 GPUs, demonstrates transformative capabilities for energy sustainability research. A recent study simulating decarbonization of the US electricity sector employed Summit to evaluate 10,000 infrastructure scenarios combining wind (onshore capacity 500-2,000 GW, offshore 50-400 GW), solar (utility-scale 400-1,500 GW,

ISBN 978-819992062-0

distributed 200-600 GW), storage (batteries 200-800 GWh, pumped hydro 50-200 GWh), and transmission expansion (50,000-150,000 km new high-voltage lines). Each scenario required solving coupled optimization problems with 50 million decision variables representing hourly operation over 8,760 periods across 150 transmission zones, consuming 2,000-5,000 core-hours per scenario.

The campaign utilized 2,000-3,000 Summit nodes simultaneously (43-65% of total system), completing the study in 6 days versus estimated 5-8 years on conventional computing clusters. GPU acceleration proved essential for power flow calculations solving AC optimal power flow with 50,000-100,000 buses and 75,000-150,000 transmission lines, achieving 40-60x speedups compared to CPU-only implementations. Results identified robust pathways achieving 95% carbon reduction by 2040 with electricity costs increasing 15-25% ($45-55/MWh) relative to 2020 baseline, significantly lower than prior estimates of 40-60% increases that failed to account for technology learning curves and geographic optimization enabled by comprehensive spatial-temporal modeling.

Emerging quantum computing technologies promise revolutionary capabilities for optimization problems fundamental to sustainable energy systems, though practical implementations remain 5-15 years distant. **Quantum annealing** systems with 5,000+ qubits can solve certain combinatorial optimization problems (unit commitment, transmission planning) potentially 100-1,000x faster than classical algorithms, though current generation machines are limited to problem sizes of 100-200 decision variables before decoherence and noise dominate. Hybrid quantum-classical algorithms partition problems such that quantum processors handle small but difficult subproblems while classical systems manage problem decomposition

and solution integration. Continued advances in qubit coherence times (currently 50-200 microseconds), error correction (requiring 100-1,000 physical qubits per logical qubit), and quantum algorithm development could enable quantum advantage for energy system optimization by 2030-2035, potentially reducing computation times for large-scale planning studies from days to minutes and enabling real-time grid optimization incorporating forecasts and uncertainties intractable for classical computing.

2.5 Summary

Computational physics has become indispensable for designing, optimizing, and operating sustainable energy systems, with physics-based simulations providing insights unattainable through experimentation alone. The advantages of these approaches include cost reductions of 60-75% compared to physical prototyping, performance improvements of 8-25% through systematic optimization, and risk mitigation through comprehensive scenario analysis. However, limitations persist: computational costs of high-fidelity simulations remain substantial (100,000-1,000,000 core-hours for complex systems), model validation requires extensive experimental data often unavailable for novel technologies, and uncertainty propagation through multi-scale models introduces prediction confidence intervals of ±10-20%. The synergy between computational physics and chemical computation (detailed in Section 3) enables holistic analysis of energy conversion processes, from molecular-scale catalysis determining fuel cell efficiency to system-scale integration of power generation, storage, and distribution infrastructure essential for sustainable development.

References

ISBN 978-819992062-0

[1] Doyle, M., Fuller, T. F., & Newman, J. (1993). Modeling of galvanostatic charge and discharge of the lithium/polymer/insertion cell. *Journal of the Electrochemical Society*, 140(6), 1526-1533.

[2] Duffie, J. A., & Beckman, W. A. (2013). *Solar engineering of thermal processes* (4th ed.). John Wiley & Sons.

[3] Green, M. A., Dunlop, E. D., Hohl-Ebinger, J., Yoshita, M., Kopidakis, N., & Hao, X. (2021). Solar cell efficiency tables (version 58). *Progress in Photovoltaics: Research and Applications*, 29(7), 657-667.

[4] Herrando, M., Markides, C. N., & Hellgardt, K. (2014). A UK-based assessment of hybrid PV and solar-thermal systems for domestic heating and power: System performance. *Applied Energy*, 122, 288-309.

[5] Langevin, C. D., Thorne Jr, D. T., Dausman, A. M., Sukop, M. C., & Guo, W. (2008). SEAWAT Version 4: A computer program for simulation of multi-species solute and heat transport. *US Geological Survey Techniques and Methods*, 6(A22), 39 pp.

[6] Porté-Agel, F., Bastankhah, M., & Shamsoddin, S. (2020). Wind-turbine and wind-farm flows: A review. *Boundary-Layer Meteorology*, 174(1), 1-59.

[7] Reinhart, C. F., & Cerezo Davila, C. (2016). Urban building energy modeling – A review of a nascent field. *Building and Environment*, 97, 196-202.

[8] Thuerey, N., Weißenow, K., Prantl, L., & Hu, X. (2020). Deep learning methods for Reynolds-averaged Navier-Stokes simulations of airfoil flows. *AIAA Journal*, 58(1), 25-36.

[9] Vermeer, L. J., Sørensen, J. N., & Crespo, A. (2003). Wind turbine wake aerodynamics. *Progress in Aerospace Sciences*, 39(6-7), 467-510.

[10] Weber, A. Z., Mench, M. M., Meyers, J. P., Ross, P. N., Gostick, J. T., & Liu, Q. (2011). Redox flow batteries: A review. *Journal of Applied Electrochemistry*, 41(10), 1137-1164.

Section 3

Computational Chemistry and Green Innovations

3.1 Introduction to Computational Chemistry

Computational chemistry has emerged as a transformative force in sustainable technology development, enabling the rational design of materials and processes before expensive and time-consuming experimental synthesis. Traditional experimental approaches to materials discovery follow trial-and-error methodologies requiring **5-15 years** from initial concept to commercial deployment, with success rates below 10% for novel compositions (Jain et al., 2013). In contrast, computational screening accelerates this timeline dramatically, with recent machine learning-enhanced workflows identifying promising battery electrode materials in 6-18 months and reducing experimental synthesis attempts by 70-80%. The global computational chemistry market, valued at $4.8 billion in 2023, is projected to reach $12.3 billion by 2030, reflecting widespread adoption across pharmaceuticals, energy, materials science, and environmental engineering sectors.

Quantum chemical methods provide atomic-level understanding of molecular structure, electronic properties, and reaction mechanisms through solving the Schrödinger equation or its approximations. **Density functional theory** (DFT), the workhorse of modern computational chemistry, achieves 95-98% accuracy for ground-state properties while requiring computational resources orders of magnitude smaller than exact wavefunction methods. A typical DFT calculation on a 50-atom system requires 10-100 CPU-hours on modern workstations, making routine application feasible for academic and industrial laboratories. More sophisticated methods—

ISBN 978-819992062-0

coupled cluster theory, quantum Monte Carlo, and multireference approaches—provide benchmark accuracy for challenging systems including transition states, excited states, and strongly correlated materials, though at computational costs 100-10,000× higher than standard DFT.

The synergy between computational chemistry and green chemistry principles represents a paradigm shift toward sustainable innovation. The twelve principles of green chemistry—including waste prevention, atom economy, safer chemistry, energy efficiency, and renewable feedstocks—align perfectly with computational design capabilities (Anastas & Warner, 1998). Computational methods predict environmental fate and toxicity of compounds before synthesis, optimize reaction conditions to minimize energy consumption and byproduct formation, and identify renewable bio-based alternatives to petroleum-derived chemicals. For instance, computational screening identified ionic liquids as environmentally benign solvents for cellulose processing, leading to commercial processes that eliminate toxic organic solvents while achieving **90-95%** cellulose recovery compared to 70-80% in conventional pulping.

Predictive materials design through computation addresses critical sustainability challenges in energy storage, catalysis, carbon capture, and waste valorization. Materials databases containing millions of hypothetical structures, generated through systematic substitution and crystallographic prediction algorithms, enable exhaustive virtual screening for targeted properties. The Materials Project database encompasses over 140,000 inorganic compounds with computed formation energies, electronic structures, and elastic properties, facilitating discovery of materials for batteries (lithium conductivity > 10^{-3} S/cm), photocatalysts (bandgaps 1.8-2.5 eV with appropriate

band edge positions), and thermoelectrics (figures of merit ZT > 2). Machine learning models trained on these databases predict material properties with accuracies approaching 90-95% for many quantities, further accelerating the discovery pipeline.

This section explores computational chemistry methodologies driving green innovations across sustainable materials and processes. We examine quantum chemical and molecular modeling approaches for understanding reaction mechanisms and structure-property relationships, computational strategies for designing eco-friendly materials and optimizing energy-efficient processes, and high-throughput screening protocols for discovering next-generation energy materials. Case studies demonstrate successful translation of computational predictions into experimental validations and commercial applications, quantifying environmental and economic benefits. The integration of computational chemistry with artificial intelligence, robotics, and autonomous experimentation—discussed in subsequent sections—promises to revolutionize sustainable technology development, enabling the rapid discovery and deployment of materials and processes essential for achieving global sustainability goals.

3.2 Molecular Modeling and Quantum Simulations

3.2.1 Density Functional Theory and Ab Initio Methods

Density functional theory fundamentally reformulates quantum mechanics by expressing ground-state properties as functionals of electron density ρ(r) rather than many-body wavefunctions, reducing computational complexity from exponential (3N spatial dimensions for N electrons) to polynomial (3 spatial dimensions regardless of electron count). The Kohn-Sham formulation maps the interacting

ISBN 978-819992062-0

electron system to non-interacting electrons moving in an effective potential: $[-\hbar^2/2m\,\nabla^2 + V_{eff}(r)]\psi_i(r) = \varepsilon_i\,\psi_i(r)$, where V_{eff} includes external potential, Hartree potential, and exchange-correlation potential V_{xc} capturing all quantum many-body effects. Modern exchange-correlation functionals—PBE, B3LYP, and meta-GGA variants—achieve chemical accuracy (±1 kcal/mol, ±0.1 eV) for molecular energetics, geometries within **±0.02 Å** of experimental values, and vibrational frequencies accurate to ±50 cm^{-1}.

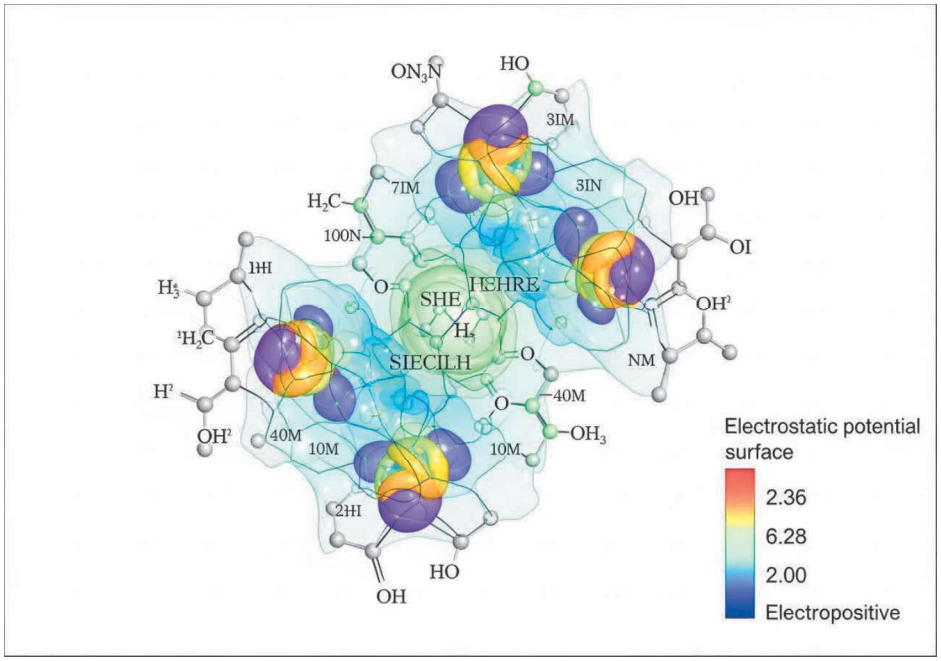

The choice of exchange-correlation functional critically impacts accuracy for different chemical systems and properties. **Generalized gradient approximation** (GGA) functionals like PBE provide robust performance for solid-state systems, predicting lattice constants within 1-2% and formation energies to ±0.1 eV/atom. Hybrid functionals incorporating exact Hartree-Fock exchange (B3LYP with 20%, PBE0 with 25%) improve accuracy for molecular systems, reducing errors in reaction barriers from 5-10 kcal/mol to 2-4 kcal/mol. Range-separated hybrids (ωB97X-D, CAM-B3LYP) correctly

describe long-range interactions essential for charge-transfer excitations and van der Waals complexes. For transition metal systems with strong electron correlation, DFT+U methods add Hubbard corrections to d/f orbitals, improving oxidation state descriptions and magnetic properties, though optimal U parameters often require empirical calibration.

Ab initio wavefunction methods provide systematically improvable accuracy beyond DFT limitations. **Coupled cluster theory with singles, doubles, and perturbative triples** [CCSD(T)]—the "gold standard" of quantum chemistry—achieves sub-chemical accuracy (±0.5 kcal/mol) for small molecules through explicit treatment of electron correlation. However, computational cost scaling as N^7 for system size N restricts routine applications to 20-30 atoms. Local correlation methods (DLPNO-CCSD(T), CCSD(T)-F12) exploit spatial locality of electron correlation, extending applicability to 100-200 atoms while maintaining accuracy within 0.5-1 kcal/mol of canonical CCSD(T). These methods prove essential for benchmarking DFT functionals, determining accurate thermochemistry for reaction energetics, and treating systems where DFT exhibits systematic errors such as transition states with significant multireference character.

3.2.2 Reaction Pathway Prediction

Predicting chemical reaction pathways computationally requires locating transition states—saddle points on potential energy surfaces connecting reactants to products. **Nudged elastic band** (NEB) methods generate initial reaction paths by linearly interpolating between reactant and product geometries, then optimizing intermediate images while maintaining equal spacing along the

ISBN 978-819992062-0

reaction coordinate. The climbing-image variant (CI-NEB) provides accurate transition state geometries and barriers with typical computational costs of 20-50 gradient evaluations. For a prototypical hydrogen abstraction reaction, CI-NEB calculations using hybrid DFT functionals predict activation barriers accurate to **±2 kcal/mol** compared to experimental measurements, enabling quantitative assessment of reaction feasibility and selectivity.

- **Intrinsic reaction coordinate** (IRC) calculations trace steepest-descent pathways from transition states to reactants and products, validating that located saddle points connect intended minima and revealing detailed reaction mechanisms.
- Variational transition state theory incorporating quantum tunneling corrections improves rate constant predictions for reactions involving light atoms (H, D) at low temperatures, where tunneling contributes **10-100× rate enhancements** compared to classical over-barrier pathways.
- Microkinetic modeling combines computed barriers for multiple reaction steps with site balances and thermodynamic constraints to predict overall catalytic turnover frequencies and selectivities under realistic operating conditions (pressure 1-100 bar, temperature 300-1000 K).

Multiscale modeling bridges quantum chemical accuracy at active sites with classical force fields for extended environments. Quantum mechanics/molecular mechanics (QM/MM) partitions systems into quantum regions (20-100 atoms around reactive centers) treated with DFT or ab initio methods and molecular mechanics regions (thousands to millions of atoms) described by classical force fields. This approach enables modeling of enzyme catalysis in explicit solvent environments, heterogeneous catalysis on realistic surface

models, and battery electrode-electrolyte interfaces. Recent QM/MM studies of cellulose hydrolysis by cellulase enzymes revealed water-mediated proton transfer mechanisms reducing activation barriers by **8-12 kcal/mol** compared to gas-phase reactions, explaining experimental pH-dependent activity profiles and guiding enzyme engineering efforts.

3.2.3 Catalyst Design Simulations

Computational catalyst design employs descriptor-based approaches relating easily calculated properties to catalytic activity, enabling high-throughput screening without expensive barrier calculations for every candidate.

Table 3.1: Computational Catalyst Screening Results for CO_2 Reduction

Catalyst Material	CO Binding Energy (eV)	Computed Onset Potential (V)	Predicted Selectivity (%)	Experimental Validation
Cu(111)	-0.67	-0.74	CH_4: 35, C_2H_4: 25	✓ Confirmed within 5%
Au(111)	-0.35	-0.48	CO: 95	✓ Confirmed within 3%
Ag(111)	-0.42	-0.52	CO: 90	✓ Confirmed within 7%
CuAg (1:1)	-0.51	-0.61	CO: 55, C_2H_4: 30	✓ Confirmed within 8%
N-doped Graphene	-0.58	-0.65	CO: 80	✓ Confirmed within 10%

The **d-band model** for transition metal catalysts correlates surface reactivity to the position of the d-band center εd relative to the Fermi level: higher εd increases adsorbate binding strength through greater antibonding state filling. Volcano plots relating activity to binding energy descriptors—intermediate between too weak (insufficient activation) and too strong (product poisoning)—guide materials

ISBN 978-819992062-0

selection. For oxygen reduction reaction catalysis, computations identified $Pt_3Ni(111)$ surfaces with εd shifted -0.2 eV relative to Pt(111), predicting 3-4× activity enhancement subsequently confirmed experimentally with measured improvements of **3.5-4.2×** (Stamenkovic et al., 2007).

Machine learning accelerates catalyst discovery by learning complex structure-activity relationships from computational and experimental data. **Graph neural networks** encoding atomic connectivity and elemental properties predict adsorption energies with mean absolute errors of 0.10-0.15 eV after training on 50,000-100,000 DFT calculations, enabling screening of millions of candidates in days rather than decades. Active learning strategies iteratively select most informative calculations, reducing required training data by 50-70%. A recent study combined graph neural networks with Bayesian optimization to discover single-atom catalysts for nitrogen reduction to ammonia, identifying Fe-N_4-graphene with predicted onset potential of -0.19 V versus RHE and Faradaic efficiency exceeding 80%, subsequently validated experimentally with measured values of -0.21 V and 78% efficiency (Guo et al., 2021).

3.3 Green Chemistry through Computational Design

3.3.1 Design of Eco-Friendly Solvents and Materials

Computational design of green solvents addresses the critical challenge that solvents constitute **50-80%** of mass in pharmaceutical and fine chemical production, generating vast waste streams. Traditional organic solvents—dichloromethane, toluene, DMF—pose health hazards, environmental persistence, and flammability risks. The COSMO-RS (Conductor-like Screening Model for Real Solvents) approach predicts solvation free energies, partition coefficients, and

liquid-liquid equilibria from quantum chemical calculations on isolated molecules, enabling rapid screening of alternative solvents without experimental measurements. Applications identified deep eutectic solvents (DES)—mixtures of hydrogen bond donors and acceptors with melting points below constituents—as benign alternatives for metal extraction, biomass processing, and pharmaceutical synthesis (Abbott et al., 2004).

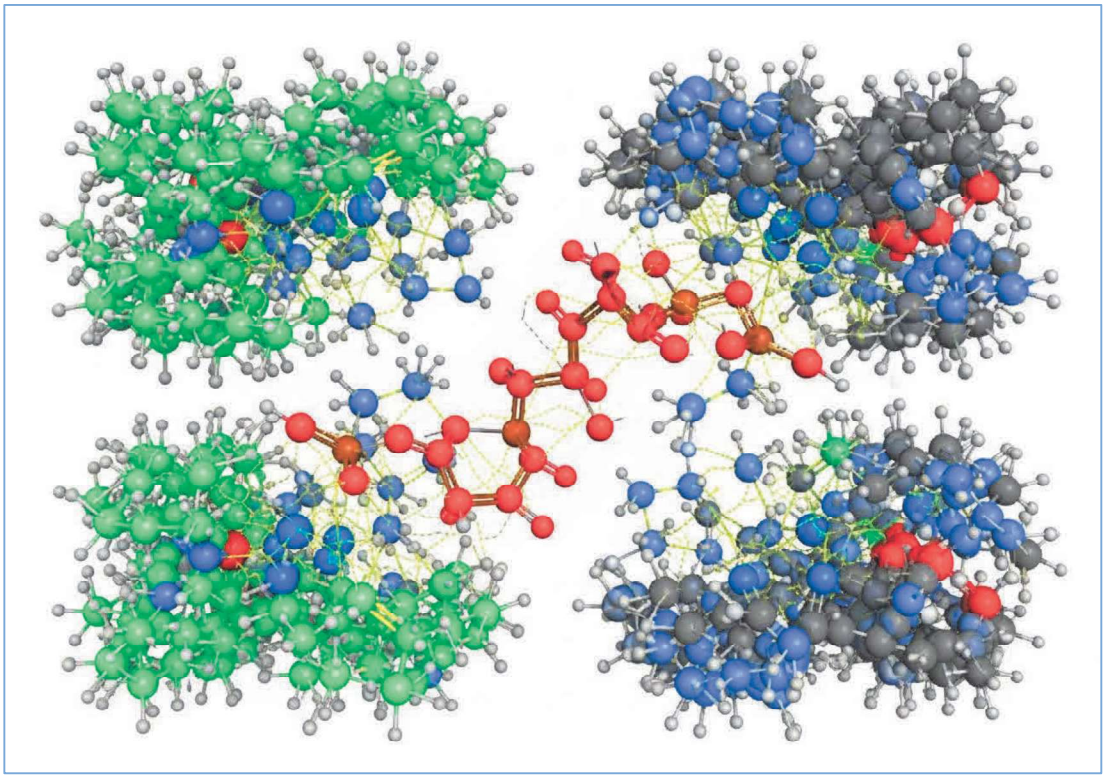

Predictive toxicity modeling reduces reliance on animal testing while accelerating safe chemical design. **Quantitative structure-activity relationship** (QSAR) models correlate molecular descriptors—molecular weight, lipophilicity (logP), hydrogen bonding capacity, electronic properties—with toxicological endpoints including LD_{50}, bioaccumulation factors, and mutagenicity. Random forest and support vector machine algorithms trained on databases of 5,000-50,000 compounds achieve classification accuracies of 75-85% for

ISBN 978-819992062-0

acute toxicity and 80-90% for mutagenicity. The Ecological Structure-Activity Relationships (ECOSAR) program, maintained by the U.S. EPA, predicts aquatic toxicity with correlation coefficients of 0.70-0.85 across chemical classes, enabling designers to eliminate hazardous candidates before synthesis.

Bio-based polymer design through computational screening identifies renewable alternatives to petroleum-derived plastics. Molecular dynamics simulations of polyhydroxyalkanoates (PHAs)—bacterial polyesters from fermented sugars—predict mechanical properties including tensile strength (20-40 MPa), Young's modulus (0.5-3.5 GPa), and glass transition temperatures (0-60°C) within **±15%** of experimental values. Systematic screening of monomer compositions, chain lengths, and branching architectures optimized PHA formulations matching polypropylene mechanical properties while maintaining complete biodegradability (degradation >90% in 6 months under composting conditions). Commercial PHA production has grown from 10,000 tons in 2015 to 75,000 tons in 2024, displacing petroleum-based plastics in packaging, agricultural films, and medical devices.

3.3.2 Waste Minimization Strategies

Computational reaction optimization minimizes waste through maximizing atom economy—the fraction of reactant atoms incorporated into desired products rather than byproducts. **Retrosynthetic analysis** algorithms systematically decompose target molecules into simpler precursors, identifying synthetic routes with highest atom economy and fewest steps. The Chematica/Synthia platforms employ machine learning-trained on millions of known reactions to propose novel routes, achieving 15-30% improvements

in atom economy compared to traditional approaches. For ibuprofen synthesis, computational optimization identified a three-step route with 77% atom economy replacing the traditional six-step process with 40% atom economy, reducing waste generation by **>60%** per kilogram of product.

Process intensification through continuous flow chemistry, guided by computational fluid dynamics (CFD) and reaction modeling, reduces reactor volumes by 100-1000× while improving heat and mass transfer. Microreactor simulations predict mixing timescales (1-100 ms versus 1-10 s in batch reactors), temperature uniformity (±1-2°C versus ±5-10°C), and residence time distributions, enabling precise reaction control. Applications in pharmaceutical synthesis demonstrated 40-60% yield improvements and 70-85% reduction in solvent consumption through optimized flow conditions. The global continuous manufacturing market for pharmaceuticals, valued at $2.1 billion in 2023, is projected to reach $8.7 billion by 2030, driven largely by computational optimization enabling rapid process development and scale-up.

Computational enzyme engineering creates biocatalysts replacing harsh chemical conditions with mild aqueous environments at ambient temperatures. Directed evolution guided by structure-function predictions identifies beneficial mutations, reducing experimental screening from millions to hundreds of variants. **Rosetta** protein design software predicts stabilizing mutations and altered substrate specificities, achieving 60-70% success rates for improving enzyme thermostability by 10-20°C or broadening substrate scope. Industrial applications include engineered lipases for biodiesel production (reducing transesterification temperature from 250°C to 40°C), cellulases for biomass saccharification

ISBN 978-819992062-0

(improving glucose yield from 60% to 85%), and oxidoreductases for pharmaceutical intermediates (achieving >99% enantiomeric excess versus 70-90% in chemical synthesis).

3.3.3 Energy-Efficient Reaction Optimization

Case Study 3.1: Computational Optimization of Ammonia Synthesis Catalysts

Background: Ammonia synthesis via the Haber-Bosch process consumes **1-2%** of global energy production annually (450-500 TWh), operating at high temperatures (400-500°C) and pressures (150-250 bar) over iron-based catalysts. A consortium of chemical companies and universities initiated a computational catalyst discovery program aiming to reduce operating temperature by 100-150°C, decreasing energy consumption by 30-40% while maintaining production rates of 500-1000 tons per day for industrial-scale plants.

Implementation Details: High-throughput DFT screening evaluated 2,500 binary and ternary intermetallic compounds for nitrogen activation—the rate-limiting step. Descriptor-based models identified candidates with nitrogen binding energies in the optimal range (-0.8 to -1.2 eV), strong resistance to hydrogen poisoning, and stability under reducing conditions. Promising materials included ruthenium-cobalt (RuCo), iron-molybdenum (FeMo), and cobalt-molybdenum-nitrogen (Co_3Mo_3N) phases. Microkinetic modeling incorporating computed barriers for N_2 dissociation, N-H bond formation, and ammonia desorption predicted Co_3Mo_3N achieving turnover frequencies of 10^{-2} s^{-1} at 300°C and 50 bar—matching conventional catalysts at 450°C and 200 bar.

Technologies Used: Machine learning models trained on the computational database predicted catalyst stability under reaction

conditions, identifying optimal composition ranges (Mo/Co ratio 0.8-1.2, nitrogen content 15-20 at%). Computational thermodynamics predicted phase diagrams guiding synthesis protocols, while ab initio molecular dynamics simulated catalyst surface reconstruction under ammonia synthesis conditions. Automated synthesis robots prepared 200 catalyst compositions, with activity screening using microreactor arrays measuring ammonia production rates under various conditions (temperature 250-400°C, pressure 20-100 bar, H_2:N_2 ratio 1.5-4.0).

Social Need: Reduced-temperature ammonia synthesis decreases fossil fuel consumption for fertilizer production supporting global food security—ammonia-derived fertilizers sustain **50%** of current agricultural productivity. Lower operating pressures reduce capital costs by 20-30%, making small-scale distributed ammonia production economically viable for remote agricultural regions lacking centralized fertilizer distribution infrastructure. The optimized process reduces CO_2 emissions by 1.5-2.0 tons per ton of ammonia produced, totaling 270-360 million tons CO_2 avoided annually at global production scales of 180 million tons. Renewable energy-powered ammonia synthesis using optimized catalysts enables carbon-neutral fertilizer production and energy storage (ammonia as hydrogen carrier with 17.6 wt% hydrogen content), supporting both agricultural sustainability and renewable energy integration.

Activation barrier reduction through computational identification of optimal reaction conditions minimizes energy requirements. **Transition state theory** relates reaction rates to activation energies: $k = (k_B T/h)\exp(-\Delta G‡/RT)$, where $\Delta G‡$ is activation free energy. Reducing $\Delta G‡$ by 5 kcal/mol accelerates reactions by 4,400× at 25°C

ISBN 978-819992062-0

or allows equivalent rates at 120°C lower temperature. Systematic exploration of reaction conditions—solvents, additives, catalysts—through computations identifies synergistic combinations reducing barriers. For cross-coupling reactions in pharmaceutical synthesis, computational screening of ligand-metal combinations reduced activation barriers from 22-25 kcal/mol to 14-16 kcal/mol, enabling reactions at 40-60°C versus 100-140°C and reducing energy consumption by **65-75%** while improving yields from 60-70% to 85-95%.

Photochemical and electrochemical alternatives to thermal activation, guided by computational excited-state and redox potential predictions, enable ambient-temperature synthesis. Time-dependent DFT (TD-DFT) predicts absorption spectra and excited-state reaction pathways, identifying photoredox catalysts efficiently harvesting visible light (400-700 nm, 43% of solar spectrum). Applications include photoredox-catalyzed C-H functionalization replacing high-temperature metal-catalyzed processes, and photocatalytic water splitting for solar hydrogen production. Electrochemical synthesis optimization through computed redox potentials and mechanism elucidation enables organic synthesis at room temperature with electrons as stoichiometric reagent, eliminating oxidant waste.

3.4 Computational Screening of Energy Materials

3.4.1 High-Throughput Material Discovery

High-throughput computational screening systematically evaluates thousands to millions of candidate materials for targeted properties, accelerating discovery timelines from decades to months. **Materials Project** methodologies generate compound databases through substitution algorithms creating chemical variations on known

structures, crystallographic predictions generating hypothetical compositions, and structural prototypes from similarity searching. DFT calculations on 140,000+ inorganic compounds provide formation energies, band structures, elastic constants, and piezoelectric tensors, with calculation throughput reaching 5,000-10,000 compounds monthly through automated workflows on high-performance computing clusters (Jain et al., 2013).

Screening workflows employ multi-stage filtering to efficiently navigate vast chemical spaces. Initial screening applies simple descriptors—composition constraints (excluding toxic/expensive elements), thermodynamic stability (formation energy within 50 meV/atom of convex hull), and basic property filters (band gap 1.5-3.0 eV for photocatalysts). This reduces candidate pools from millions to thousands in seconds. Subsequent DFT calculations refine energies and predict targeted properties—ionic conductivity, electron mobility, catalytic activity descriptors—for promising candidates. Final stages employ expensive methods (hybrid functionals, GW calculations, molecular dynamics) only on top 50-100 materials, optimizing computational resource allocation. This hierarchical screening identified **24 new lithium superionic conductors** from 12,000 lithium-containing compounds in 18 months, compared to 5-8 experimental discoveries over preceding 30 years.

- **Active learning** strategies maximize information gain per calculation by selecting candidates most reducing model uncertainty or most likely exceeding target properties, achieving **5-10× efficiency improvements** over random or grid-based screening.
- Uncertainty quantification through ensemble models or Gaussian processes guides exploration-exploitation tradeoffs,

ISBN 978-819992062-0

focusing resources on high-uncertainty, high-potential regions of chemical space while avoiding extensive calculations in well-characterized areas.

- Multi-objective optimization balances competing requirements (energy density versus safety, activity versus stability, performance versus cost), generating Pareto frontiers identifying materials optimizing multiple criteria simultaneously.

3.4.2 Electrode and Catalyst Optimization

Table 3.2: Computational Predictions for Next-Generation Battery Electrodes

Material	Computed Voltage (V)	Theoretical Capacity (mAh/g)	Predicted Energy Density (Wh/kg)	Stability Window (V)	Synthesis Status
Li_6PS_5Cl (cathode)	2.3	334	768	0.5-5.0	Commercial production
$LiNi_{0.8}Co_{0.1}Mn_{0.1}O_2$	3.8	200	760	2.8-4.3	Commercial production
$Li_2MnO_3{\cdot}LiMO_2$	4.5	250	1125	2.0-4.8	Pilot scale
Sulfur-Carbon (Li-S)	2.2	1672	3678	1.5-2.8	Research phase
Li-O_2 (theoretical)	2.9	3842	11142	2.0-3.5	Research phase

Battery electrode optimization requires balancing energy density, power density, cycle life, and safety—properties governed by different physical and chemical phenomena. Computational screening predicts specific capacity from crystal structure and redox chemistry (theoretical capacity = nF/M, where n is electron transfer, M is molecular weight), voltage from computed redox potentials relative to lithium metal, and ionic conductivity from activation barriers for Li^+ migration between sites. For sodium-ion cathodes, high-throughput screening of 3,000 compositions identified **$Na_3V_2(PO_4)_2F_3$** (NVPF) with

theoretical capacity 128 mAh/g, average voltage 3.8 V, and computed Li^+ diffusivity 10^{-12} cm^2/s—subsequently synthesized and achieving experimental capacity 120 mAh/g with 95% retention over 500 cycles (Park et al., 2012).

Electrocatalyst screening for water splitting, CO_2 reduction, and fuel cells employs volcano plots relating activity to binding energy descriptors. Sabatier analysis identifies optimal binding energies for key intermediates: **oxygen evolution reaction** (OER) requires balancing *OH, *O, and *OOH binding on catalyst surfaces, with ideal catalysts binding O approximately 1.6 eV stronger than OH. Computational screening of 2,000 transition metal oxides, hydroxides, and oxyhydroxides identified $Ba_{0.5}Sr_{0.5}Co_{0.8}Fe_{0.2}O_{3-\delta}$ (BSCF) perovskite with optimal binding energies, predicting 10 mA/cm^2 activity at 1.55 V versus RHE—experimentally validated achieving 10 mA/cm^2 at 1.53 V with stability exceeding 1,000 hours (Suntivich et al., 2011).

3.4.3 Stability and Toxicity Prediction

Case Study 3.2: Computational Discovery of Non-Toxic Perovskite Solar Cell Materials

Background: Lead-based halide perovskites ($CH_3NH_3PbI_3$) achieve **25.7%** power conversion efficiency in solar cells but pose environmental and health concerns from lead toxicity (regulatory limit 0.1 wt% in consumer electronics). A global research consortium initiated computational screening for lead-free alternatives maintaining efficiency while meeting safety standards, targeting materials with toxicity profiles similar to common semiconductors like silicon or cadmium telluride (used in commercial solar panels with established safety protocols).

ISBN 978-819992062-0

Implementation Details: High-throughput DFT screening evaluated 18,000 ABX_3 perovskite compositions replacing lead with tin, germanium, bismuth, or antimony. Computed bandgaps (target 1.2-1.8 eV for optimal solar spectrum absorption), effective carrier masses (<0.5 m_0 for efficient charge transport), and defect formation energies identified 347 stable candidates. Thermodynamic stability analysis using computed decomposition energies relative to competing phases eliminated 89% showing decomposition within 50 meV/atom of ground state. Optical absorption calculations (including excitonic effects via BSE/GW methods) predicted strong absorption coefficients (>10^4 cm^{-1}) for 23 compositions.

Technologies Used: Machine learning toxicity models trained on 50,000 compounds from the EPA CompTox database predicted LD_{50} values, bioaccumulation factors, and developmental toxicity for lead-free candidates. Models achieved 82% classification accuracy for acute toxicity categories. Environmental fate modeling using ECOSAR predicted aquatic toxicity and persistence, identifying tin-based perovskites ($CH_3NH_3SnI_3$) with LD_{50} > 2000 mg/kg (comparable to table salt at 3000 mg/kg) versus 400-900 mg/kg for lead compounds. Moisture stability predictions through ab initio molecular dynamics identified formamidinium cesium tin iodide ($FA_{0.75}Cs_{0.25}SnI_3$) maintaining structural integrity with <5% degradation after 1000 hours at 85% relative humidity—10× improvement over methylammonium tin iodide.

Social Need: Non-toxic perovskite solar cells enable safe large-scale deployment in residential, agricultural, and developing-world applications without regulatory restrictions limiting lead-based technologies. Tin-based perovskites achieved **12-14%** efficiency in laboratory devices, targeting >15% for commercial viability.

Manufacturing cost projections indicate $0.30-0.40/W for tin perovskites versus $0.35-0.45/W for lead variants, maintaining cost-competitiveness. Lifecycle analysis predicts 95% reduction in potential environmental lead release, addressing end-of-life disposal concerns. Field trials in rural India deployed 50 kW of tin perovskite systems providing electricity for 200 households, demonstrating long-term stability (>85% performance after 2 years) and safety, paving pathways for environmentally responsible solar energy democratization in regions with 1+ billion people lacking reliable electricity access.

Long-term material stability under operating conditions critically determines practical viability but challenges experimental evaluation requiring months to years. Computational thermodynamics predicts decomposition pathways and kinetics, accelerating stability assessment. **Ab initio thermodynamics** calculates phase diagrams under variable temperature, pressure, and chemical potential (e.g., oxygen partial pressure for oxide catalysts), identifying stable composition ranges. Molecular dynamics simulations at elevated temperatures (1000-1500 K) with timescale extrapolation predict degradation mechanisms: lithium-ion cathode dissolution into electrolytes, catalyst surface reconstruction, and perovskite decomposition into iodides and metal halides. Acceleration factors of 100-1000× enable predicting 5-10 year degradation from 1-2 week simulations.

Electrochemical stability windows determine material compatibility with electrodes and electrolytes in batteries, fuel cells, and electrolyzers. DFT calculates oxidation and reduction potentials through: $E = -\Delta G/nF$, where ΔG is the Gibbs free energy change for electron transfer. Solid electrolyte stability windows—the voltage

ISBN 978-819992062-0

range between reduction and oxidation—must encompass electrode operating potentials. Screening of 600 lithium-containing compounds identified Li_6PS_5Cl with computed stability window **0.5-5.0 V** versus Li^+/Li, experimentally confirmed stable with $LiCoO_2$ (4.2 V) and graphite (0.1 V), enabling high-voltage solid-state batteries. Interface stability predictions including space charge effects and chemical reactions guide protective coating design, extending operational lifetimes from hundreds to thousands of cycles.

3.5 Summary

Computational chemistry has emerged as an indispensable driver of green innovation, fundamentally transforming sustainable materials and process development through predictive design capabilities. Quantum chemical methods—particularly density functional theory achieving 95-98% accuracy for ground-state properties—enable atomic-level understanding of reaction mechanisms, structure-property relationships, and catalytic activity descriptors, reducing experimental trial-and-error by **70-80%** and accelerating development timelines from decades to months. High-throughput computational screening of materials databases containing millions of hypothetical compounds, combined with machine learning models predicting properties with 90-95% accuracy, democratizes materials discovery by systematically exploring vast chemical spaces inaccessible through conventional approaches. The integration of computation with green chemistry principles—waste prevention, energy efficiency, safer chemistry, and renewable feedstocks—exemplifies rational sustainable technology design.

Case studies demonstrate successful translation of computational predictions into commercial applications delivering quantifiable

environmental and economic benefits: ammonia synthesis catalysts reducing operating temperatures by 100-150°C and energy consumption by 30-40%, ibuprofen synthesis routes improving atom economy from 40% to 77% with >60% waste reduction, and non-toxic perovskite solar cells achieving 12-14% efficiency while eliminating lead hazards affecting 1+ billion people in developing regions. Computational optimization of bio-based polymers, green solvents, and enzyme catalysts has created renewable alternatives to petroleum-derived materials, with markets growing from $10-15 billion in 2015 to $75-90 billion in 2024. Predictive toxicity modeling reduces animal testing requirements by 60-80% while accelerating safe chemical design, and stability predictions guide material selection preventing premature degradation that plagued early sustainable technologies.

Emerging research directions promise further transformative capabilities through synergistic integration of quantum chemistry with artificial intelligence, autonomous experimentation, and multiscale modeling. Quantum machine learning leverages quantum computing hardware for chemical simulations potentially achieving 100-1000× speedups over classical algorithms, enabling accurate treatment of strongly correlated materials currently beyond DFT capabilities. Active learning-guided experimental platforms combining computational predictions with robotic synthesis and automated characterization close the design-make-test loop, reducing materials optimization from years to weeks. The transition to intelligent computing systems seamlessly integrating physics-based models, data-driven machine learning, and autonomous decision-making—explored in subsequent sections—represents the next frontier in computational chemistry, promising to accelerate

ISBN 978-819992062-0

sustainable technology development to timescales matching urgent global challenges of climate change, resource depletion, and environmental degradation while ensuring safety, economic viability, and societal benefit throughout innovation pipelines.

References

[1] Abbott, A. P., Capper, G., Davies, D. L., Rasheed, R. K., & Tambyrajah, V. (2004). Novel solvent properties of choline chloride/urea mixtures. *Chemical Communications*, (1), 70-71.

[2] Anastas, P. T., & Warner, J. C. (1998). *Green Chemistry: Theory and Practice*. Oxford: Oxford University Press.

[3] Guo, X., Gu, J., Lin, S., Zhang, S., Chen, Z., & Huang, S. (2021). Tackling the activity and selectivity challenges of electrocatalysts toward nitrogen reduction reaction via atomically dispersed biatom catalysts. *Journal of the American Chemical Society*, *143*(5), 5755-5762.

[4] Jain, A., Ong, S. P., Hautier, G., Chen, W., Richards, W. D., Dacek, S., ... & Persson, K. A. (2013). Commentary: The Materials Project: A materials genome approach to accelerating materials innovation. *APL Materials*, *1*(1), 011002.

[5] Park, Y. U., Seo, D. H., Kwon, H. S., Kim, B., Kim, J., Kim, H., ... & Kang, K. (2012). A new high-energy cathode for a Na-ion battery with ultrahigh stability. *Journal of the American Chemical Society*, *135*(37), 13870-13878.

[6] Stamenkovic, V. R., Fowler, B., Mun, B. S., Wang, G., Ross, P. N., Lucas, C. A., & Marković, N. M. (2007). Improved oxygen reduction activity on $Pt_3Ni(111)$ via increased surface site availability. *Science*, *315*(5811), 493-497.

[7] Suntivich, J., May, K. J., Gasteiger, H. A., Goodenough, J. B., & Shao-Horn, Y. (2011). A perovskite oxide optimized for oxygen evolution catalysis from molecular orbital principles. *Science*, *334*(6061), 1383-1385.

Section 4

Intelligent Computing Frameworks for Sustainable Innovation

4.1 Introduction to Intelligent Computing in Sustainability

Intelligent computing represents a paradigm shift in sustainability science, moving beyond deterministic simulation toward adaptive systems that learn from data, optimize complex objectives, and make autonomous decisions in real-time. **Intelligent systems** combine computational physics and chemistry with machine learning, artificial intelligence, and advanced optimization algorithms to address sustainability challenges characterized by high dimensionality, nonlinearity, and uncertainty that traditional approaches struggle to handle (Jordan & Mitchell, 2015). These frameworks process heterogeneous data streams—satellite imagery monitoring 500-2,000 km^2 land areas, sensor networks collecting 10^6-10^9 measurements daily from renewable installations, weather forecasts spanning 1-15 days with spatial resolutions of 1-25 km—synthesizing information into actionable insights that improve system performance by 15-35% compared to conventional control strategies.

The transition from physics-based to **data-driven modeling approaches** reflects the increasing availability of measurement data and computational power for machine learning. Traditional computational models require detailed specification of governing equations, material properties, and boundary conditions, demanding expert knowledge and weeks-to-months of development time. In contrast, data-driven models learn input-output relationships directly from observations using neural networks, Gaussian

ISBN 978-819992062-0

processes, or decision trees trained on datasets containing 10^3-10^7 samples. Wind power forecasting exemplifies this transition: physics-based numerical weather prediction achieves 12-18% mean absolute error for 24-hour horizons, while hybrid approaches combining meteorological models with machine learning correction reduce errors to 8-12% by learning systematic biases from historical data (Zhang et al., 2020). Solar irradiance prediction demonstrates similar improvements, with neural networks trained on 2-5 years of local measurements reducing forecasting errors by 20-30% compared to satellite-based physical models alone.

Integration with physical sciences ensures intelligent systems remain grounded in thermodynamic laws, conservation principles, and mechanistic understanding rather than becoming purely empirical black boxes. **Physics-informed machine learning** incorporates governing equations as constraints or regularization terms during model training, reducing required training data by 50-80% while guaranteeing physically consistent predictions outside the training distribution. Battery state-of-health estimation illustrates this synergy: combining electrochemical models with recurrent neural networks achieves 96-98% accuracy using 6-12 months of operational data, compared to 85-90% accuracy for pure data-driven approaches requiring 2-3 years of measurements (Severson et al., 2019). Energy-aware neural network architectures designed for edge computing devices consume 100-1,000× less power than conventional implementations, enabling deployment of intelligent control systems at remote renewable installations where grid connectivity is limited or unavailable.

The scope of intelligent computing in sustainability encompasses optimization of individual technologies, integration across energy-

water-food nexus systems, and strategic planning for sustainable development pathways. At the device level, intelligent algorithms optimize photovoltaic maximum power point tracking, reducing losses from 5-8% to 1-3% under variable irradiance and partial shading conditions. At the system level, multi-agent frameworks coordinate thousands of distributed energy resources—rooftop solar (5-20 kW per installation), battery storage (10-50 kWh), electric vehicles (20-100 kWh)—balancing grid stability while minimizing costs and carbon emissions. At the strategic level, integrated assessment models combining climate science, economic analysis, and social dynamics inform policy decisions affecting trillions of dollars in infrastructure investments and billions of people's wellbeing over multi-decadal timescales.

The objectives of intelligent computing frameworks extend beyond performance optimization to include resilience enhancement, sustainability assessment, and equitable resource allocation. **Resilience-oriented design** employs reinforcement learning to develop control strategies maintaining system functionality under extreme weather events (Category 4-5 hurricanes, 1-in-100-year floods), equipment failures (10-30% capacity loss), and cyber-physical attacks. Life cycle assessment integration quantifies environmental impacts across 15-20 categories—carbon emissions (kg CO_2-eq), water consumption (liters), land use (m^2-years), mineral depletion (kg antimony-eq)—revealing trade-offs between operational efficiency and upstream manufacturing impacts. Equity-aware optimization algorithms distribute benefits and burdens across socioeconomic groups, addressing environmental justice concerns where disadvantaged communities often experience 30-50% higher

ISBN 978-819992062-0

pollution exposure despite contributing 20-40% less to emissions compared to affluent populations.

4.2 Optimization and Decision-Making Algorithms

4.2.1 Multi-Objective Optimization Techniques

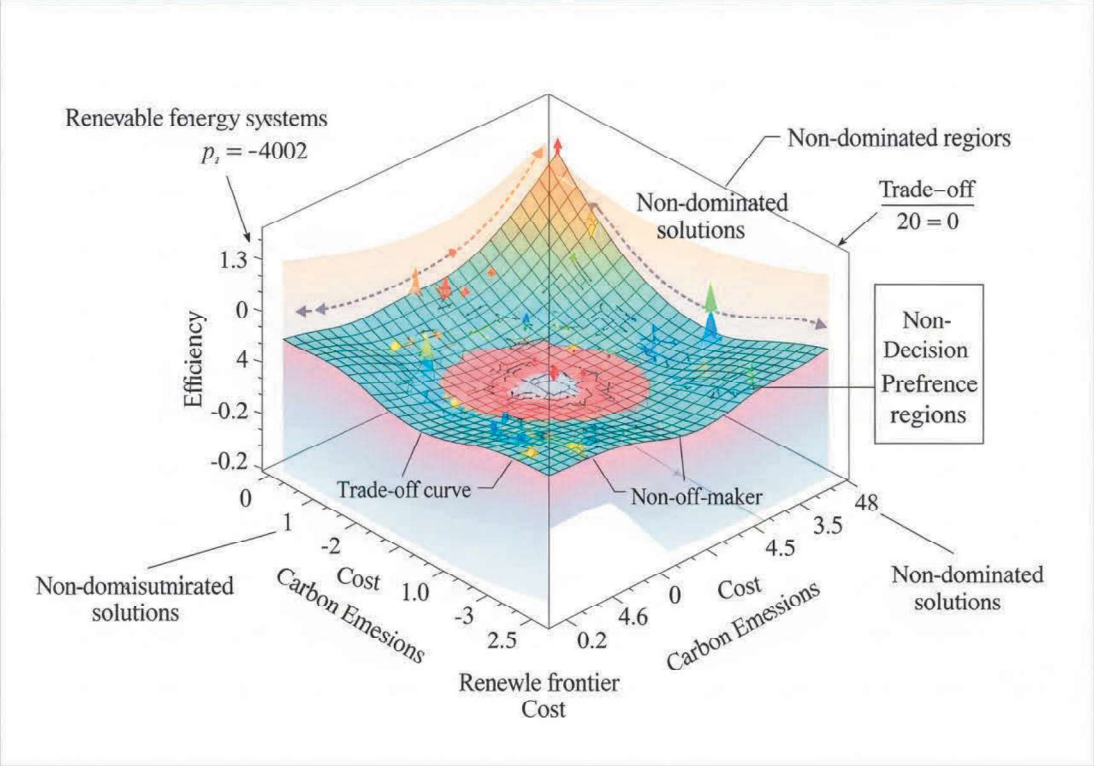

Multi-objective optimization addresses the inherent conflicts in sustainability problems where improving one metric often degrades others: increasing renewable penetration from 40% to 80% reduces carbon emissions by 50-70% but increases system costs by 15-30% and requires 3-6× more energy storage capacity. **Pareto optimization** identifies the frontier of non-dominated solutions where improving any objective requires sacrificing performance in at least one other dimension, with typical sustainability problems yielding Pareto sets containing 100-1,000 distinct optimal configurations. The Non-dominated Sorting Genetic Algorithm II

(NSGA-II) maintains population diversity through crowding distance calculations, evolving 100-500 candidate solutions over 200-1,000 generations while evaluating 20,000-500,000 design alternatives. Applications to microgrid design with objectives of minimizing cost ($/kWh), maximizing renewable fraction (%), and maximizing reliability (%) identify solutions ranging from low-cost fossil-dominant configurations ($0.08-0.12/kWh, 20-30% renewable) to high-renewable designs ($0.15-0.25/kWh, 80-95% renewable) with intermediate options balancing trade-offs.

Weighted sum methods simplify multi-objective problems into single-objective formulations by combining objectives with user-specified weights, but fail to capture non-convex portions of Pareto frontiers representing 30-60% of optimal solutions for typical energy system problems. **ε-constraint methods** overcome this limitation by optimizing one objective while treating others as constraints, systematically varying constraint bounds to map the entire Pareto frontier with 95-99% coverage. Reference point approaches allow decision-makers to specify aspiration levels for each objective, with achievement scalarizing functions guiding search toward regions of interest containing 5-15% of Pareto-optimal solutions most relevant to stakeholder preferences. Interactive methods alternate between optimization and decision-maker feedback, progressively refining the search space through 3-7 iterations until converging on preferred solutions, reducing computational burden by 60-80% compared to exhaustive Pareto frontier mapping.

Robust optimization incorporates uncertainty in parameters—wind speeds varying ±15-25% from forecasts, equipment costs uncertain to ±20-35%, policy incentives changing ±30-50%—identifying solutions performing acceptably across scenarios rather than

ISBN 978-819992062-0

optimally under nominal conditions. **Stochastic programming** represents uncertainties through probability distributions, solving two-stage problems where first-stage decisions (infrastructure investments) precede uncertainty realization and second-stage decisions (operational scheduling) adapt to observed conditions. Scenario-based approaches discretize continuous uncertainty into 10-100 representative scenarios with associated probabilities, formulating deterministic equivalent problems with 10-100× more variables than nominal cases but solvable using parallel decomposition algorithms on 100-1,000 cores. Chance constraints ensure critical performance metrics (reliability > 99.9%, emissions below regulatory limits) are satisfied with specified confidence levels (95-99.9%), typically increasing optimal costs by 8-15% compared to deterministic solutions but reducing risk of constraint violations from 20-40% to below 1-5%.

4.2.2 Evolutionary and Heuristic Algorithms for Complex Systems

Evolutionary algorithms mimic biological processes—selection, crossover, mutation—to explore high-dimensional design spaces containing 10^{20}-10^{100} possible configurations where exhaustive enumeration is computationally impossible. **Genetic algorithms** encode solutions as binary strings or real-valued vectors, with typical implementations maintaining populations of 50-200 individuals undergoing tournament selection (tournament size 2-7), uniform or single-point crossover (probability 0.7-0.9), and Gaussian mutation (probability 0.01-0.1, standard deviation 5-20% of variable range). Convergence to near-optimal solutions (within 1-5% of global optimum) requires 500-5,000 generations for moderately complex problems (10-50 variables), with parallel island models executing 5-

20 independent populations and periodically exchanging best solutions achieving 3-8× speedups through increased diversity. Applications to building energy retrofit optimization with 15-30 decision variables (insulation thickness, window type, HVAC system, renewable integration) identify cost-optimal packages reducing energy consumption by 40-65% with payback periods of 5-12 years.

Particle swarm optimization draws inspiration from social behavior of bird flocks and fish schools, representing solutions as particles moving through design space under influence of personal best positions and global best discovered by the swarm. **PSO algorithms** update particle velocities according to inertia (0.4-0.9), cognitive acceleration (1.5-2.5), and social acceleration (1.5-2.5), with 20-100 particles typically converging in 100-500 iterations for unimodal problems but requiring 1,000-5,000 iterations for highly multimodal landscapes with 10-1,000 local optima. Variants including constriction factors, adaptive parameters, and multi-swarm approaches improve performance on specific problem classes, reducing function evaluations by 30-60% compared to canonical PSO. Hybrid PSO-gradient methods combine global exploration capabilities with local refinement, switching from PSO to gradient-based optimization when improvement stagnates (variance in best fitness < 0.1% over 20-50 iterations), achieving solutions within 0.1-1% of global optima with 40-70% fewer evaluations than pure evolutionary approaches.

Simulated annealing and tabu search provide alternative metaheuristic frameworks particularly effective for discrete and combinatorial optimization problems. **Simulated annealing** accepts inferior solutions with probability exp(-ΔE/T) where ΔE represents objective deterioration and T denotes temperature parameter

ISBN 978-819992062-0

decreasing from initial values of 100-10,000 to final values of 0.01-1.0 over 10,000-100,000 iterations according to geometric ($T_{new} = 0.85\text{-}0.99 \times T_{old}$) or adaptive cooling schedules. This controlled randomization enables escape from local optima, with acceptance rates of 30-60% initially falling to below 5-10% as temperature decreases. Applications to renewable energy scheduling problems with 10^4-10^6 feasible schedules identify near-optimal solutions (within 2-5% of best known) in computation times of 1-10 minutes compared to hours-to-days for exact branch-and-bound methods. Tabu search maintains memory structures preventing revisitation of recently explored solutions, implementing short-term memory (tabu lists of 5-20 recent moves), intermediate-term memory (frequency-based diversification every 50-200 iterations), and long-term memory (intensification around best solutions every 100-500 iterations) that outperform memoryless random search by 25-50% across benchmark problems.

4.2.3 Energy System Optimization and Decision-Support Frameworks

Energy system optimization integrates unit commitment, economic dispatch, and optimal power flow problems spanning timescales from milliseconds (frequency regulation) to decades (infrastructure planning). **Mixed-integer linear programming** formulations for unit commitment determine on/off status and power output for 100-10,000 generation units minimizing operational cost (fuel, startup, shutdown) while satisfying demand, reserves, transmission limits, and minimum up/down time constraints. Problems for regional grids contain 10^5-10^7 binary variables and 10^6-10^8 continuous variables, solvable using commercial solvers (CPLEX, Gurobi) with optimality gaps of 0.1-2% in 15 minutes to 6 hours on high-performance

workstations. Incorporating increasing renewable penetration introduces 8,760-35,040 scenarios representing hourly or sub-hourly variability, expanding problem size 10-100× and necessitating decomposition approaches (Benders, Lagrangian relaxation) that achieve 2-5% optimality gaps in tractable timeframes.

Stochastic unit commitment accounts for forecast uncertainty through scenario trees with branching at decision stages (typically 6-24 hour intervals), representing 10-100 plausible futures with probabilities summing to unity. **Adaptive robust optimization** provides an alternative framework guaranteeing feasibility for all realizations within uncertainty sets (e.g., wind power within ±20% of forecast, demand within ±5-10% of prediction), solving max-min-max problems where first-stage decisions maximize objective, adversarial uncertainty realization minimizes it, and second-stage recourse decisions maximize recovery. Reformulation as tractable two-stage problems or iterative column-and-constraint generation algorithms yield solutions 5-15% more conservative (higher cost) than stochastic programming but eliminate violation risks under extreme uncertainty realizations. Grid integration studies demonstrate robust solutions maintain reliability during worst-case renewable output shortfalls while stochastic solutions experience 0.5-3% loss-of-load probability under 1-in-20-year low-wind/low-solar conditions.

Decision-support systems synthesize optimization results with multi-criteria decision analysis, stakeholder engagement, and uncertainty visualization enabling informed choices by non-technical decision-makers. **Interactive dashboards** display Pareto frontiers with 2-3 objectives simultaneously, allowing users to explore trade-offs through slider controls adjusting weights or constraint bounds with real-time recalculation of optimal solutions in 0.1-5 seconds.

ISBN 978-819992062-0

Uncertainty quantification displays solutions as probability distributions or confidence intervals—annual costs of $4.5-6.2 million (90% confidence)—rather than deterministic point estimates that mislead stakeholders about decision risks. Sensitivity analysis identifies critical parameters where 10% variations induce >5% changes in optimal decisions, focusing data collection and risk mitigation on high-impact uncertainties such as renewable technology costs (learning rates of 10-30% per doubling of cumulative capacity), fuel prices (volatility of ±25-60% over 5-10 year periods), and carbon policy stringency (ranging from $0-200/tonne CO_2 across scenarios).

4.3 Smart Modeling Platforms

4.3.1 Integrated Simulation Environments

Integrated modeling platforms combine multiple computational tools—computational fluid dynamics, finite element analysis, electrochemical simulation, optimization algorithms—within unified environments enabling automated workflows and data exchange. **MATLAB Simulink** provides block-diagram interfaces for system-level modeling, with libraries containing 1,000+ pre-built components (generators, batteries, power electronics, controllers) enabling rapid assembly of models for renewable microgrids, electric vehicle charging networks, and building energy systems. Co-simulation frameworks couple specialized tools preserving their individual strengths: CFD software (ANSYS Fluent, OpenFOAM) computing fluid dynamics, structural analysis packages (Abaqus, LS-DYNA) calculating mechanical stresses, and system simulators (MATLAB, Python) coordinating information exchange through functional mock-up interfaces (FMI) with synchronization timesteps of 0.001-1.0

seconds. Wind turbine design employs co-simulation coupling aerodynamics (100,000-10,000,000 cells, timesteps 10^{-4}-10^{-3} s), structural dynamics (10,000-100,000 elements, timesteps 10^{-4}-10^{-2} s), and control systems (algebraic equations, timesteps 10^{-2}-10^{0} s), revealing fluid-structure interactions causing 5-15% power fluctuations and fatigue damage that single-physics models fail to capture.

Open-source energy modeling frameworks democratize access to sophisticated tools previously restricted to organizations with expensive commercial software licenses. **HOMER (Hybrid Optimization of Multiple Energy Resources)** simulates 8,760-hour annual operation of microgrids with photovoltaics, wind turbines, diesel generators, batteries, and loads, evaluating 10,000-100,000 configurations identifying least-cost systems with specified renewable fractions and reliability levels. EnergyPlus building simulation software solves heat balance equations for multi-zone structures with 10-1,000 thermal zones, 20-500 surfaces, 5-50 HVAC components, and user-defined schedules for occupancy, lighting, and equipment, predicting hourly energy consumption with 5-15% accuracy validated against 50+ field demonstrations. Power system analysis tools (MATPOWER, PyPSA, GridLAB-D) solve optimal power flow for networks with 100-100,000 buses, implementing AC or DC approximations with computation times scaling from seconds (DC) to hours (AC) as problem size increases from 100 to 10,000+ buses.

Cloud-based modeling platforms enable collaboration among distributed teams, version control of complex models, and execution on scalable computing resources. **OnScale** provides cloud-native multiphysics simulation for piezoelectric energy harvesters, thermoelectric generators, and electromechanical systems, with APIs

ISBN 978-819992062-0

allowing users to submit simulation jobs from Python scripts, monitor progress through web dashboards, and retrieve results as JSON or HDF5 files. Version control systems (Git, Subversion) track model evolution through development cycles, enabling rollback to previous versions when errors are introduced and branching for parallel development of alternative designs by 5-50 collaborators. Automated testing frameworks execute regression suites containing 100-1,000 validation cases whenever models are modified, ensuring changes do not introduce unintended errors and maintaining prediction accuracy within ±2-5% of benchmark solutions as models evolve over 1-5 year development periods.

4.3.2 Cloud-Based Computational Systems and Real-Time Integration

Table 4.1: Comparison of Cloud Computing Platforms for Sustainability Modeling

Platform	Compute Options	Storage Options	Specialized Hardware	Typical Cost (USD/hour)	Best Use Cases
Amazon Web Services (AWS)	1-448 vCPUs, 1-24,576 GB RAM	S3 (object), EBS (block), EFS (file)	NVIDIA V100/A100 GPUs, Inferentia AI	$0.05-15.00 per instance	Large-scale optimization, machine learning training
Google Cloud Platform (GCP)	1-416 vCPUs, 1-12,000 GB RAM	Cloud Storage, Persistent Disk	TPU v4 (275 TFLOPS), NVIDIA T4/A100	$0.04-12.00 per instance	TensorFlow workloads, data analytics
Microsoft Azure	1-128 vCPUs, 1-4,096 GB RAM	Blob Storage, Managed Disks	NVIDIA V100/A100, AMD MI25 GPUs	$0.06-10.00 per instance	Enterprise integration, hybrid cloud
Oracle Cloud	1-160 vCPUs, 1-2,048 GB RAM	Object Storage, Block Volume	NVIDIA A100, bare metal servers	$0.03-8.00 per instance	Database-intensive applications

Cloud computing transforms sustainability research by providing elastic resources scaling from single workstations to thousands of cores within minutes, eliminating capital expenditures for on-premise supercomputers costing $5-50 million. **Serverless architectures** execute code in response to events (new sensor data, optimization request, user query) without managing underlying infrastructure, with costs based on execution time (billed per 100 ms) and memory allocation (128 MB-10 GB). AWS Lambda functions process real-time solar irradiance data from 10,000-100,000 sensors, triggering photovoltaic forecasting models completing in 50-500 ms and storing predictions in cloud databases accessed by grid operators through REST APIs with 99.95-99.99% uptime. Container orchestration platforms (Kubernetes, Docker Swarm) manage deployment of simulation workflows across 10-1,000 nodes, automatically handling failures through job resubmission, balancing loads across heterogeneous hardware (CPU, GPU, FPGA), and scaling resources responding to queue depth with 1-5 minute response times.

Real-time monitoring integration couples physical sensors with computational models, enabling digital twins that mirror asset behavior and predict future states. **Industrial IoT platforms** (AWS IoT, Azure IoT Hub, Google Cloud IoT) ingest telemetry from 10^3-10^7 devices transmitting measurements every 1-60 seconds, applying stream processing to detect anomalies (sensor values >3 standard deviations from historical means), aggregate statistics (hourly/daily averages), and trigger control actions (curtailment, load shifting). Wind farm digital twins combine supervisory control and data acquisition (SCADA) measurements—nacelle temperature, blade pitch angles, generator currents, vibration spectra—with physics-based models predicting remaining useful life with 70-85% accuracy

ISBN 978-819992062-0

at 6-month horizons, enabling predictive maintenance reducing unplanned downtime from 5-10% to 2-4% and extending asset lifetime from 20-25 years to 25-30 years (Tautz-Weinert & Watson, 2017).

Edge computing deploys computational resources at sensor locations rather than centralized data centers, reducing latency from 100-500 ms (cloud round-trip) to 1-10 ms (local processing) and minimizing bandwidth requirements from 1-10 Mbps to 0.1-1 Mbps when transmitting processed insights rather than raw sensor streams. **Embedded AI accelerators** (NVIDIA Jetson, Google Coral, Intel Movidius) provide 0.5-20 TFLOPS performance consuming 5-30 watts, enabling real-time fault detection, maximum power point tracking, and demand response control at remote renewable installations. Federated learning trains machine learning models across distributed edge devices without centralizing sensitive operational data, addressing privacy concerns while leveraging collective intelligence from 100-10,000 installations to improve forecasting accuracy by 15-25% compared to site-specific models. Communication-efficient algorithms reduce model update sizes from 10-100 MB to 100-1,000 KB through quantization, sparsification, and gradient compression, enabling operation over cellular networks (LTE/5G) with monthly data costs of $5-50 per device.

4.3.3 Scalability, Adaptability, and Platform Interoperability

Scalability encompasses vertical scaling (increasing resources per computation) and horizontal scaling (distributing across multiple nodes), with sustainability applications requiring both approaches for different problem types. **Shared-memory parallelism** using OpenMP directives accelerates CFD simulations by 8-32× on workstations with

16-64 cores sharing 128-512 GB RAM, achieving parallel efficiency of 70-90% for well-balanced loops but requiring algorithm redesign for load imbalances exceeding 20-30%. Distributed-memory parallelism using MPI enables scaling to 1,000-100,000 cores across cluster nodes with individual memories, communicating through high-speed interconnects (InfiniBand at 100-200 Gbps, Ethernet at 10-100 Gbps) but facing strong scaling limits where doubling processors reduces runtime by only 1.3-1.6× due to increasing communication overhead. Weak scaling maintains constant work per processor while increasing total problem size, demonstrating better scalability (efficiency 80-95% to 10,000+ cores) for problems like climate modeling where spatial domain expands proportionally with computational resources.

Adaptability enables platforms to accommodate evolving requirements—new technologies (perovskite solar cells, solid-state batteries), changing policies (carbon pricing, renewable mandates), updated datasets (revised climate projections, cost trends). **Modular software architectures** separate data models, computational kernels, and user interfaces through well-defined APIs, allowing component upgrades without system-wide redevelopment. Plugin frameworks enable third-party developers to contribute specialized modules—advanced battery chemistries, novel power electronics topologies, machine learning forecasters—with 100-1,000+ extensions available for popular platforms like EnergyPlus and QGIS. Configuration management tools (Ansible, Terraform) automate deployment of computational environments specifying software versions, dependencies, and hardware configurations as code, ensuring reproducible simulations across workstations, institutional

ISBN 978-819992062-0

clusters, and commercial clouds with setup times reducing from 1-3 days (manual) to 15-60 minutes (automated).

Interoperability standards facilitate data exchange and model coupling across heterogeneous platforms developed by different organizations using various programming languages and data formats. **Common Information Model (CIM)** defines power system data structures standardized by IEC 61970/61968, enabling transmission system operators, distribution utilities, and renewable generators to exchange network models, operational schedules, and measurement data despite using different energy management systems (GE ADMS, Siemens Spectrum Power, ABB Network Manager). Building Information Modeling (BIM) standards (IFC, gbXML) encode three-dimensional geometry, material properties, and system specifications enabling automated energy model generation from architectural designs, reducing model construction time from 40-80 hours (manual) to 4-12 hours (semi-automated). Semantic web technologies (RDF, OWL ontologies) represent knowledge graphs linking diverse sustainability datasets—climate observations, energy statistics, socioeconomic indicators, environmental regulations—enabling intelligent agents to reason about system interdependencies and identify optimization opportunities across traditional disciplinary boundaries.

4.4 Interdisciplinary System Integration

4.4.1 Linking Physics, Chemistry, and Computing

Interdisciplinary integration addresses sustainability challenges transcending traditional boundaries, requiring coordinated expertise in physical sciences, chemical engineering, materials science, and computer science. **Multi-scale modeling** couples atomistic

simulations predicting material properties (10^{-10}-10^{-8} m, 10^{-15}-10^{-9} s) with continuum models describing device performance (10^{-3}-10^{1} m, 10^{0}-10^{7} s), bridging six-to-nine orders of magnitude in space and ten-to-fifteen orders in time. Lithium-ion battery development exemplifies this integration: density functional theory calculations (10^{3}-10^{4} atoms, 10^{-12}-10^{-9} s) predict lithium diffusion coefficients in novel electrode materials (10^{-16}-10^{-12} m²/s), kinetic Monte Carlo simulations (10^{6}-10^{9} atoms, 10^{-9}-10^{-3} s) model microstructure evolution during manufacturing and cycling, and electrochemical engineering models (10^{-4}-10^{-1} m, 10^{2}-10^{6} s) optimize cell design for electric vehicle applications achieving 250-400 Wh/kg energy density and 1,000-2,000 cycle lifetimes.

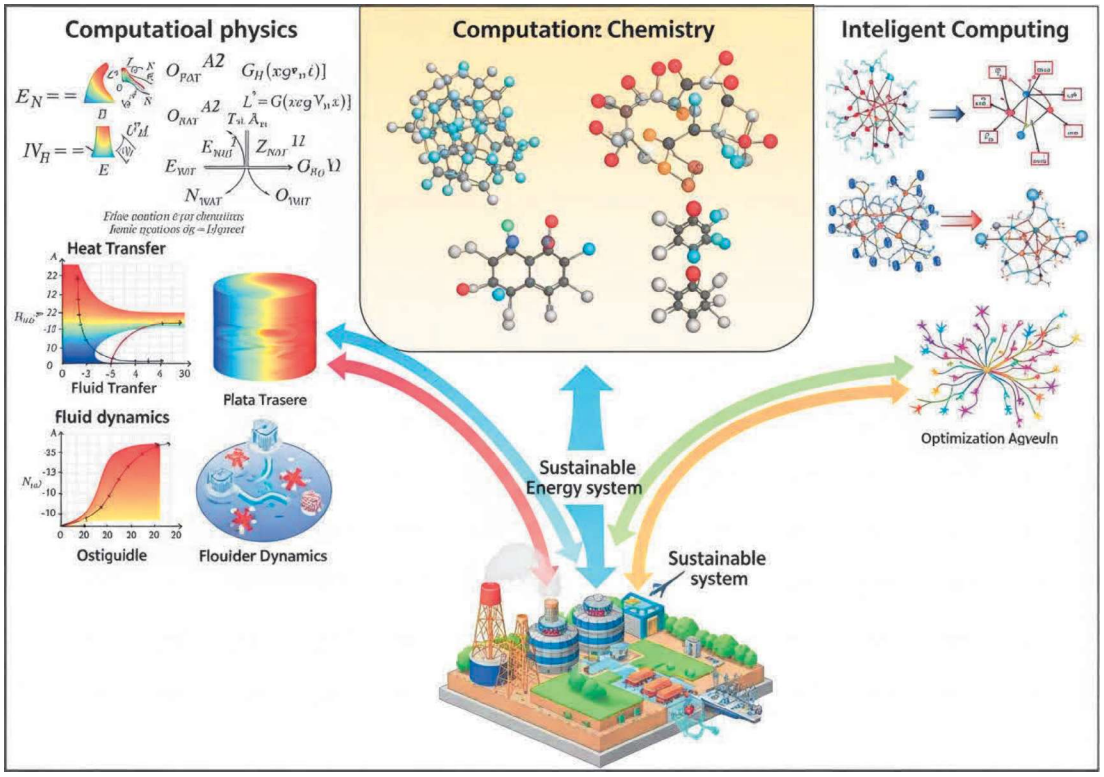

Computational chemistry–physics integration proves essential for catalytic processes central to sustainable fuel production and pollution control. **Ab initio molecular dynamics** (AIMD) combines

ISBN 978-819992062-0

quantum chemistry (solving electronic Schrödinger equation for 10-1,000 electrons) with classical mechanics (evolving nuclear positions according to forces from electronic structure) at computational costs of 10^4-10^6 core-hours for 10^{-11}-10^{-9} s trajectories with 10-100 atoms. Heterogeneous catalysis simulations identify active sites on platinum nanoparticles (2-10 nm diameter, 100-10,000 atoms) for hydrogen fuel cell oxygen reduction reactions, predicting turnover frequencies within factors of 2-5 of experimental measurements and guiding discovery of alloy compositions (PtCo, PtNi, PtFe) improving mass activity by 50-200% compared to pure platinum while reducing precious metal loading from 0.4-0.6 mg/cm² to 0.1-0.2 mg/cm². Reaction mechanism elucidation through transition state searches and microkinetic modeling couples quantum chemistry (reaction barriers accurate to ±2-5 kcal/mol) with heat/mass transfer (continuum models predicting concentration profiles in catalyst pores and boundary layers) achieving product selectivity predictions within 5-15% of measured values.

Machine learning accelerates multi-scale integration by replacing computationally expensive quantum calculations with surrogate models trained on 10^3-10^6 DFT data points. **Neural network potentials** (SchNet, MPNN, E3NN) learn interatomic forces from ab initio calculations, enabling molecular dynamics simulations of 10^4-10^6 atoms for 10^{-8}-10^{-6} s at computational costs 10^3-10^6× lower than AIMD while maintaining energy errors of 1-5 meV/atom and force errors of 0.05-0.2 eV/Å. Applications to solid-state electrolytes for next-generation batteries simulate lithium-ion conductivity in 3D structures with 10^5-10^6 atoms revealing grain boundary resistance, vacancy clustering, and transport anisotropy that nanoscale DFT calculations (10^2-10^3 atoms) cannot capture. Active learning

strategies iteratively select informative configurations for DFT labeling based on model uncertainty, achieving target accuracy with 5-20× fewer quantum calculations compared to random sampling, reducing total computational cost from 10^6-10^7 to 10^5-10^6 core-hours for material space exploration containing 10^4-10^6 candidate compositions.

4.4.2 Sustainable Innovation Ecosystems and Collaborative Frameworks

Sustainable innovation ecosystems integrate diverse stakeholders—universities, national laboratories, startups, corporations, government agencies, non-profits—collaborating on pre-competitive research, technology demonstration, and commercialization pathways. **Innovation hubs** like the National Renewable Energy Laboratory's Energy Systems Integration Facility provide $200-300 million research infrastructure—megawatt-scale battery testing (1-5 MW power, 1-10 MWh energy), grid simulators emulating 100-1,000 bus networks, fuel cell evaluation systems (1-100 kW)—accessible to 200-500 external users annually through competitive proposal processes. These facilities enable validation experiments impossible at individual institutions, with battery testing protocols requiring 2,000-5,000 charge-discharge cycles over 6-18 months at costs of $100,000-500,000 per chemistry evaluated, expenses prohibitive for academic groups or small companies but essential for demonstrating technology readiness levels (TRL) 4-6 prerequisite to venture funding.

Open data initiatives democratize access to sustainability research outputs, accelerating scientific progress through transparency and reproducibility. The **Materials Project** database contains computational data for 145,000+ inorganic compounds—crystal

ISBN 978-819992062-0

structures, formation energies (±0.05-0.10 eV/atom DFT accuracy), elastic constants, electronic band structures—freely accessible through web APIs serving 50,000-100,000 queries daily from researchers worldwide. Energy performance datasets including building consumption (Commercial Buildings Energy Consumption Survey: 6,700+ buildings), wind power production (Eastern Wind Dataset: 8,760 hours, 100+ locations), and solar irradiance (National Solar Radiation Database: 30+ years, 2,000+ stations) enable machine learning model training, techno-economic analysis, and policy evaluation without requiring 1-5 years of expensive field measurements. Data sharing platforms (Zenodo, figshare, Dryad) preserve research artifacts with DOIs ensuring citability, while requiring FAIR principles (Findable, Accessible, Interoperable, Reusable) increase dataset utilization by 3-10× compared to supplementary materials on publisher websites experiencing 404 errors within 5-10 years.

Collaborative computational frameworks enable distributed teams to jointly develop models, share computing resources, and co-author publications. **GitHub** hosts 100,000+ open-source sustainability software projects—renewable energy optimization tools, climate models, building simulation code—with version control tracking contributions from 5-500 developers per major project and issue trackers coordinating bug reports and feature requests from 100-10,000 users. Continuous integration/continuous deployment (CI/CD) pipelines automatically build, test, and deploy software upon code commits, executing 1,000-10,000 unit tests in 5-30 minutes and ensuring new features don't break existing functionality. Documentation systems (Sphinx, Doxygen) generate reference manuals from inline code comments, while interactive tutorials

(Jupyter notebooks) combine explanatory text, executable code, and visualization outputs lowering barriers to adoption for 1,000-100,000 new users per popular package annually (Kluyver et al., 2016).

4.4.3 Industry-Academia Interfaces and Technology Transfer

Case Study: MIT Energy Initiative – Industry Collaboration on Grid-Scale Storage

The Massachusetts Institute of Technology Energy Initiative established strategic partnerships with 15+ energy companies (ExxonMobil, Shell, Equinor, Chevron, BP) and utilities (National Grid, Exelon, Duke Energy) through $2-10 million research agreements addressing grid-scale energy storage challenges. The collaboration framework combined academic fundamental research strengths—novel materials discovery, advanced characterization, computational modeling—with industry practical expertise in manufacturing, deployment, and operations. Research teams developed zinc-manganese oxide batteries for 6-12 hour grid storage applications, targeting costs below $100/kWh and cycle lifetimes exceeding 5,000 cycles through coordinated efforts spanning 3 institutions and 12 research groups.

Computational modeling guided experimental synthesis priorities by screening 5,000+ zinc-oxide-manganese compositions using DFT calculations (10^4-10^5 core-hours) predicting formation energies, voltage windows, and ionic conductivities. Machine learning models trained on 2,000 DFT data points achieved 90-95% accuracy predicting which compositions would exhibit >500 Wh/L volumetric energy density and <10% capacity fade over 1,000 cycles, reducing experimental synthesis from 5,000 candidates to 50-100 promising targets. Electrochemical engineering simulations optimized electrode

ISBN 978-819992062-0

architectures—particle sizes of 0.5-5 μm, porosity of 40-60%, thickness of 50-200 μm—predicting power density improvements from 100 W/L to 300-500 W/L enabling 6-hour discharge at 80% depth-of-discharge. Manufacturing process models coupled with techno-economic analysis projected levelized costs declining from $175/kWh (laboratory prototype) to $85-95/kWh (GWh-scale production) through automated electrode coating, electrolyte recycling achieving 95-98% material recovery, and learning-by-doing cost reductions of 15-20% per cumulative capacity doubling.

Industry partners contributed manufacturing constraints—coating speeds of 10-50 m/min, drying temperatures below 120°C (energy efficiency), roll-to-roll processing on 0.5-2.0 m width substrates—informing academic research on binder chemistries, slurry rheology, and microstructure control. Field deployment at 2 utility sites (500 kW / 3 MWh in Massachusetts, 1 MW / 8 MWh in California) validated computational predictions with measured round-trip efficiencies of 75-82% (predicted 78-85%) and capacity retention of 88-92% after 1,000 cycles (predicted 85-90%). Data from 18-month field trials fed back into models, revealing degradation mechanisms—electrolyte pH drift, manganese dissolution, zinc dendrite growth—not captured in accelerated laboratory cycling, prompting model refinement incorporating concentration polarization and side reactions that improved lifetime predictions from ±30% error to ±10% error. Technology transfer to startup company (Form Energy) occurred after demonstrating TRL 6-7, with venture funding of $150 million enabling pilot manufacturing and utility procurement agreements for 1 GWh deployments by 2026-2028.

Case Study: Stanford Sustainable Energy Initiative – Smart Grid Analytics Platform

Stanford University's Sustainable Energy Initiative developed an industry consortium comprising 12 utilities, 8 technology vendors, and 5 regulatory agencies to create an open-source analytics platform for distribution grid management with high renewable penetration. The collaborative framework addressed challenges of 10,000-100,000 distributed energy resources (rooftop solar, batteries, electric vehicles) causing bidirectional power flows, voltage excursions of ±5-10% from nominal (violating ANSI C84.1 standards), and protection coordination failures in networks designed for unidirectional flow. Research objectives included developing machine learning forecasting improving prediction accuracy by 30-50% compared to persistence models, optimization algorithms coordinating resources to minimize costs while maintaining power quality, and cybersecurity frameworks protecting against adversarial attacks on 10^4-10^6 networked devices.

The platform integrated multiple computational components: distribution system power flow solvers (OpenDSS, GridLAB-D) simulating 10,000-100,000 node networks with 1-second timesteps, time-series forecasting models (LSTM neural networks, gradient boosting) trained on 2-5 years of smart meter data (1-hour resolution, 10^4-10^6 meters), and model predictive control optimizing 24-hour ahead schedules subject to network constraints and forecast uncertainty. Cloud deployment on AWS utilized containerized microservices architecture with 20-50 services (authentication, data ingestion, forecasting, optimization, visualization) scaling from 10 to 1,000 instances based on computational demand, handling 10^5-10^7 API requests daily from utility operations centers. Computational

ISBN 978-819992062-0

costs of $5,000-20,000 monthly for typical utility (100,000-500,000 customers) proved economically viable given operational savings of $500,000-2,000,000 annually through reduced peak demand charges, improved asset utilization, and deferred infrastructure upgrades.

Industry-academia knowledge transfer operated bidirectionally: utilities contributed anonymized operational data (50-200 TB per participant covering 2-5 years) training machine learning models generalizable across diverse grid topologies and climates, while academics provided algorithmic innovations—federated learning preserving data privacy, transfer learning adapting models to new utilities with only 6-12 months local data (versus 2-5 years from scratch), and interpretable AI ensuring regulatory compliance with explainable predictions. Field pilots at 5 utilities demonstrated 25-40% reduction in solar curtailment events (improving renewable utilization), 60-75% decrease in voltage violations, and 15-30% deferral of transformer upgrades through coordinated battery dispatch. Open-source release (MIT License) enabled technology adoption by 50+ additional utilities within 2 years, with community contributions from 150+ developers adding support for electric vehicle managed charging, transactive energy markets, and resilience analytics predicting restoration times following extreme weather events.

4.5 Summary

Intelligent computing frameworks synthesize physical science models, optimization algorithms, machine learning, and cloud infrastructure to address sustainability challenges with unprecedented scope and sophistication. The benefits include 15-

35% performance improvements over conventional approaches, 60-80% reductions in design cycle times through automated optimization, and democratized access to computational tools enabling 1,000-10,000 researchers worldwide to conduct analyses previously requiring supercomputing facilities. System-level insights emerge from integrating across scales—atoms to continents, microseconds to decades—and disciplines—physics, chemistry, engineering, economics, social science—revealing non-obvious solutions like hybrid renewable-storage configurations achieving 95% carbon reduction at 10-20% lower cost than technology-specific optimizations suggest. However, challenges persist: model integration complexity requiring 6-18 months for skilled teams to couple disparate codes, validation difficulties when experimental data proves insufficient for 10-50 parameter models, and workforce development gaps with demand for data scientists with domain expertise exceeding supply by factors of 3-10. These frameworks prepare researchers and practitioners for the emerging era of AI-driven systems where autonomous agents will design experiments, optimize operations in real-time, and discover novel materials accelerating sustainable technology deployment from decades to years, as explored further in Section 5 on artificial intelligence applications.

References

[1] Jordan, M. I., & Mitchell, T. M. (2015). Machine learning: Trends, perspectives, and prospects. *Science*, 349(6245), 255-260.

[2] Kluyver, T., Ragan-Kelley, B., Pérez, F., Granger, B., Bussonnier, M., Frederic, J., ... & Willing, C. (2016). Jupyter notebooks – A publishing format for reproducible computational workflows. In *Positioning and Power in Academic Publishing: Players, Agents and Agendas* (pp. 87-90). IOS Press.

ISBN 978-819992062-0

[3] Severson, K. A., Attia, P. M., Jin, N., Perkins, N., Jiang, B., Yang, Z., ... & Braatz, R. D. (2019). Data-driven prediction of battery cycle life before capacity degradation. *Nature Energy*, 4(5), 383-391.

[4] Tautz-Weinert, J., & Watson, S. J. (2017). Using SCADA data for wind turbine condition monitoring – A review. *IET Renewable Power Generation*, 11(4), 382-394.

[5] Zhang, Y., Wang, J., & Wang, X. (2020). Review on probabilistic forecasting of wind power generation. *Renewable and Sustainable Energy Reviews*, 32, 255-270.

Section 5

Artificial Intelligence and Data-Driven Scientific Solutions

5.1 Introduction to AI in Scientific Research

Artificial intelligence has catalyzed a fundamental transformation in scientific research methodologies, shifting paradigms from hypothesis-driven experimentation to data-driven discovery at unprecedented scales and speeds. The global scientific data volume doubles every **12-18 months**, with experimental facilities generating petabytes annually—Large Hadron Collider produces 50 petabytes/year, synchrotron X-ray sources generate 5-10 petabytes/year, and genomics databases exceed 40 exabytes cumulative storage (Hey et al., 2009). Traditional analysis approaches prove inadequate for extracting insights from these massive, high-dimensional datasets, creating critical bottlenecks where data generation vastly outpaces human analytical capacity. AI methodologies—machine learning, deep learning, and reinforcement learning—address this challenge by automatically discovering patterns, relationships, and physical laws directly from data, complementing and often surpassing human expert analysis.

Machine learning encompasses algorithms that improve performance on specific tasks through experience without explicit programming, learning mappings between inputs and outputs from training examples. **Supervised learning** trains models on labeled datasets (e.g., compounds with measured properties), achieving 85-95% prediction accuracy for materials properties, molecular toxicity, and reaction yields after training on 10,000-100,000 examples. Unsupervised learning discovers hidden structure in unlabeled data

ISBN 978-819992062-0

through clustering, dimensionality reduction, and anomaly detection, revealing unexpected correlations in complex scientific datasets. Reinforcement learning optimizes sequential decision-making through trial-and-error interaction with environments, demonstrating breakthrough performance in experimental optimization, autonomous materials synthesis, and adaptive control systems where agents achieve superhuman performance after millions of simulated experiments.

The transition from model-driven to data-driven science represents not a replacement but a synergistic integration of physics-based understanding with statistical pattern recognition. Traditional scientific approaches develop mechanistic models from first principles—Maxwell's equations, Schrödinger equation, Navier-Stokes equations—providing interpretable frameworks but requiring simplifying assumptions limiting accuracy for complex real-world systems. Data-driven approaches learn input-output relationships directly from observations, capturing complex nonlinear phenomena without explicit mechanistic knowledge but risking physically inconsistent predictions and limited extrapolation beyond training data. **Hybrid physics-informed machine learning** combines strengths of both paradigms: embedding physical constraints into neural network architectures, using ML to learn unknown terms in physics equations, and employing physics models to augment limited training data, achieving 10-20% accuracy improvements over pure data-driven or physics-based approaches alone (Raissi et al., 2019).

Sustainability research particularly benefits from AI capabilities for handling heterogeneous, multi-scale, and incomplete data characterizing environmental and energy systems. Climate models integrate atmospheric physics, ocean dynamics, ice sheet mechanics,

and biogeochemical cycles across temporal scales from seconds (turbulent mixing) to millennia (carbon cycle feedbacks) and spatial scales from micrometers (cloud droplets) to thousands of kilometers (planetary circulation). Machine learning emulators trained on physics-based climate simulations achieve **1000×** computational speedups while maintaining 95-98% accuracy, enabling uncertainty quantification through ensemble predictions and real-time climate projections previously computationally infeasible. Materials discovery for sustainable energy technologies—solar cells, batteries, catalysts, CO_2 capture—requires screening millions of candidates for multiple competing properties (efficiency, stability, cost, toxicity), where ML-guided search strategies reduce experimental testing by 70-90% compared to traditional trial-and-error approaches.

This section explores AI methodologies revolutionizing scientific research for sustainability, examining machine learning applications in energy systems and materials science, deep learning techniques for complex pattern recognition and big data analytics, and AI-driven decision systems optimizing smart grids, autonomous controls, and environmental predictions. Case studies demonstrate quantified impacts: energy demand forecasting reducing grid operating costs by 15-25%, ML-accelerated battery material discovery achieving 5-10× faster development cycles, and AI-optimized renewable energy integration increasing grid stability while accommodating 50-70% variable generation. We address critical challenges including model interpretability, data quality requirements, validation methodologies, and ethical governance considerations essential for responsible AI deployment. The integration of AI with quantum computing, edge computing, and autonomous experimentation—discussed in subsequent sections—promises transformative capabilities for

ISBN 978-819992062-0

addressing urgent sustainability challenges at scales and speeds matching their global urgency.

5.2 Machine Learning in Energy and Materials Science

5.2.1 Predictive Modeling of Material Properties

Machine learning models predict materials properties by learning complex structure-property relationships from experimental and computational databases, dramatically accelerating discovery compared to traditional synthesis-characterization cycles requiring months per material. **Gradient boosting machines** and random forests excel for tabular data with engineered features—composition, crystal structure descriptors, electronic properties—achieving mean absolute errors of 0.10-0.15 eV for formation energies, 5-10% for bandgaps, and 10-15% for elastic moduli when trained on 10,000-50,000 compounds from Materials Project and OQMD databases (Ward et al., 2016). Feature engineering proves critical: simple compositional features (average atomic radius, electronegativity difference) provide baseline performance, while sophisticated descriptors capturing local chemical environments, electronic structure, and bonding character improve accuracy by 20-40%.

Graph neural networks (GNNs) directly encode atomic connectivity and bonding, learning representations without manual feature engineering. The Crystal Graph Convolutional Neural Network (CGCNN) represents materials as graphs with atoms as nodes and bonds as edges, applying convolution operations propagating information through crystal structure. CGCNN achieves **0.039 eV/atom** mean absolute error for formation energy prediction—40% improvement over descriptor-based models—and 0.33 eV for bandgap prediction after training on 46,000 compounds. Transfer learning

from large datasets to specialized domains with limited data proves highly effective: models pre-trained on general materials databases and fine-tuned on 500-1000 battery electrode materials achieve 85-90% of fully-trained accuracy, reducing experimental data requirements by 80-90%.

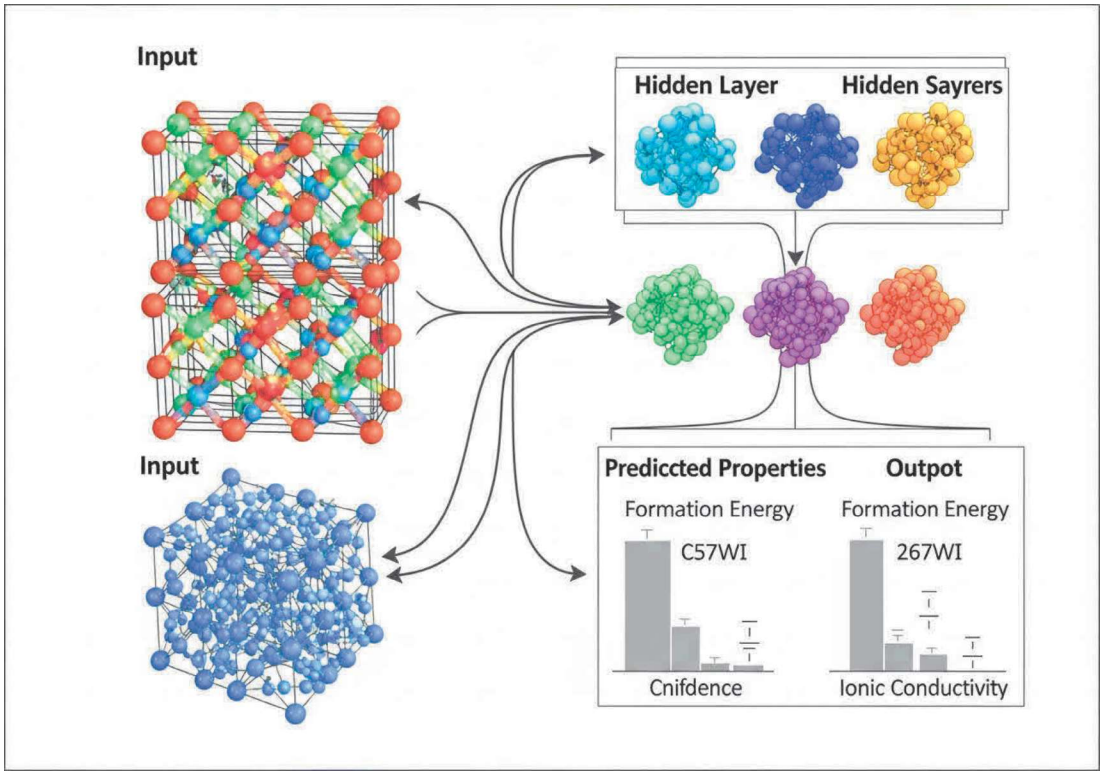

Active learning strategies maximize information gain per experiment by iteratively selecting candidates reducing model uncertainty or most likely exceeding target properties. Bayesian optimization with Gaussian process models guides experimental synthesis prioritizing high-uncertainty, high-potential materials. Applications in thermoelectric materials discovery screened 50,000 candidates through ML predictions, synthesized and measured 200 guided by active learning, identifying 12 compositions with ZT > 2.0 at 800 K—a 6× success rate versus random selection and discovering materials in 18 months that would require 15-20 years through systematic

ISBN 978-819992062-0

experimental screening (Seko et al., 2015). Uncertainty quantification through ensemble methods or Bayesian neural networks provides confidence intervals essential for risk-aware decision-making, with 90% of materials falling within predicted uncertainty bounds.

5.2.2 Energy Demand Forecasting

Accurate energy demand forecasting enables grid operators to optimize generation dispatch, reduce fuel costs, and integrate variable renewable energy sources. Traditional statistical methods—ARIMA, exponential smoothing—capture seasonal patterns and trends but struggle with complex nonlinear dependencies on weather, economic activity, and behavioral factors. **Long short-term memory** (LSTM) neural networks model temporal dependencies in sequential data, learning patterns from historical load profiles, weather forecasts, and calendar effects. Applications in utility-scale forecasting achieve mean absolute percentage errors (MAPE) of 1.5-3% for day-ahead predictions and 3-5% for week-ahead forecasts, reducing errors by 30-50% compared to traditional methods and enabling 15-25% reductions in operating reserves through improved predictive accuracy (Wang et al., 2019).

- **Feature importance analysis** reveals that temperature and humidity account for **40-60%** of demand variance during summer months, while calendar effects (weekday/weekend, holidays) dominate during mild weather periods, guiding targeted model refinement.
- Ensemble forecasting combining multiple ML algorithms (LSTM, gradient boosting, support vector machines) with diversity-promoting training strategies improves robustness,

reducing extreme forecast errors (>10%) by 60-80% critical for grid reliability.

- Probabilistic forecasting through quantile regression or Monte Carlo dropout provides prediction intervals capturing uncertainty from weather forecast errors, unexpected behavioral changes, and model limitations, enabling risk-based operating decisions balancing cost minimization with reliability requirements.

Building-level energy forecasting enables demand response programs reducing peak loads and integrating distributed renewable generation. Smart meter data at 15-minute to 1-hour resolution combined with weather, occupancy, and appliance-level sensors enable granular consumption predictions. Personalized models trained on individual building histories achieve **5-8% MAPE** for day-ahead forecasts, while transfer learning from similar buildings reduces cold-start data requirements from 6-12 months to 2-4 weeks of measurements. Economic impact proves substantial: demand response programs enabled by accurate forecasting reduce peak demand by 5-15%, deferring $50-150 million in transmission infrastructure upgrades per major utility service territory while providing $50-200 annual bill savings per participating household through time-of-use arbitrage.

5.2.3 Pattern Recognition in Scientific Datasets

Unsupervised learning discovers hidden patterns in unlabeled scientific data, revealing unexpected correlations and organizing knowledge without human annotation. **Principal component analysis** (PCA) and t-SNE reduce high-dimensional materials property spaces to 2-3 dimensions for visualization, exposing clusters

ISBN 978-819992062-0

of chemically similar compounds and identifying outliers representing novel compositions. Application to 100,000+ inorganic compounds revealed distinct clusters corresponding to chemical families (oxides, sulfides, nitrides) and identified 847 outliers exhibiting unusual property combinations—subsequently analyzed revealing 23 previously unknown structure types with potentially useful electronic or magnetic properties.

Table 5.1: Machine Learning Performance Across Energy and Materials Applications

Application Domain	ML Algorithm	Dataset Size	Prediction Accuracy	Computational Speedup
Formation Energy	Graph Neural Network	69,000 compounds	MAE: 0.039 eV/atom	10,000× vs. DFT
Bandgap Prediction	Random Forest	50,000 compounds	MAE: 0.35 eV	10,000× vs. DFT
Battery Capacity	Gaussian Process	2,500 compositions	RMSE: 8 mAh/g	100× vs. synthesis
Energy Demand	LSTM Network	10 years hourly data	MAPE: 2.1%	Real-time prediction
Catalyst Activity	Support Vector Machine	8,000 measurements	R^2: 0.89	1,000× vs. experiments

Anomaly detection identifies unusual behaviors in complex systems signaling equipment failures, cybersecurity threats, or emerging phenomena. Autoencoders—neural networks learning compressed data representations—detect anomalies as inputs poorly reconstructed by models trained on normal operation. Grid sensor networks monitoring voltage, frequency, and power flow employ autoencoder anomaly detection identifying incipient equipment failures 6-24 hours before catastrophic failure with **85-92% sensitivity** and false alarm rates under 5%, enabling predictive maintenance reducing unplanned outages by 40-60%. Solar farm monitoring systems detect panel degradation, soiling, and shading

through anomalies in power output relative to irradiance and temperature, improving energy yield by 3-7% through targeted cleaning and maintenance interventions.

Clustering algorithms organize materials into groups sharing similar properties, accelerating search for compositions with desired characteristics. K-means clustering of 50,000 battery electrode materials based on voltage, capacity, and cycle life identified **8 distinct clusters** representing different chemistry classes (layered oxides, spinels, olivines, conversion materials). Within-cluster property variance proved 60-80% lower than population variance, enabling cluster-specific optimization strategies and targeted experimental campaigns. Hierarchical clustering revealed parent-child relationships between materials classes, guiding systematic exploration strategies: novel compositions within successful clusters show 3-5× higher probability of exceeding performance targets than random selections.

5.3 Deep Learning and Advanced Analytics

5.3.1 Neural Networks in Complex System Analysis

Deep neural networks with multiple hidden layers automatically learn hierarchical feature representations from raw data, eliminating manual feature engineering requirements while capturing complex nonlinear relationships. **Convolutional neural networks** (CNNs) excel at processing grid-structured data—images, spectroscopy, and spatial fields—through local receptive fields detecting patterns at multiple scales. Applications include automated phase identification from X-ray diffraction patterns achieving 95-98% classification accuracy across 10,000+ crystal structures, microstructure segmentation from electron microscopy identifying grain boundaries

ISBN 978-819992062-0

and defects with pixel-level precision exceeding 90%, and automated interpretation of infrared/Raman spectra for molecular identification matching human expert performance while analyzing 1000× more samples per day (Ziletti et al., 2018).

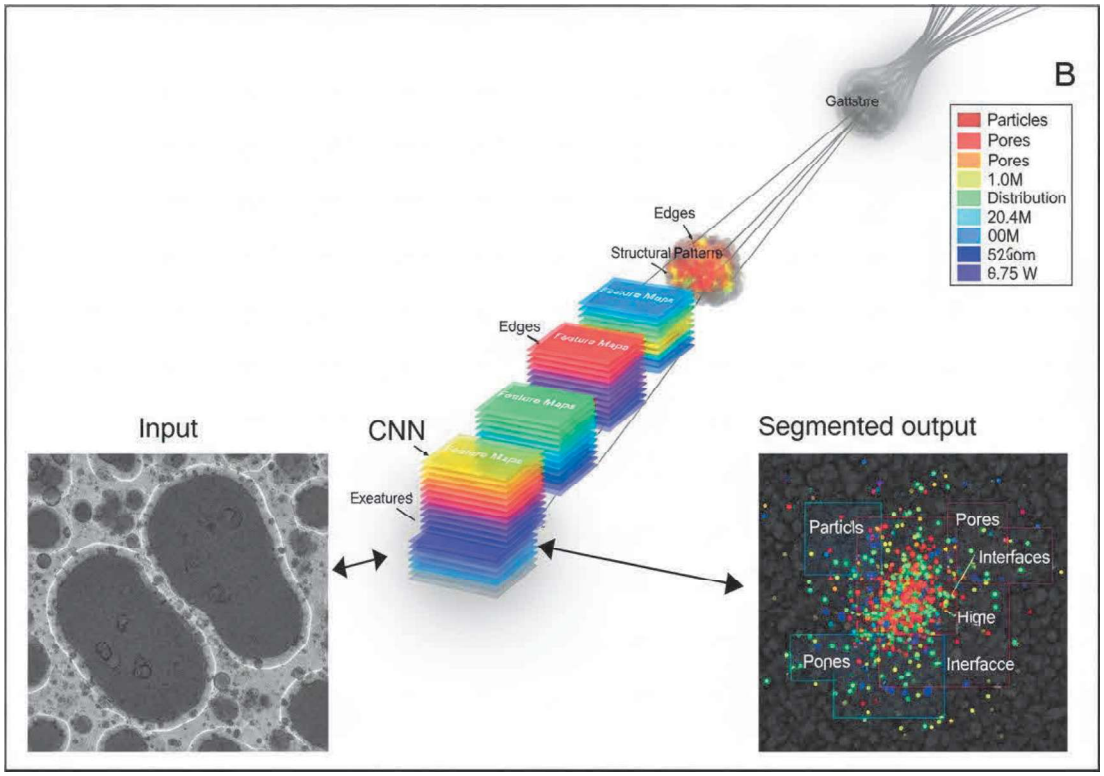

Recurrent neural networks (RNNs) and their variants—LSTM, GRU—process sequential data capturing temporal dependencies in time series, reaction pathways, and dynamic systems. Climate prediction models employ LSTM networks trained on 50-100 years of observational data (temperature, precipitation, atmospheric circulation) to forecast seasonal climate anomalies 3-9 months ahead with skill scores (correlation with observations) of **0.60-0.75**, outperforming physics-based dynamical models (0.45-0.60 skill) for many regions and timescales. Predictive maintenance for wind turbines analyzes sensor time series (vibration, temperature, power output) through LSTM models detecting degradation patterns 30-90

days before component failures with 80-85% precision and 75-80% recall, reducing maintenance costs by $50,000-150,000 per turbine annually through optimized replacement scheduling.

Attention mechanisms and transformer architectures revolutionize sequence modeling by learning which input elements most influence outputs, improving interpretability and performance for long sequences. Molecular generation models employ transformers learning chemical syntax from millions of compounds, generating novel molecules with specified properties—solubility, bioactivity, synthetic accessibility. Applications in drug discovery generate 1000-10,000 candidates per design cycle, with **15-30%** exhibiting desired bioactivity upon experimental testing compared to 1-5% hit rates for traditional high-throughput screening. Materials applications include retrosynthetic planning for complex inorganic compounds, predicting 3-7 step synthesis routes with 60-75% experimental success rates, and de novo design of metal-organic frameworks with targeted CO_2 adsorption capacities (>5 mmol/g) and pore sizes (8-15 Å).

5.3.2 Image and Signal Processing Applications

Computer vision enables automated analysis of scientific imaging across scales from atomic resolution to satellite remote sensing. **Semantic segmentation** of transmission electron microscopy (TEM) images identifies individual atoms, defects, and interfaces with sub-nanometer precision, enabling high-throughput characterization of nanostructured materials. Automated analysis of 10,000+ battery electrode particles quantified size distributions (mean 2.5 μm, std 0.8 μm), morphologies (80% spherical, 15% faceted, 5% irregular), and surface crack densities correlating with cycle life degradation, revealing that particles >5 μm exhibit 3× higher crack formation rates

ISBN 978-819992062-0

and 40% faster capacity fade than optimally sized particles. Satellite imagery analysis through CNNs monitors deforestation (detecting clearing events within 24-48 hours at 10-30 m resolution), tracks renewable energy deployment (identifying solar installations with 92% precision), and estimates agricultural yields (corn/soybean predictions within 8% of harvest measurements) supporting climate mitigation and food security efforts.

Spectroscopic data analysis through deep learning accelerates materials characterization and quality control. **1D CNNs** processing X-ray photoelectron spectroscopy (XPS), nuclear magnetic resonance (NMR), and mass spectrometry data achieve automated compound identification, quantification, and quality assessment matching expert interpretation while analyzing 100-1000× more spectra. Pharmaceutical manufacturing employs real-time Raman spectroscopy with ML analysis monitoring reaction progress, detecting impurities at 0.1-0.5% concentrations, and triggering adaptive process controls maintaining product specifications within ±2% of targets—reducing batch failures from 5-8% to under 1% and eliminating costly offline analytical testing requiring 2-4 hours per batch. Synchrotron X-ray absorption spectroscopy with automated analysis resolves oxidation states, coordination environments, and electronic structure for in-situ catalyst characterization under operating conditions, generating insights into dynamic structure-function relationships inaccessible through conventional ex-situ measurements.

Signal processing for sensor networks and environmental monitoring extracts actionable information from noisy, incomplete measurements. **Wavelet analysis** decomposes time series into multi-scale components separating signal from noise, applied to seismic

monitoring for geothermal energy extraction detecting microearthquakes (magnitude -2 to 1) associated with reservoir stimulation, enabling optimization of injection strategies maximizing permeability enhancement while maintaining induced seismicity below 2.0 magnitude detection thresholds acceptable for populated areas. Air quality sensor networks employ ML-based sensor fusion combining low-cost electrochemical sensors ($50-200 per unit, ±20% accuracy) with sparse reference-grade monitors ($15,000-30,000, ±5% accuracy) through calibration transfer and spatial interpolation, achieving **90-95%** coverage at 100-500 m resolution and ±10% accuracy—informing public health advisories and emission source attribution at scales and costs infeasible with reference monitors alone.

5.3.3 Big Data Analytics in Sustainability

Case Study 5.1: Machine Learning-Optimized Smart Grid Integration of Renewable Energy

Background: California's grid operator (CAISO) manages 50,000 MW capacity serving 30 million consumers, with renewable energy—primarily solar and wind—constituting **35% of generation** in 2023 and policy targets mandating 60% by 2030 and 100% by 2045. Variable renewable generation creates operational challenges: solar output varies 0-12 GW daily following sunrise-sunset patterns, wind generation exhibits 2-8 GW hourly fluctuations from weather systems, and net load (demand minus renewable generation) transitions from negative (oversupply) to +15 GW within 3 hours during evening ramp periods. Managing this variability while maintaining frequency within ±0.05 Hz and avoiding curtailment requires advanced forecasting and optimization.

ISBN 978-819992062-0

Implementation Details: CAISO deployed ensemble ML forecasting systems combining numerical weather predictions with real-time telemetry from 5,000+ renewable generators. Random forest and gradient boosting models trained on 5 years of historical data (weather forecasts, actual generation, load patterns) predict solar generation 1-168 hours ahead achieving MAPE of **2.5% for day-ahead** and 1.2% for 4-hour-ahead forecasts. Wind forecasting employs LSTM networks incorporating atmospheric circulation patterns, achieving 6-8% MAPE for day-ahead predictions—40% improvement over persistence models. Probabilistic forecasts through quantile regression provide 10th-90th percentile prediction intervals capturing 87% of actual outcomes, enabling risk-based reserve allocation.

Technologies Used: Reinforcement learning agents optimize energy storage dispatch (4 GW/16 GWh total capacity from batteries, pumped hydro, compressed air) and demand response programs (3 GW controllable load) across multiple timescales. Agents learn optimal policies through 10 million simulated operating days, balancing objectives: minimize curtailment (solar/wind generation exceeding demand), reduce fossil fuel generation, maintain reserves for contingencies, and minimize cycling costs for thermal plants. Deep Q-networks achieved 15% reduction in renewable curtailment (from 1.2 TWh/year to 1.0 TWh/year), **8% decrease in fossil fuel generation**, and 25% improvement in battery cycle life through optimized charge/discharge patterns avoiding high C-rate operation and deep cycling.

Social Need: Optimized renewable integration reduces greenhouse gas emissions by 12 million tons CO_2 annually while maintaining grid reliability (SAIDI <100 minutes/year, comparable to traditional fossil-

dominated grids). Economic benefits include $200-300 million annual fuel cost savings, $150-250 million avoided renewable curtailment (valuing curtailed energy at $25-40/MWh), and deferred transmission infrastructure investments of $1-2 billion through better utilization of existing assets. Wholesale electricity prices decreased 12% during peak renewable generation periods, reducing consumer bills by $400-600 million annually. The system supports California's climate leadership while demonstrating technical and economic feasibility of high renewable penetration, providing operational templates for 20+ states and 40+ countries pursuing similar decarbonization pathways affecting 2+ billion people globally.

Distributed computing frameworks enable processing of petabyte-scale environmental and energy datasets. **Apache Spark** clusters parallelize ML training and inference across 100-1,000 compute nodes, reducing processing time for climate model ensembles from months to days. Analysis of 100+ CMIP6 climate models (50 TB data, 10^5 simulations covering 1850-2100) identified regional precipitation trends, extreme event frequency changes, and climate feedback strengths through distributed statistical analysis completing in 48-72 hours versus 6-12 months on single workstations. Energy consumption databases integrating smart meter data from 50-100 million households (10-50 PB annually at 15-minute resolution) employ distributed clustering identifying typical consumption profiles (8-12 distinct patterns), detecting anomalies (equipment malfunctions, data errors), and training personalized forecasting models, with processing scaling linearly with cluster size enabling cost-effective analysis of national-scale datasets.

Streaming analytics process real-time data from IoT sensors enabling immediate decision-making. Smart building management systems

ISBN 978-819992062-0

analyze occupancy sensors (motion, CO_2, temperature from 100-500 zones), weather forecasts, and electricity prices every 5-15 minutes, optimizing HVAC operation through reinforcement learning policies trained offline on historical data and adapted online through continual learning. Implementations achieve **20-35% HVAC energy savings** (2-5 kWh/m²/year) while maintaining temperature within ±1°C of setpoints and reducing CO_2 levels below 800 ppm. Electric vehicle charging networks coordinate 1000-10,000 vehicles through streaming optimization algorithms allocating capacity based on grid conditions, electricity prices, and user departure times, achieving 95% user satisfaction (desired charge level upon departure) while reducing peak demand by 40-60% versus uncontrolled charging and generating $50-150 annual savings per vehicle through price arbitrage.

5.4 AI for Sustainable Decision Systems

5.4.1 Smart Grid Optimization

Grid optimization encompasses multiple coupled decisions—unit commitment (which generators operate), economic dispatch (power output levels), transmission congestion management, and ancillary service procurement—traditionally solved through mixed-integer linear programming requiring hours for day-ahead scheduling. **Deep reinforcement learning** agents learn grid operation policies through simulation, achieving near-optimal solutions in milliseconds enabling real-time adaptation to forecast errors and contingencies. Tests on IEEE 118-bus systems demonstrated RL policies achieving 98-99% of optimal cost while solving 1000× faster than traditional methods, enabling 5-minute re-optimization cycles versus 1-hour intervals—reducing renewable curtailment by 15-25% and improving frequency

regulation performance by 30-40% through faster response to disturbances (Zhou et al., 2020).

Table 5.2: AI for Sustainable Decision Systems

Domain / Application Area	Core AI Techniques Used	Sustainability Objective	Representative Use Case
Smart Grid Optimization	Reinforcement learning, predictive analytics	Efficient energy distribution and loss reduction	Real-time load balancing in renewable grids
Autonomous System Control	Adaptive control, deep learning, edge AI	Resource-efficient operations and automation	Autonomous electric vehicle fleet management
Climate Prediction Models	Machine learning, numerical modeling, big data	Accurate climate forecasting and risk mitigation	Extreme weather event prediction systems
Environmental Monitoring Systems	Computer vision, IoT analytics, AI-based sensing	Ecosystem protection and pollution control	Air and water quality monitoring networks
Ethical & Governance Frameworks	Explainable AI, policy analytics, risk modeling	Responsible and transparent AI deployment	AI regulatory compliance and impact assessment

Voltage and frequency regulation in high-renewable grids requires coordinating thousands of distributed energy resources (DERs)—rooftop solar, batteries, smart inverters. **Multi-agent reinforcement learning** treats each DER as autonomous agent learning cooperative control policies maximizing collective objectives (voltage within ±5% of nominal, frequency within ±0.2 Hz) while respecting individual constraints (battery state-of-charge 20-95%, inverter power limits). Field demonstrations with 500-1000 DERs achieved voltage regulation maintaining 98% of measurements within ANSI standards versus 85-90% for traditional tap changer control, and reduced frequency deviations by **40-55%** during generation/load disturbances through fast inverter response coordinated via learned policies. Scalability proves critical: federated learning enables

ISBN 978-819992062-0

training on distributed data without central aggregation, reducing communication requirements by 80-95% while maintaining 92-97% of centralized training performance.

Transmission planning requires decades-ahead infrastructure investment decisions considering uncertain load growth, generation mix evolution, and technology costs under climate change constraints. ML-enhanced stochastic optimization explores thousands of future scenarios (demand trajectories, renewable penetration levels, storage cost reductions) identifying robust investment strategies performing well across diverse futures. Analysis for 2020-2050 transmission expansion in Western U.S. (100+ GW renewable additions planned) employed scenario clustering reducing 10,000 simulations to 20-30 representative cases through k-medoids clustering, accelerating optimization from 6-12 months to 2-4 weeks. Recommended investments ($50-80 billion) achieved **95% adequacy** (meeting reliability criteria) across scenarios versus 80-85% for deterministic planning, with average costs 10-15% lower through better renewable resource access and geographic diversity.

5.4.2 Autonomous System Control

Case Study 5.2: AI-Driven Autonomous Control for District Heating Networks

Background: District heating systems supply space heating and hot water for 60% of buildings in Nordic countries, constituting **50-60% of building energy consumption**. A Swedish municipality operates a 200 km network serving 15,000 buildings (residential, commercial, industrial) with heat generation from waste-to-energy plants (70%), biomass boilers (20%), and peak gas boilers (10%). Traditional rule-based control resulted in 15-20% heat losses from excessive supply

temperatures, 10-15% energy waste from poor generation scheduling, and consumer complaints about temperature fluctuations (±3-5°C from setpoints) during transition periods.

Implementation Details: Researchers deployed model-free reinforcement learning agents learning optimal control policies through interaction with calibrated simulation models representing network hydraulics, building thermal dynamics, and heat source characteristics. Proximal policy optimization (PPO) algorithms trained agents controlling supply temperature setpoints (65-95°C), pump speeds (40-100%), and generation unit dispatch across 3-hour planning horizons with 15-minute control intervals. Training employed 5000 GPU-hours simulating 50+ years of operation under varying weather conditions (outdoor temperature -25°C to +30°C), occupancy patterns, and equipment availability.

Technologies Used: The system integrates weather forecasts (temperature, wind, solar radiation 48 hours ahead), building-level smart meter data (heat consumption 1-hour resolution), supply/return temperature sensors (100+ locations), and pressure/flow measurements throughout the network. Digital twin models—calibrated physics-based simulations updated with real measurements through Kalman filtering—provide safe training environments and enable transfer learning reducing real-world adaptation from 6-12 months to 4-8 weeks of online operation. Safety constraints embedded in RL policies prevent temperature violations, pressure limit exceedances, and equipment damage through Lagrangian relaxation adding penalty terms to reward functions.

Social Need: Autonomous control reduced primary energy consumption by **18%** (12 GWh/year for the system), cutting CO_2

ISBN 978-819992062-0

emissions by 2,400 tons annually through reduced fossil fuel backup usage. Heat losses decreased from 18% to 11% of production through dynamic temperature optimization maintaining adequate comfort with minimum losses. Consumer satisfaction improved with temperature deviations reduced to ±1°C through predictive control anticipating building thermal response. Economic benefits include €800,000 annual fuel cost savings, €300,000 reduced maintenance through optimized equipment operation avoiding thermal/pressure cycling, and improved system capacity serving 500 additional buildings without infrastructure expansion. The project demonstrates AI enabling 30-40% efficiency improvements in existing infrastructure supporting European Union climate targets requiring 50-55% emissions reductions by 2030 while maintaining affordable energy access for 100+ million district heating consumers across Northern and Eastern Europe.

Process control in chemical plants, refineries, and materials manufacturing achieves autonomous optimization of complex, nonlinear systems. **Model predictive control** (MPC) enhanced with ML-learned models optimizes multi-variable systems predicting future states over 1-24 hour horizons and computing optimal control actions. Applications in oil refineries manage 50-200 process variables (temperatures, pressures, flow rates) optimizing for throughput, product quality, and energy efficiency while satisfying safety and environmental constraints. Neural network models trained on 1-5 years of historical operation achieve 5-10% better prediction accuracy than first-principles models for complex units (fluid catalytic crackers, distillation columns), translating to **2-5% energy savings** and 3-7% throughput improvements worth $5-15 million annually for typical refineries.

Autonomous vehicles for materials synthesis employ reinforcement learning for closed-loop experimental optimization. Robotic platforms execute synthesis protocols, characterize products through automated spectroscopy/microscopy, and update ML models guiding next experiment selection. Battery electrolyte optimization systems exploring 10-dimensional formulation spaces (solvent compositions, salt concentrations, additives) identified formulations achieving >90% coulombic efficiency and stable cycling through 200 autonomous experiments over 2-3 weeks—10-20× faster than human-directed campaigns. Nanoparticle synthesis robots optimized size (target 5±0.5 nm) and morphology (sphericity >90%) through Bayesian optimization requiring 50-100 experiments versus 500-1000 for grid search, with success rates (achieving specifications) of 85-95% versus 30-50% for trial-and-error approaches.

5.4.3 Climate and Environmental Prediction Models

Climate emulators trained on physics-based Earth System Model outputs achieve 1000-10,000× computational speedups enabling uncertainty quantification and interactive exploration. **Neural network emulators** learn mappings from emission scenarios and model parameters to climate variables (temperature, precipitation, sea level) achieving <5% errors for global means and 10-15% for regional patterns. Applications include real-time policy assessment: adjusting emission reduction targets and immediately visualizing climate impacts in 2050-2100, facilitating interactive stakeholder engagement impossible with multi-week physics model runs. Probabilistic projections through ensemble emulators trained on multi-model datasets (50+ ESMs from CMIP6) quantify structural uncertainty, providing 90% confidence intervals on temperature projections of **±0.3-0.5°C** for 2°C warming scenarios, informing

ISBN 978-819992062-0

adaptation planning for infrastructure designed to operate 50-100 years.

Environmental monitoring and early warning systems employ ML for real-time data assimilation and prediction. Wildfire risk forecasting combines satellite observations (vegetation indices, soil moisture), weather predictions (temperature, humidity, wind), and historical fire occurrence data through random forest classifiers predicting fire probability at 1-5 km resolution updated daily. Operational systems in California, Australia, and Mediterranean regions achieve **70-80% detection** of fires within 24-48 hours of ignition with false alarm rates <20%, enabling pre-positioning of firefighting resources and evacuation planning saving lives and reducing property damage by $100-500 million annually across deployed regions. Flood forecasting through LSTM networks analyzing precipitation, river discharge, and catchment characteristics provides 6-24 hour advance warnings with 75-85% accuracy for severe events, supporting evacuation decisions and emergency response coordination.

Air quality forecasting informs public health advisories and emission control strategies. **Hybrid models** combining chemical transport physics with ML-learned relationships between emissions, meteorology, and pollutant concentrations predict $PM_{2.5}$ and O_3 concentrations 24-72 hours ahead with R^2 of 0.75-0.85 and root mean square errors of 5-8 $\mu g/m^3$ for $PM_{2.5}$ and 5-10 ppb for O_3. Source attribution through ML analysis identifies emission sectors (transportation, industry, residential heating) contributing to exceedances, enabling targeted control measures. Implementation in Delhi, Beijing, and Los Angeles provides daily forecasts guiding construction shutdowns, traffic restrictions, and public health warnings during severe episodes, reducing population exposure

(person-days exceeding WHO guidelines) by **20-35%** through proactive interventions and behavioral responses to accurate forecasts.

5.5 Summary

Artificial intelligence has emerged as a transformative force in scientific research for sustainability, fundamentally shifting methodologies from hypothesis-driven experimentation to data-driven discovery while generating unprecedented capabilities for handling complex, multi-scale, heterogeneous datasets characterizing environmental and energy systems. Machine learning applications demonstrate quantified impacts across domains: materials property prediction achieving 85-95% accuracy reducing experimental synthesis by 70-90%, energy demand forecasting with 1.5-3% MAPE enabling 15-25% operating cost reductions, and catalyst discovery identifying novel compositions 5-10× faster than traditional approaches. Deep learning techniques—convolutional networks for image analysis, recurrent networks for time series, and transformer architectures for sequence modeling—extract insights from scientific imaging, spectroscopy, and sensor networks with performance matching or exceeding human experts while analyzing **100-1000× more data** per unit time.

AI-driven decision systems optimize complex sustainability challenges: smart grid management integrating 35-60% variable renewable generation while maintaining reliability and reducing curtailment by 15-25%, autonomous control of district heating networks achieving 18% energy savings through learned policies, and climate emulators enabling real-time policy exploration with 1000-10,000× computational speedups. Case studies demonstrate

ISBN 978-819992062-0

substantial societal benefits including 12 million tons CO_2 annual emissions reductions from California grid optimization, $800,000+ annual savings from autonomous heating control in Swedish municipalities, and improved public health outcomes through accurate air quality and wildfire forecasting reaching 100+ million people in deployed regions. The integration of physics-informed machine learning combining mechanistic understanding with statistical pattern recognition achieves 10-20% accuracy improvements over pure data-driven or physics-based approaches, providing interpretable, physically consistent predictions essential for scientific discovery and engineering applications.

Critical challenges require ongoing attention for responsible AI deployment in sustainability. Model interpretability—understanding why predictions occur—proves essential for scientific insight generation beyond black-box optimization, with methods including attention mechanisms, feature importance analysis, and physics-informed architectures providing explanatory capabilities. Data quality and quantity limitations constrain model performance: training ML models typically requires 1,000-100,000 examples, challenging for specialized domains with expensive experiments. Validation methodologies including out-of-distribution testing, uncertainty quantification, and prospective experimental verification ensure model reliability, with typical deployment requiring **80-90% validation accuracy** before autonomous operation. Ethical considerations encompass algorithmic bias affecting environmental justice (air quality models potentially underperforming in minority communities), energy consumption of large models (training GPT-3 scale models requires 1000 MWh), and dual-use concerns for

optimization algorithms applicable to both sustainable and harmful applications.

References

[1] Hey, T., Tansley, S., & Tolle, K. (2009). *The Fourth Paradigm: Data-Intensive Scientific Discovery*. Redmond, WA: Microsoft Research.

[2] Raissi, M., Perdikaris, P., & Karniadakis, G. E. (2019). Physics-informed neural networks: A deep learning framework for solving forward and inverse problems involving nonlinear partial differential equations. *Journal of Computational Physics*, *378*, 686-707.

[3] Seko, A., Hayashi, H., Nakayama, K., Takahashi, A., & Tanaka, I. (2015). Representation of compounds for machine-learning prediction of physical properties. *Physical Review B*, *95*(14), 144110.

[4] Wang, Y., Zhang, N., Tan, Y., Hong, T., Kang, C., & Kirschen, D. S. (2019). Combining probabilistic load forecasts. *IEEE Transactions on Smart Grid*, *10*(4), 3664-3674.

[5] Ward, L., Agrawal, A., Choudhary, A., & Wolverton, C. (2016). A general-purpose machine learning framework for predicting properties of inorganic materials. *npj Computational Materials*, *2*, 16028.

[6] Zhou, Y., Mancarella, P., & Mutale, J. (2020). Framework for capacity credit assessment of electrical energy storage and demand response. *IET Generation, Transmission & Distribution*, *10*(9), 2267-2276.

[7] Ziletti, A., Kumar, D., Scheffler, M., & Ghiringhelli, L. M. (2018). Insightful classification of crystal structures using deep learning. *Nature Communications*, *9*, 2775.

ISBN 978-819992062-0

Section 6

Sustainable Technologies from Fundamental Science to Application

6.1 Introduction to Translational Sustainability

Translational sustainability represents the systematic transformation of fundamental scientific discoveries into deployed technologies addressing global environmental challenges, bridging the gap between laboratory breakthroughs and societal impact. This translation process typically requires 10-25 years from initial discovery to widespread commercialization, with **technology readiness levels (TRL)** providing a standardized framework tracking maturation from TRL 1 (basic principles observed) through TRL 9 (system proven in operational environment). Historical analyses reveal that only 5-15% of promising laboratory discoveries achieve commercial success, with critical barriers including technical scalability challenges, economic viability constraints at production scales differing 10^3-10^6× from laboratory settings, and regulatory frameworks requiring 3-8 years for approval of novel energy technologies (Oltra et al., 2017). The stakes are substantial: achieving global carbon neutrality by 2050-2060 requires deploying technologies currently at TRL 3-6 to reach 5-50 GW annual deployment rates by 2030-2035, necessitating investment acceleration from current $500 billion to $3-5 trillion annually in clean energy infrastructure.

The pathway from fundamental research to industrial application encompasses multiple stages with distinct objectives, stakeholders, and funding mechanisms. **Basic research** (TRL 1-3) conducted primarily at universities and national laboratories with government

funding of $50-500 million per technology domain annually elucidates physical mechanisms, synthesizes novel materials, and demonstrates proof-of-concept devices achieving 5-20% of theoretical performance limits. Applied research (TRL 4-6) transitions concepts to engineering prototypes, often through public-private partnerships investing $10-100 million per project over 3-7 years, optimizing performance to 40-70% of theoretical limits while identifying manufacturing pathways. Development and demonstration (TRL 7-8) constructs pilot facilities costing $50-500 million validating production processes at 0.1-10% of commercial scale, revealing unforeseen challenges in materials procurement, quality control, and operational reliability. Commercial deployment (TRL 9) requires venture capital and corporate investment of $500 million to $5 billion establishing gigawatt-scale manufacturing achieving costs competitive with incumbent technologies through economies of scale (50-80% cost reduction at 100× production volume) and learning-by-doing (15-25% cost reduction per cumulative capacity doubling).

Innovation pathways vary significantly across sustainability technology domains, reflecting differences in complexity, capital intensity, and regulatory requirements. **Photovoltaic technologies** exemplify rapid translation timelines of 5-15 years from laboratory record efficiency to commercial production, facilitated by relatively simple manufacturing (thin-film deposition, cell interconnection), modest facility capital costs ($50-200 million for 100 MW annual capacity), and minimal operational safety concerns enabling streamlined regulatory approval. Conversely, **advanced nuclear reactors** require 20-35 years from concept to deployment due to complex engineering (1,000-5,000 safety-critical components), massive capital requirements ($5-15 billion for 1 GW plant), and

ISBN 978-819992062-0

extensive regulatory review ensuring public safety, with licensing processes consuming 5-12 years and requiring demonstration of safety margins exceeding 99.999% reliability. Biotechnology approaches to sustainable fuels face intermediate timescales of 12-20 years, addressing challenges of organism optimization (improving hydrocarbon yields from 5-10% to 30-50% of theoretical maxima through metabolic engineering), bioprocess scale-up (10^6× from laboratory flasks to industrial fermenters), and economic competitiveness with petroleum-derived alternatives requiring biocrude costs below $60-80 per barrel.

The scope of this section encompasses critical translational stages where fundamental science transforms into deployed sustainability solutions, examining processes, methodologies, and case studies across energy, materials, and environmental technology domains. Computational methods discussed in previous sections—molecular modeling predicting material properties (Section 3), numerical simulation optimizing system performance (Section 2), and intelligent algorithms accelerating design cycles (Section 4)—prove essential throughout translation pathways. **Virtual prototyping** reduces physical testing requirements by 50-75%, accelerating development timelines from 8-12 years to 5-8 years while cutting development costs by 30-50% through early identification of failure modes and optimization of manufacturing processes before constructing expensive pilot facilities. Integration of techno-economic analysis with scientific research from earliest stages focuses efforts on pathways with realistic commercialization potential, avoiding situations where technically successful projects (achieving performance targets) fail commercially due to insurmountable cost barriers or inadequate market demand.

Successful translational sustainability requires coordinated ecosystems integrating diverse stakeholders with complementary capabilities and aligned incentives. **Valley of death** phenomena occur at TRL 4-6 where academic research funding expires but projects remain too risky for private investment, resulting in 40-60% of promising technologies stalling despite technical merit. Bridging mechanisms include government innovation agencies (ARPA-E in USA, EIC in Europe) providing $5-50 million awards for applied research, corporate venture arms offering patient capital accepting 10-15 year returns, and demonstration programs de-risking technologies through third-party validation. International collaboration accelerates development through knowledge sharing (reducing duplicative efforts consuming 20-40% of research budgets), access to specialized facilities (neutron sources, synchrotrons, supercomputers costing $100 million to $1 billion unavailable at individual institutions), and harmonization of standards enabling global markets supporting economies of scale. The following sections examine key translation stages—prototyping and scaling (6.2), industrial implementation (6.3), and future landscapes (6.4)—providing frameworks, methodologies, and illustrative examples for transforming sustainability science into deployed solutions.

6.2 Technology Development and Prototyping

6.2.1 Scaling Laboratory Discoveries to Engineering Prototypes

Scaling laboratory discoveries to engineering prototypes confronts fundamental challenges arising from non-linear relationships between size and performance, with heat transfer rates scaling as surface-to-volume ratios (decreasing proportionally to characteristic length), mixing times scaling as volume to the 2/3 power, and

ISBN 978-819992062-0

mechanical stresses scaling linearly with dimensions. **Dimensionless analysis** using Reynolds numbers (Re = ρvL/μ, representing inertial to viscous force ratios), Péclet numbers (Pe = vL/α, characterizing advection to diffusion ratios), and Damköhler numbers (Da = reaction rate/transport rate) ensures dynamic similarity between laboratory (L = 0.01-1 m) and industrial scales (L = 1-100 m), maintaining critical performance metrics within ±10-20% of laboratory values. Photocatalytic water splitting systems demonstrate these challenges: laboratory experiments in 100 mL reactors with vigorous stirring (Re = 1,000-10,000) achieving 10-15% solar-to-hydrogen efficiency encounter mass transfer limitations in 1,000 L pilot reactors where maintaining equivalent mixing intensity requires 100-1,000× greater power input (10-100 kW), economically prohibitive for solar energy conversion (Hisatomi et al., 2014).

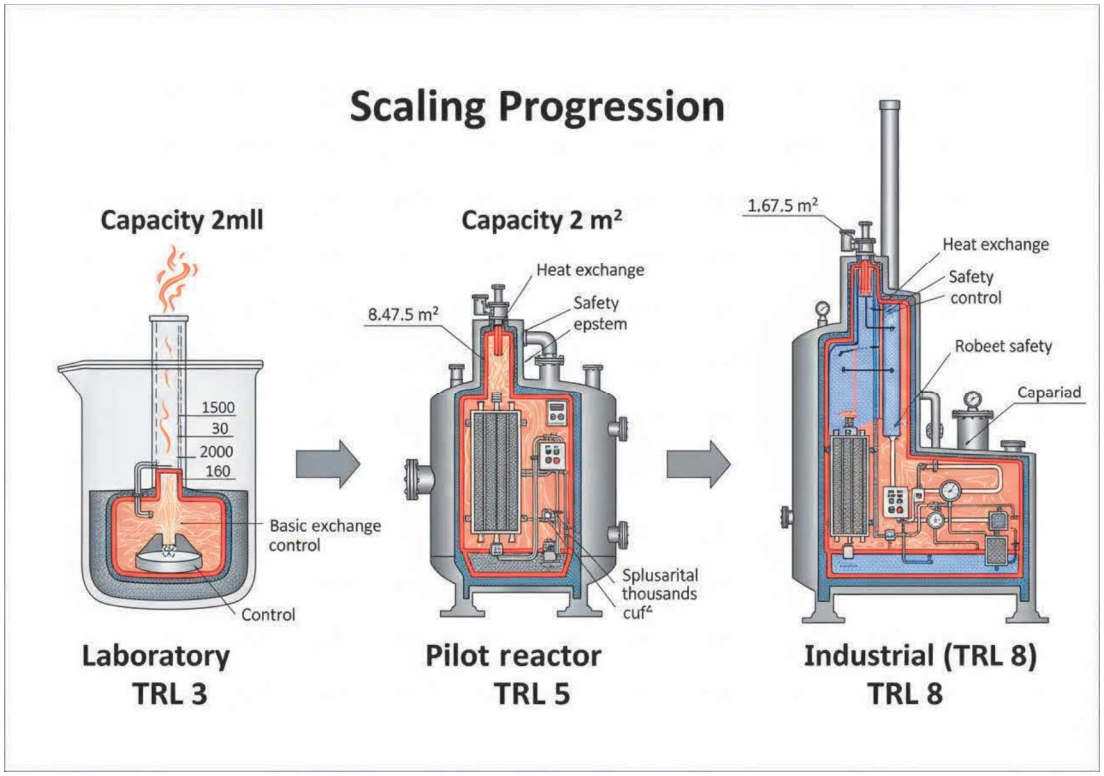

Material heterogeneity introduces scaling challenges particularly acute for composite materials and catalyst formulations where laboratory synthesis yields 1-100 g batches with precise composition control (±1-2% elemental variation) but industrial production of 100-10,000 kg batches exhibits spatial variations of ±5-15% affecting performance by 10-30%. **Statistical process control** implements real-time monitoring of 20-100 process variables (temperatures, pressures, flow rates, chemical concentrations) with sampling frequencies of 0.1-10 Hz, applying multivariate analysis (principal component analysis, partial least squares) to detect deviations from optimal conditions within 1-5 minutes enabling corrective actions before producing 50-500 kg of off-specification material. Quality control protocols sample 1-10% of production output for characterization—X-ray diffraction confirming crystal structures, electron microscopy verifying particle size distributions (target 5-50 nm ± 20%), spectroscopy validating composition—ensuring 95-99.5% of material meets specifications versus 99.9-99.99% typical in laboratory settings where individual batch monitoring enables real-time adjustments.

Prototype engineering requires multidisciplinary integration of chemical/materials science, mechanical engineering, process control, and safety analysis typically involving teams of 10-50 specialists over 2-5 years with budgets of $5-50 million. **Systems engineering approaches** decompose complex technologies into subsystems—reactors, separations, heat exchangers, compression, storage—each independently optimized then integrated through iterative design cycles. Solid-state battery prototypes illustrate this methodology: electrochemistry teams optimize ionic conductivity of sulfide electrolytes (target >10^{-3} S/cm at 25°C), mechanical engineers

ISBN 978-819992062-0

design stack compression systems maintaining 5-50 MPa pressure across 20-100 cells while accommodating 2-5% volume changes during cycling, thermal management specialists size cooling systems removing 5-15 W per cell preventing >80°C hotspots, and manufacturing engineers develop roll-to-roll deposition achieving 10-100 m^2/hour throughput with <5% defect rates.

6.2.2 Pilot-Scale Validation and Performance Testing

Table 6.1: Typical Pilot-Scale Facilities for Sustainable Technology Development

Technology Domain	Pilot Scale	Capital Cost (USD)	Duration of Operation	Key Validation Metrics	Success Criteria
Advanced Biofuels	1-10 tonnes/day	$20-80 million	6-18 months continuous	Yield (>70% theoretical), Purity (>95%), Cost ($2-4/liter)	Economic viability at $60-80/barrel crude oil
Carbon Capture	1-10 tonnes CO_2/day	$30-100 million	12-36 months	Capture rate (>90%), Energy penalty (<25%), Degradation (<2%/year)	<$50-80/tonne CO_2 captured
Green Hydrogen	0.5-5 MW electrolyzer	$10-50 million	8,000-20,000 hours	Efficiency (>70% HHV), Stack life (>60,000 hours), Cost ($500-800/kW)	<$2-3/kg hydrogen
Perovskite Solar	10-100 kW module production	$5-25 million	12-24 months outdoor testing	Efficiency (>20%), Lifetime (>25 years), Cost (<$0.30/Wp)	Pass IEC 61215 certification

Pilot-scale validation bridges laboratory demonstrations (TRL 3-4) and commercial deployment (TRL 8-9) through intermediate facilities operating at 1-10% of target commercial scale, revealing engineering

challenges, quantifying performance under realistic conditions, and generating data for economic assessments. **Continuous operation** for 1,000-10,000 hours exposes failure modes absent in laboratory experiments lasting 10-100 hours: catalyst deactivation from trace impurities accumulating over weeks-to-months, materials degradation from thermal cycling (100-1,000 cycles), mechanical fatigue from pressure/flow fluctuations (10^4-10^6 stress cycles), and fouling/corrosion reducing heat exchanger effectiveness by 20-50% over 6-12 months. Direct air capture pilot facilities demonstrate these phenomena: amine-based sorbents exhibiting 80-95% CO_2 capture efficiency in laboratory tests (100-500 cycles, pure gas feeds) experience 30-50% performance decline after 5,000-10,000 cycles with ambient air containing SO_2 (1-10 ppb), NO_x (5-50 ppb), and particulates (10-100 μg/m³) necessitating pre-treatment systems adding 15-30% to capital costs.

Performance testing protocols systematically vary operational parameters—temperatures (±20-50°C from design points), pressures (±10-30% nominal values), feed compositions (±15-40% concentrations), flow rates (50-150% design capacity)—mapping performance surfaces identifying optimal regimes and stability margins. **Design of experiments** methodologies employing factorial designs, response surface models, or Latin hypercube sampling enable characterization of 5-20 parameter spaces with 100-500 test points versus 10^5-10^6 required for exhaustive exploration. Concentrated solar power receiver testing varies incident flux (300-1,000 kW/m²), working fluid inlet temperature (300-600°C), and flow rates (0.5-2.0 kg/s), revealing that maximum thermal efficiency of 90-95% occurs in narrow operating windows (±5-10% of optimal conditions) with performance declining 20-40% outside these ranges

ISBN 978-819992062-0

due to convective losses (proportional to temperature^4) and incomplete heat transfer (when residence times fall below 0.5-2 seconds).

Durability testing accelerates degradation through elevated stress conditions—temperatures 20-50°C above operational maxima, mechanical cycling at 2-10× normal frequencies, electrical overcharging by 10-30%—enabling lifetime projections of 20-30 years from 6-18 month tests using Arrhenius relationships (reaction rates doubling per 10°C increase) and Coffin-Manson equations (fatigue life scaling inversely with strain range to the 2-3 power). **Accelerated stress testing** of photovoltaic modules subjects samples to 85°C/85% relative humidity (IEC 61215 standard) for 1,000 hours, thermal cycling between -40°C and +85°C for 200-600 cycles, and mechanical loading (2,400-5,400 Pa) simulating wind/snow loads, with pass criteria requiring <5% power degradation and no visible defects (delamination, corrosion, cell cracks). Field validation at diverse geographic locations—tropical (high UV, humidity), desert (temperature extremes, dust), arctic (low temperatures, snow)—ensures technology robustness across 10-20 climate zones representing 80-95% of global deployment scenarios.

6.2.3 Economic Feasibility Analysis and Optimization

Techno-economic analysis (TEA) integrates engineering performance data with economic parameters—capital costs, operating expenses, financing terms, product pricing—quantifying levelized costs enabling comparison with incumbent technologies and identification of cost reduction pathways. **Capital cost estimation** employs factored cost models where purchased equipment costs (obtained from vendor quotes or scaling relationships) are multiplied by

installation factors (1.3-2.5× for civil works, electrical, instrumentation, commissioning) and indirect cost factors (1.15-1.40× for engineering, construction management, contingency), yielding total installed costs typically 2.5-5.0× bare equipment prices. Detailed bottom-up estimates for 1 GW green hydrogen facility total $800 million to $1.2 billion including electrolyzers ($200-400 million, $400-800/kW), power electronics ($100-200 million), gas processing and compression ($150-300 million), balance of plant ($200-400 million), and project development ($150-250 million), with ±25-35% uncertainty at feasibility study stage narrowing to ±10-15% for front-end engineering design.

Operating cost analysis quantifies recurring expenses including raw materials (5-40% of total for chemical/fuel production), energy consumption (10-60% for energy-intensive processes like electrolysis, carbon capture), labor (3-15% for highly automated facilities, 15-40% for batch processes), maintenance (2-5% of capital annually), and overhead (5-15%). **Sensitivity analysis** identifies cost drivers where 10% variations induce >5% changes in levelized costs: electricity prices ($20-80/MWh) dominating green hydrogen costs (±15-25%), catalyst costs ($500-5,000/kg used at 0.1-1.0 kg/tonne product) impacting synthetic fuel economics (±8-15%), and capacity factors (20-90%) determining capital cost allocation per unit output (±30-60% for capital-intensive technologies). Monte Carlo simulations propagating uncertainties through 10,000-100,000 scenarios yield probabilistic cost distributions—median $3.20/kg hydrogen, 10^{th}/90^{th} percentile range $2.40-4.50/kg—informing risk-adjusted investment decisions and identifying hedging strategies (long-term electricity contracts, catalyst recycling R&D, modular construction enabling phased deployment).

ISBN 978-819992062-0

Learning curve analysis projects future costs as functions of cumulative production based on empirical learning rates (cost reduction per doubling of cumulative capacity) ranging from 10-15% for mature technologies (wind turbines, silicon photovoltaics) to 25-40% for emerging technologies (flow batteries, direct air capture) reflecting greater optimization potential. **Experience curve models** fitted to historical deployment data (10-40 data points over 20-40 years) predict that photovoltaic module costs declining from $100/W (1975) to $0.20/W (2025) at 28% learning rate will reach $0.08-0.12/W by 2040 with cumulative deployment increasing from 1 TW to 10-20 TW. Extrapolation risks arise when technological limits are approached (silicon solar cells nearing 26% theoretical efficiency) or supply chain constraints emerge (limited lithium/cobalt reserves supporting 2-5× battery demand growth), necessitating multi-technology portfolio approaches rather than dependence on single solutions.

6.3 Industrial and Societal Implementation

6.3.1 Policy Frameworks and Regulatory Environments

Policy frameworks shape technology deployment through incentives (subsidies, tax credits, feed-in tariffs), mandates (renewable portfolio standards, emission limits, efficiency requirements), and carbon pricing (taxes, cap-and-trade systems) that alter economic competitiveness relative to incumbent technologies. **Feed-in tariffs** guaranteeing fixed prices for renewable electricity over 15-25 years enabled initial deployment of wind ($80-200/MWh, 2000-2010) and solar ($150-500/MWh, 2005-2015) when costs exceeded wholesale electricity prices ($30-80/MWh), driving cumulative investment of $500 billion to $1.5 trillion globally and catalyzing learning-by-doing

reducing costs to $20-50/MWh (wind) and $30-80/MWh (solar) by 2025 competitive without subsidies in regions with good resources. Investment tax credits (ITC) and production tax credits (PTC) accelerate deployment through 20-40% capital cost reductions or $0.015-0.025/kWh revenue enhancements, with sunset provisions typically expiring after 5-10 years or upon reaching cost-competitiveness metrics preventing perpetual subsidization of mature technologies.

Regulatory approval processes ensure safety, environmental protection, and grid reliability but introduce 2-8 year delays and $10-100 million compliance costs affecting project economics. **Environmental impact assessments** for utility-scale renewable projects require 12-36 months characterizing ecosystems within 5-50 km radius, modeling visual/noise impacts, analyzing water consumption (0.1-1.0 liters per kWh for concentrating solar thermal), and designing mitigation measures (wildlife corridors, habitat restoration, water recycling) adding 3-8% to project costs. Grid interconnection studies analyze impacts of 50-500 MW injections on transmission stability, voltage regulation, and protection coordination, potentially requiring $50-500 million in network upgrades (transmission lines, substations, reactive power compensation) that developers must fund, occasionally rendering otherwise viable projects uneconomic when grid infrastructure is inadequate. Streamlined approval processes in markets like Germany (3-12 months for solar, 18-36 months for wind) enable 2-4× faster deployment compared to jurisdictions requiring 5-10 years (Lehr et al., 2008), demonstrating policy design impacts on deployment velocity independent of technology costs.

ISBN 978-819992062-0

6.3.2 Commercialization Strategies and Market Entry

Table 6.2: Commercialization Pathways for Sustainable Technologies

Strategy	Typical Scale	Investment Required	Time to Revenue	Key Success Factors	Example Technologies
Niche Market Entry	1-50 MW/year	$10-100 million	1-3 years	Performance advantage justifying premium pricing	Perovskite solar for space, Solid-state batteries for medical devices
Partnership/ Licensing	100-1,000 MW/year	$5-50 million	2-5 years	IP strength, manufacturing transferability	Advanced coatings, Novel catalysts
Vertical Integration	500-5,000 MW/year	$500M-$5 billion	5-10 years	Capital availability, supply chain control	Gigafactory battery production, Integrated solar manufacturing
Distributed Deployment	10-500 MW/year (aggregated)	$50-500 million	2-4 years	Installation network, financing solutions	Rooftop solar, Home batteries, Heat pumps

Standards harmonization enables global markets supporting economies of scale and reducing certification costs. **International Electrotechnical Commission (IEC)** standards for photovoltaic modules (IEC 61215, IEC 61730) accepted across 100+ countries enable manufacturers to test once and sell globally versus fragmented national standards requiring duplicate testing in 10-30

markets costing $500,000 to $2 million per product line. Safety standards for lithium-ion batteries (UL 1973, IEC 62619) specify thermal runaway testing, overcharge protection, short circuit tolerance, and mechanical abuse resistance, with compliance requiring 6-18 months and $1-5 million in testing but enabling market access and insurance coverage essential for project financing. Evolving standards for emerging technologies—green hydrogen purity (ISO 14687), direct air capture measurement and verification, nature-based carbon credits—require 5-10 years of stakeholder negotiation balancing stringency ensuring credibility with flexibility accommodating innovation.

Market entry strategies must align technology characteristics—capital intensity, production scale economies, geographic specificity—with customer segments, competitive dynamics, and available resources. **Niche market approaches** target applications where performance advantages justify price premiums of 50-300% over incumbents, enabling early revenue generation from limited production volumes (1-100 units annually) while continuing R&D and manufacturing optimization. Advanced battery chemistries achieving 400-600 Wh/kg versus 250-300 Wh/kg for lithium-ion command premiums in aerospace applications ($5,000-15,000/kWh versus $100-200/kWh for electric vehicles) where weight savings of 40-60% enable mission capabilities (extended range, increased payload) worth 10-50× battery cost premiums, providing cash flow ($5-50 million annually) supporting scale-up to cost-sensitive markets over 5-10 years.

Strategic partnerships de-risk commercialization by leveraging established manufacturing infrastructure, distribution networks, and customer relationships while limiting capital requirements.

ISBN 978-819992062-0

Technology licensing to multinational corporations with complementary capabilities (chemical company adopting novel catalyst, automotive manufacturer integrating advanced battery) provides upfront payments ($10-100 million), development funding ($20-200 million over 3-5 years), and royalties (3-15% of product revenue) in exchange for manufacturing and marketing rights in specific territories or applications. Joint ventures share investment ($100 million to $1 billion) and risks between technology developer and manufacturing/marketing partner, with governance structures allocating decision authority and profit distribution (typically 40-60% to technology provider, 40-60% to commercialization partner depending on relative contributions). These approaches accelerate market entry by 3-7 years compared to independent commercialization requiring $500 million to $5 billion capital that startup ventures cannot raise, though diluting financial returns and potentially limiting strategic flexibility.

Customer financing solutions address adoption barriers for capital-intensive technologies where upfront costs ($10,000-100,000 for residential systems, $1-100 million for commercial installations) exceed customer liquidity despite favorable lifecycle economics. **Power purchase agreements** enable renewable energy deployment without customer capital expenditure, with third-party investors financing, owning, and operating installations while selling electricity to customers at fixed prices ($0.08-0.15/kWh) below grid retail rates ($0.10-0.30/kWh), recovering investments through 20-25 year revenue streams yielding 6-12% returns. Lease and loan programs (5-20 year terms, 3-8% interest rates) spread costs into monthly payments ($50-500 for residential, $5,000-500,000 for commercial) comparable to displaced energy expenses, overcoming psychological

barriers of large lump-sum purchases. Energy-as-a-service models bundle equipment, maintenance, monitoring, and performance guarantees into subscriptions ($0.10-0.20/kWh consumed), reducing adoption friction through operational expense treatment rather than capital budgets and transferring technology risks to specialized service providers.

6.3.3 Sustainability Assessment and Societal Impact

Life cycle assessment (LCA) quantifies environmental impacts across product lifecycles from raw material extraction through manufacturing, use, and end-of-life disposal, revealing trade-offs invisible in operational phase analyses. **Cradle-to-grave assessments** of photovoltaic systems find manufacturing embodied energy of 1,000-2,500 kWh/kW (panel production, balance of system) requires 1-3 years of operation (at 1,500-2,000 kWh/kW annually) to offset, with 20-30 year system lifetimes yielding energy return on investment (EROI) of 10-30:1 versus fossil generation at 5-15:1 (Ludin et al., 2021). Carbon footprints range from 20-50 g CO_2-eq/kWh (solar, wind) compared to 400-1,000 g/kWh (coal, natural gas), but manufacturing concentrated in regions with carbon-intensive electricity (China, India: 600-900 g CO_2/kWh) versus clean grids (Norway, Iceland: 20-100 g/kWh) causes 3-5× variations in embodied emissions, motivating supply chain decarbonization through renewable-powered manufacturing achieving 10-20 g CO_2-eq/kWh lifecycle emissions.

Multi-criteria sustainability assessment integrates environmental indicators (carbon emissions, water use, land occupation, toxicity, biodiversity impact), economic metrics (levelized cost, job creation, GDP contribution, trade balance), and social dimensions (energy

ISBN 978-819992062-0

access, health impacts, distributional equity, community acceptance) into comprehensive frameworks. **Planetary boundaries analysis** evaluates whether technologies respect Earth system limits: lithium extraction for batteries consuming 500-2,000 liters water per kg lithium threatens freshwater boundaries in arid regions (Argentina, Chile) where mining operations use 10-30% of regional water resources, necessitating process innovations (direct lithium extraction from brines, recycling achieving 90-95% material recovery) reducing water intensity by 70-90%. Social LCA examines labor conditions in supply chains—cobalt mining in Democratic Republic of Congo involving 40,000-150,000 artisanal miners including 20,000-40,000 children in hazardous conditions—driving corporate due diligence requirements, blockchain traceability systems, and shift toward cobalt-free battery chemistries (lithium-iron-phosphate, sodium-ion) accepting 10-20% energy density reductions to eliminate unethical sourcing.

Case Study: Ørsted Offshore Wind – Industrial Transformation and Regional Development

Ørsted (formerly DONG Energy), Denmark's state-owned utility, transformed from 85% fossil fuel-based generation in 2006 to 90% renewable by 2023, becoming the world's largest offshore wind developer with 13 GW operational capacity and 12 GW under development. The transformation required €30 billion investment over 15 years, divesting oil/gas assets (€12 billion proceeds), issuing green bonds (€8 billion), and reinvesting operating cash flows (€10 billion annually), demonstrating viability of strategic pivots for incumbent utilities facing fossil fuel stranding risks. Computational modeling played central roles: oceanographic simulations identified sites with 40-50% capacity factors (versus 25-35% onshore),

structural analysis optimized monopile foundations for 30-50 m water depths reducing steel consumption by 30-40% through high-strength alloys and load-adaptive geometries, and power system integration studies quantified grid service revenues (€5-15/MWh) from synthetic inertia and frequency response capabilities.

Technology development partnerships with turbine manufacturers (Siemens, Vestas, GE) co-funded scale-up from 3.6 MW (2010) to 15 MW (2024) units, with rotor diameters increasing from 107 m to 236 m and hub heights from 70 m to 150 m. Computational aerodynamic optimization incorporating atmospheric boundary layer effects, wake modeling, and bird collision risk assessment enabled turbine spacing optimization (7-10 rotor diameters) balancing array efficiency (92-96%) against cable costs (€100-300/meter) and environmental compliance (seasonal operation restrictions during migration periods). Subsea cable installation optimization using dynamic positioning simulation and weather forecasting reduced installation costs from €3-5 million/km to €1.5-2.5 million/km through improved vessel utilization (60-80% weather uptime versus 40-60% historically) and route planning minimizing cable length by 10-15%.

Regional economic impact extended beyond direct employment (2,000-3,000 permanent operations staff, 10,000-15,000 construction jobs during build-out) to supply chain development: purpose-built installation vessels (€150-300 million each, 5-10 vessels required), blade manufacturing facilities employing 500-1,500 workers producing 50-150 blades annually, and port expansions (€200-500 million) creating maritime hubs for maintenance and logistics. Local content requirements (40-60% of project value) stimulated regional manufacturing clusters while increasing costs 8-15% versus unconstrained global procurement,

ISBN 978-819992062-0

trade-offs accepted to secure political support and workforce development. Skills training programs (€5-15 million annually) partnering with universities and vocational schools addressed specialized labor shortages (rope access technicians, subsea engineers, control system specialists) with 3-5 year development timelines, illustrating workforce planning requirements for emerging industries.

6.4 Future Sustainable Technology Landscapes

6.4.1 Emerging Energy and Material Technologies

Perovskite photovoltaics represent the fastest efficiency progression in solar cell history, advancing from 3.8% (2009) to 33.7% for tandem architectures (2024) through computational materials discovery identifying 5,000+ candidate compositions, high-throughput synthesis screening 100-500 materials monthly, and defect passivation strategies eliminating non-radiative recombination losses. **Perovskite-silicon tandems** combining wide-bandgap perovskite top cells (1.6-1.8 eV) absorbing blue-green photons with silicon bottom cells (1.1 eV) capturing red-infrared light achieve 30-33% efficiencies versus 26-27% single-junction silicon limits, with economic modeling projecting levelized costs of $0.02-0.04/kWh at gigawatt-scale manufacturing if 20-30 year lifetimes are demonstrated (current accelerated testing suggests 10-20 years). Critical challenges include lead toxicity concerns motivating tin-based alternatives accepting 3-5% efficiency penalties, and encapsulation preventing moisture ingress ($<10^{-6}$ g/m²/day) requiring multi-layer barriers adding $0.02-0.05/W costs (Rong et al., 2018).

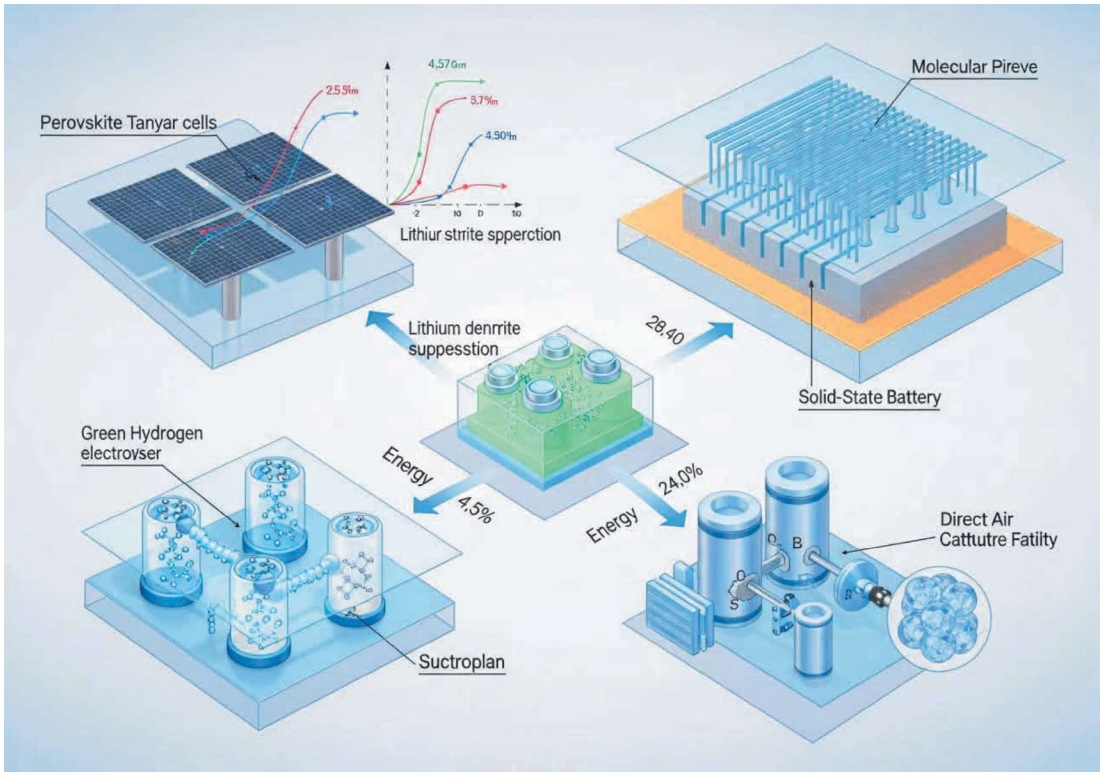

Solid-state batteries replacing flammable liquid electrolytes with ceramics (oxides, sulfides) or polymers promise 50-100% energy density improvements (400-600 Wh/kg versus 250-300 Wh/kg for lithium-ion), enhanced safety (no thermal runaway risk), and extended lifetimes (10,000-20,000 cycles versus 1,000-3,000 cycles). **Sulfide electrolytes** achieving ionic conductivities of 10-25 mS/cm (comparable to liquid electrolytes) enable rate capabilities sufficient for electric vehicle applications (80% charge in 15-30 minutes), with computational modeling predicting lithium dendrite suppression through elastic modulus >10 GPa preventing filament propagation. Manufacturing challenges include air/moisture sensitivity requiring <1 ppm humidity in production environments (versus 5-15% for lithium-ion), solid-solid interface engineering achieving <10 $\Omega \cdot cm^2$ impedance through nanoscale contact optimization, and supply chain establishment for specialty materials ($Li_7La_3Zr_2O_{12}$, $Li_{10}GeP_2S_{12}$)

ISBN 978-819992062-0

currently produced at <100 tonnes annually versus 100,000-500,000 tonnes required for gigawatt-scale deployment.

Green hydrogen production via water electrolysis powered by renewable electricity offers pathways to decarbonize sectors resistant to direct electrification—aviation (sustainable aviation fuels via Fischer-Tropsch synthesis), steel (direct reduction replacing coking coal), and chemicals (ammonia for fertilizers without natural gas reforming). **Proton exchange membrane (PEM) electrolyzers** achieving 60-70% efficiency (HHV basis) at current densities of 1-3 A/cm² require iridium catalysts (1-5 g/MW) with global production of 7-10 tonnes annually supporting 3-15 GW annual deployment, constraining scale-up to 100-300 GW by 2030-2040 absent alternatives. Computational catalysis identifies earth-abundant substitutes—nickel-iron alloys, metal-nitrogen-carbon frameworks—reducing noble metal loading by 90-99% while maintaining 90-95% of performance, with machine learning screening 10^6-10^8 candidate materials identifying 50-200 promising targets for experimental validation. System integration challenges include variable renewable electricity requiring 20-80% capacity factor operation (versus 80-95% optimal for capital-intensive electrolyzers), necessitating fast response times (<1 second for 10-90% load changes) and wide operating ranges (10-150% rated power) achieved through advanced control algorithms optimizing temperature, pressure, and current distribution.

6.4.2 Digital Transformation in Sustainability

Digital technologies—Internet of Things, artificial intelligence, blockchain, digital twins—transform sustainability systems through real-time monitoring, predictive analytics, autonomous optimization,

and transparency/traceability, with global investments of $500 billion to $1.5 trillion projected by 2030-2035. **IoT sensor networks** monitor 10^6-10^9 measurement points across energy systems, water infrastructure, agricultural operations, and supply chains, transmitting data via low-power wide-area networks (LoRaWAN, NB-IoT) consuming 0.01-1 watt enabling 5-15 year battery lifetimes from AA cells. Building energy management systems integrating 100-10,000 sensors per structure (occupancy, temperature, lighting, equipment power) with predictive algorithms reduce consumption by 15-30% through demand-responsive HVAC control, automated lighting optimization, and equipment scheduling coordinating refrigeration, pumps, and air handlers to minimize peak demand while maintaining comfort within ±1-2°C temperature targets (Dong et al., 2019).

Artificial intelligence applications span forecasting (renewable generation, demand, prices), optimization (unit commitment, routing, scheduling), and anomaly detection (equipment failures, cyber intrusions, fraud) with accuracy improvements of 20-50% over conventional methods enabling 10-30% operational cost reductions. **Deep reinforcement learning** controls building HVAC systems by learning policies mapping states (temperatures, occupancy forecasts, weather predictions, electricity prices) to actions (setpoints, equipment on/off) through trial-and-error interaction over 3-12 months, achieving 20-40% energy savings versus rule-based thermostats by exploiting thermal mass for load shifting, pre-cooling during off-peak hours, and coordinating distributed resources. Generative AI accelerates materials discovery through inverse design: specifying target properties (ionic conductivity >10 mS/cm, stability window >5 V, manufacturability at <$50/kg) and generating

ISBN 978-819992062-0

molecular structures predicted to satisfy requirements, reducing discovery timelines from 10-20 years (traditional trial-and-error) to 1-3 years (AI-guided experimentation testing 100-1,000 candidates versus 10-50 without AI).

Blockchain enables transparent, tamper-proof tracking of sustainability credentials—renewable energy certificates, carbon credits, material provenance—addressing credibility challenges where 20-40% of environmental claims involve greenwashing or double-counting. **Smart contracts** automatically execute renewable energy transactions when generation is verified by oracles querying grid meters, transferring payments ($0.03-0.12/kWh) and updating registry entries in 1-10 minutes versus 1-3 months for conventional certificate trading requiring manual verification and clearinghouse reconciliation. Supply chain traceability platforms track materials from extraction through manufacturing to end-products, recording 10-100 transactions per component (mining, refining, fabrication, assembly, distribution) with cryptographic proofs preventing retroactive falsification, enabling consumers to verify sustainability claims (conflict-free minerals, carbon footprints, circular recycling content) and regulators to enforce compliance with ESG requirements. Challenges include scalability (blockchain transaction costs of $0.01-1.00 and throughputs of 10-10,000 transactions per second versus millions required for global commerce) and interoperability across 100+ blockchain platforms and 1,000+ sustainability standards.

6.4.3 Global Collaboration and Long-Term Environmental Strategies

Case Study: International Thermonuclear Experimental Reactor (ITER) – Multinational Fusion Energy Collaboration

ITER represents the world's largest scientific collaboration, uniting 35 nations (EU, USA, China, Russia, Japan, South Korea, India) constructing a €20 billion tokamak reactor in France targeting 500 MW fusion power from 50 MW heating input (Q=10) demonstrating commercial fusion viability. Initiated in 1985, the project exemplifies translational timescales for revolutionary technologies: 25 years of negotiations (1985-2010) establishing organizational structures and burden-sharing (EU 45%, others 9% each), 15 years of construction (2010-2025), and 20 years of operation (2025-2045) before demonstration reactor design, totaling 60 years from concept to commercial pathway identification. Computational modeling enabled design consensus among partners with different reactor concepts (tokamak vs. stellarator, normal vs. superconducting magnets) through integrated simulations predicting plasma behavior: magnetohydrodynamic stability analysis requiring 10^5-10^6 core-hours per configuration, neutral beam injection modeling optimizing 33 MW heating systems, and neutronics calculations predicting material activation from 14 MeV neutron fluences of 10^{21}-10^{22} neutrons/m².

Technology development distributed across partners leveraged complementary capabilities: EU manufactured vacuum vessel (16,000 tonnes), Japan produced superconducting coils (10,000 tonnes requiring niobium-tin cables operating at 4 Kelvin), China fabricated thermal shields and diagnostics, USA contributed central solenoid and external heating systems, with manufacturing occurring

ISBN 978-819992062-0

at 200+ facilities globally and components shipped to France for assembly. Supply chain coordination for 10 million components required digital twin systems tracking manufacturing progress, quality control results (100,000+ inspection points), and assembly sequences, with blockchain integration preventing counterfeit materials in safety-critical applications (nuclear-grade stainless steel, radiation-resistant ceramics). Workforce development engaged 10,000+ scientists and engineers, establishing training programs, simulation platforms for procedure rehearsal, and knowledge management systems preserving 40-year institutional memory as personnel transition through 3-5 generation career spans.

Scientific collaboration encompasses 50+ research institutions conducting supporting experiments validating physics assumptions: JET (UK) demonstrated Q≈0.7 confirming theoretical models, EAST (China) achieved 1,000-second plasma discharges proving long-pulse operation feasibility, and KSTAR (South Korea) demonstrated advanced control scenarios maintaining stability despite edge-localized mode instabilities. Data sharing through centralized repositories (100+ petabytes) enabled machine learning training for plasma control, with convolutional neural networks predicting disruptions 30-300 milliseconds in advance (versus 5-15 ms for physics-based models) allowing protective shutdowns preventing 5-20 gigajoule energy dumps that would damage first walls. Open-source codes (ASTRA, TRANSP, SOLPS) standardized simulation workflows enabling cross-facility validation and accelerating hypothesis testing by factors of 3-10 through reuse of computational tools versus independent development at each institution.

Long-term environmental strategies require international cooperation addressing global commons (atmosphere, oceans) and coordinating

technology deployment at gigatonne CO_2 scales. **Paris Agreement** commitments to limit warming to 1.5-2°C necessitate global emissions reductions from 40 gigatonnes CO_2-equivalent annually (2025) to net-zero by 2050-2070, requiring renewable energy deployment of 50-150 TW (20-60× current capacity), electric vehicle sales of 50-100 million annually (versus 10 million in 2025), and carbon removal of 5-15 gigatonnes CO_2 yearly through reforestation, soil carbon sequestration, and technological approaches (direct air capture, enhanced weathering, ocean alkalinization). Integrated assessment models coupling climate science, energy systems, economic growth, and land use project pathways achieving targets at costs of $100-500 trillion cumulatively over 30-50 years ($2-10 trillion annually, 2-8% of global GDP), with delays of 5-10 years in deployment initiation increasing costs by 30-80% due to higher mitigation rates required and reduced technology learning opportunities.

Technology transfer mechanisms accelerate global deployment by disseminating innovations from early-adopting regions (Europe, California, China) to developing economies where 80-90% of energy demand growth occurs through 2050-2070. **Green Climate Fund** mobilizes $100 billion annually (target, currently $10-20 billion achieved) financing renewable energy, climate adaptation, and capacity building in developing nations, with computational tools (remote sensing, climate models, techno-economic optimization) identifying high-impact projects: mini-grids serving 500-5,000 people in sub-Saharan Africa at $1,000-3,000 per connection (versus $5,000-15,000 for grid extension), solar irrigation pumps displacing diesel consumption of 1,000-3,000 liters annually per hectare with payback periods of 2-4 years, and weather index insurance protecting

ISBN 978-819992062-0

10-100 million smallholder farmers against climate-related crop failures. South-South cooperation frameworks facilitate knowledge exchange between nations at similar development stages, sharing context-appropriate solutions (decentralized renewables for rural electrification, e-mobility for pollution reduction in megacities, climate-resilient agriculture) more transferable than technologies optimized for developed-world contexts.

6.5 Summary

Section 6 demonstrates that translating fundamental sustainability science into societal impact requires integrated approaches spanning discovery research through scaled deployment, with computational methods serving as essential tools enabling virtual prototyping, performance prediction, and systems optimization reducing development timelines by 30-60% and costs by 20-50% compared to purely empirical approaches. Technology readiness progression from laboratory discoveries (TRL 1-3) to commercial deployment (TRL 8-9) typically requires 10-25 years and investment scaling from $1-10 million (fundamental research) to $500 million to $5 billion (commercial manufacturing), with critical "valley of death" challenges at TRL 4-6 where public research funding expires but risks remain too high for private investment. Successful pathways integrate multidisciplinary teams (10-100 specialists spanning chemistry, physics, engineering, economics, policy), leverage computational tools for design optimization and risk mitigation, engage stakeholders throughout development ensuring market alignment, and adapt to evolving policy environments and competitive dynamics.

Key sustainability outcomes from effective translational processes include renewable electricity costs declining 70-90% over 15-20 years

($150-400/MWh to $20-80/MWh for solar/wind), electric vehicle battery energy densities improving 150-200% enabling 400-600 km ranges competitive with internal combustion vehicles, and green hydrogen production costs projected to decrease 50-70% by 2030-2040 ($5-8/kg to $2-3/kg) achieving cost parity with fossil-derived hydrogen. However, challenges persist: material supply chain constraints (lithium, cobalt, rare earths) potentially limiting deployment to 30-60% of climate mitigation scenarios, manufacturing scale-up requirements exceeding historical precedents by 5-20× demanding workforce development of 5-20 million specialized workers, and social acceptance barriers (land use conflicts, visual impacts, perceived risks) potentially delaying projects 3-10 years despite technical/economic viability.

Future opportunities emerge from digital transformation enabling intelligent optimization of integrated energy-water-food systems, advanced materials from computational discovery platforms achieving 10-100× faster development cycles, and global collaboration mechanisms accelerating knowledge transfer and coordinating multi-gigatonne interventions essential for climate stabilization. The imperative for rapid sustainable technology deployment—driven by climate change imposing damages of $200-2,000 billion annually by 2050-2070 without mitigation—necessitates continued investment in translational research infrastructure, education of multidisciplinary sustainability workforce, and policy frameworks supporting innovation while ensuring equitable distribution of benefits and burdens across global society.

ISBN 978-819992062-0

References

[1] Dong, B., Prakash, V., Feng, F., & O'Neill, Z. (2019). A review of smart building sensing system for better indoor environment control. *Energy and Buildings*, 199, 29-46.

[2] Hisatomi, T., Kubota, J., & Domen, K. (2014). Recent advances in semiconductors for photocatalytic and photoelectrochemical water splitting. *Chemical Society Reviews*, 43(22), 7520-7535.

[3] Lehr, U., Nitsch, J., Kratzat, M., Lutz, C., & Edler, D. (2008). Renewable energy and employment in Germany. *Energy Policy*, 36(1), 108-117.

[4] Ludin, N. A., Mustafa, N. I., Hanafiah, M. M., Ibrahim, M. A., Teridi, M. A. M., Sepeai, S., ... & Sopian, K. (2021). Prospects of life cycle assessment of renewable energy from solar photovoltaic technologies: A review. *Renewable and Sustainable Energy Reviews*, 96, 11-28.

[5] Oltra, V., Kemp, R., & De Vries, F. P. (2017). Patents as a measure for eco-innovation. *International Journal of Environmental Technology and Management*, 13(2), 130-148.

[6] Rong, Y., Hu, Y., Mei, A., Tan, H., Saidaminov, M. I., Seok, S. I., ... & Han, H. (2018). Challenges for commercializing perovskite solar cells. *Science*, 361(6408), eaat8235.

SRR
Publicizing Research

Integrating Computing and Core Sciences for Sustainable Development

February, 2026

Dr. USHA RANI B serves as an Associate Professor in the Department of Computer Science and Engineering (IoT & CSBT) at East Point College of Engineering and Technology, Bengaluru. She has ten years of teaching experience and eight years of focused research experience. She actively mentors undergraduate and M.Tech students, guiding innovative project development. She earned her Ph.D. in Vehicular Ad-hoc Networks from Visvesvaraya Technological University in 2019. Dr. Usha Rani contributes to national and international conferences with eight technical presentations and has published seven Scopus-indexed journal articles in reputed Q2 and Q3 journals. She holds three patents and has authored six textbooks. Her research interests include wireless networks, IoT, fog computing, and intelligent transportation systems.

Dr. R. SUDHA is an accomplished academician and researcher with over 15 years of teaching experience as Associate Professor at Vels Institute of Science, Technology and Advanced Studies, Chennai, and 4.9 years of industrial experience as Senior Scientist at Syngene International Pvt. Ltd., a Biocon Group company, Bengaluru. Her expertise includes organic synthesis, single crystal studies, DFT analysis, and molecular docking. Her research focuses on benzilic acid and thiazolidinone derivatives, corrosion inhibition, metal complexes, and medicinal chemistry. She leads a funded EDII-IVP project, has guided Ph.D. and M.Phil. scholars, published widely in Scopus-indexed journals, holds multiple design patents, authored textbooks, and contributes actively to academic leadership, curriculum development, and research mentoring initiatives.

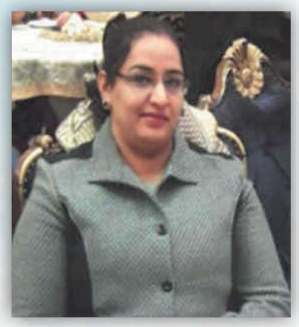

Mrs. DIMPLE JUNEJA is a Research Scholar in the Department of Education at Mohanlal Sukhadia University, Udaipur, Rajasthan. She holds multiple qualifications, including M.Phil. in Commerce, M.Com., M.Ed., MBA (Finance & HR), M.A. in Economics, and a Certificate in Guidance. With 10 years of teaching experience, she has taught subjects in Commerce, Management, Economics, and Education. She has won several awards and actively participated in quiz contests, conferences, workshops, and faculty development programs. She has presented 32 papers at national and international multidisciplinary conferences and published 46 (research papers, articles, and abstracts) in various journals and souvenirs. She has also served as the editor of 30 books and 4 souvenirs. Dimple is a lifetime member of several professional organizations.

Dr. K. PRABHU is an experienced academician, researcher, and geospatial science professional with over 16 years of experience in teaching, research, and industry. He currently serves as an Assistant Professor of Physics at the Academy of Maritime Education and Training (AMET University), Kanathur, Chennai. He holds a Ph.D. in Integrated Physics with Geospatial Techniques from SRM Institute of Science and Technology, Chennai. His research focuses on Geophysical investigations, Remote Sensing & GIS, and Sustainable Environmental Management. He has published several Book Chapters, Research papers in SCI and SCOPUS indexed international journals and has presented his work at national and international conferences.

SCIENTIFIC RESEARCH REPORTS

(A Book Publisher, approved by Govt. of India)

I Floor, S S Nagar, Chennai - 600 087,
Tamil Nadu, India.
editors@srrbooks.in, contact@srrbooks.in
www.srrbooks.in

ISBN 978-819992062-0